Quantum Optics In Structured Radiation Reservoirs

Søren Bay

Institute of Physics and Astronomy
University of Aarhus

1998

Contents

Preface **v**

1 Prologue **1**
1.1 Thesis outline 2

2 Photonic Crystals **5**
2.1 Introduction 5
2.2 The Maxwell equations 6
2.2.1 A photonic band gap in the scalar approximation. 9
2.3 Experimental and theoretical results. 11
2.4 Construction 14
2.5 Applications 16

3 Atom-Atom interaction at the edge of a photonic band gap **21**
3.1 Introduction 21
3.2 The Model 23
3.2.1 Atom-Atom interaction in free space vacuum 25
3.2.2 Atom-Atom interaction in a cavity 25
3.3 Calculation of the couplings 26
3.4 Revisiting the resolvent operator equations 31
3.5 The inversion 34
3.6 The wave functions in time domain 36
3.6.1 One atom 36
3.6.2 Two atoms at the band edge ($\delta = 0$) 37
3.6.3 Small interatomic separation. 39
3.7 The photonic population distribution 41
3.7.1 One atom 41
3.7.2 Two atoms 42
3.8 Summary 44

4 Strongly non-Lorentzian emission spectra in a radiative cascade **47**
4.1 Introduction 47
4.2 The system 48

4.3 Spectrum . . . 49
4.3.1 Lower transition coupled to PBG . . . 50
4.3.2 Upper transition coupled to PBG . . . 53
4.4 Summary . . . 54

5 Fluorescence into flat and structured radiation continua: An atomic density matrix without a master equation 57
5.1 Introduction . . . 57
5.2 The model . . . 58
5.3 Monte-Carlo wave functions . . . 59
5.4 A master equation in the Born-approximation . . . 64
5.5 Conclusions . . . 67

6 Superradiance in a structured radiation reservoir 71
6.1 Introduction . . . 71
6.2 The model . . . 73
6.2.1 Pseudo-mode description . . . 74
6.2.2 Adiabatic elimination of strongly damped mode . . . 76
6.3 Dynamics . . . 76
6.4 Population trapping . . . 79
6.4.1 Analytical approximation to the atomic population distribution . . . 79
6.5 Decay rate in the long time limit . . . 80
6.6 Mean-value equations . . . 85
6.6.1 Mean-value equations in the symmetry breaking approximation . . . 85
6.6.2 Excitation conserving decorrelation . . . 88
6.7 Concluding remarks . . . 90

7 Epilogue 91
7.1 Thesis summary and conclusions . . . 91
7.2 Outlook . . . 92

A Comment on "Resonance fluorescence near a photonic band gap edge: Dressed-state Monte-Carlo wave function approach." 95
A.1 Comment . . . 95

B Resolvent Operator 99
B.1 The resolvent operator . . . 99
B.2 The inversion . . . 101
B.3 The pole approximation . . . 102

C Resumé 105

Bibliography 109

Preface

This thesis is presented for the Faculty of Science at the University of Aarhus as part of the requirements for the Ph.D-degree in physics.

During my Ph.D-studies, I have had the opportunity to visit the theory group at the Max-Planck Institute for Quantum Optics (MPQ) in Garching, Germany. I would like to thank all my friends at the institute for making these visits so enjoyable. I am in particular grateful to the group secretary Renate Weise-McKnight for helping me with all the practical problems during my time in Munich and for the pleasant atmosphere she creates in the group, and I am indebted to Prof. Peter Lambropoulos for suggesting this project and for his hospitality and warm support during my Ph.D-studies.
I am certainly indebted to my supervisor Klaus Mølmer as well for his guidance during my Ph.D-studies and for his creative inputs which have made very valuable contributions to the work presented here. Further his relaxed style has provided an easy-going atmosphere at the 6th floor although more serious-minded people soon learned to close their office doors when Klaus would enter the office I share with Larsch to tell jokes or discuss various kinds of surgery... Finally, I would like to thank my office mate Larsch and all my friends at the Institute in Aarhus for good company.

The work presented in this thesis has resulted in a number of publications [1, 2, 3, 4, 5, 6]. Chapter 3 is based on Refs. [1, 2], chapter 4 on Ref. [3] and chapter 5 is based on Ref. [4] but results on the non-markovian master equation have been added. Chapter 6 is based on Ref. [5] and Ref. [6] is included in appendix A.

Chapter I

Prologue

Dissipation is present in systems ranging from macroscopic size down to microscopic systems governed by quantum mechanics such as an atom. For an atom, the dominant source of dissipation is the coupling to the many modes of the electromagnetic vacuum field which results in the Lamb shift in frequency of the atomic levels and the spontaneous decay rate which renders all excited states unstable. Spontaneous decay is often considered an inherent property of an atom but manipulation of the boundary conditions of the electromagnetic field can strongly alter the characteristics of spontaneous decay [7, 8]. In fact, embedding an atom in a near-resonant cavity thereby amplifying the coupling to one or a few modes of the reservoir leads to an enhancement or suppression of the atomic spontaneous decay depending on the parameters of the system.
In a theoretical description of an atom in a cavity, the resonant cavity mode(s) interacting with the atom is singled out from the background of harmonic oscillator modes and treated on an equal footing with the atomic degrees of freedom whereas the remaining background of weakly coupled modes is treated perturbatively resulting in a shift in frequency and a decay width for the atom.
Recently, however, new types of materials have appeared which possess structured reservoirs that can not be modelled satisfactorily using these standard methods. This includes phonon reservoirs in semiconductors and in particular photon reservoirs in photonic crystals. Photonic crystals are novel materials in which the spatial modulation of the dielectric constant leads to the formation of band structure for the electromagnetic field in close analogy to the electronic band structure in solids. The presence of gaps in the band structure for the electromagnetic field implies that no photonic modes exist for a range of frequencies in the crystal.
The recurrent theme of this thesis is the interaction of small quantum systems with a structured radiation reservoir and the motivation for these studies is two-fold. First, the introduction of structured reservoirs leads to a whole range of new phenomena: For instance in the spontaneous decay of a two-level atom located inside a photonic band gap (PBG) material and near-resonant with the edge of a PBG, Rabi-like oscillations may occur in a transient regime and in

the long-time limit a significant part of the excitation may remain localized at the site of the atom (the so-called photon-atom state) as opposed to the exponential decay of an atom in free space where eventually the atom loses all its excitation. These novel effects occur without the introduction of a defect mode in the crystal but simply due to the structures in the continuum.
A second motivation for these studies is to investigate the validity of the approximations normally employed when dealing with a reservoir. The Markov (or pole) approximation assuming a flat reservoir is of course invalidated in a structured reservoir but we show in chapter 5 that also the Born-approximation which neglects correlations between the atom and the reservoir field modes is no longer valid. New methods are thus required and in chapter 5, we present a novel technique based on the resolvent operator and Monte-Carlo wave functions techniques.

1.1 Thesis outline

Concluding this introductory chapter, let us outline the remainder of this thesis.
The general emphasis in this thesis is on the impact of a modified radiation reservoir on atomic dynamics. Although structured reservoirs are encountered in many contexts, our main focus is on the structured radiation reservoir in photonic crystals. Photonic crystals do, however, constitute a very active field of research in themselves and the next chapter is thus dedicated to a presentation of these novel structures. We present theoretical and experimental investigations of these crystals and various schemes for their construction as well as possible applications.
In chapter 3, we investigate two closely spaced atoms interacting through the narrow band of strongly coupled modes at the edge of a photonic band gap. The resonant dipole-dipole interaction (RDDI) is strongly modified for atomic transition frequencies in the vicinity of the band gap edge, but we show that an analytical approximation to the RDDI agrees very well with the exact RDDI obtained by numerical integration using the exact dispersion relation. Having established the value of the RDDI, we can derive the amplitudes for the two atoms without resorting to the pole-approximation which is necessary due to the strongly modified mode structure in the dielectric host.
In chapter 4, an atomic ladder system is investigated. In particular we focus on the emission spectrum and show that a range of new structures appear in the spectrum of a cascaded system when one of the transitions is in the vicinity of the band gap edge.
In chapter 5, we investigate an atomic Λ-system with one transition coupled to a laser field and a flat continuum of vacuum modes and the other transition coupled to field modes near the edge of a photonic band gap. The system requires simultaneous treatment of Markovian and non-Markovian dissipation processes, and to treat the system dynamics, we propose a formalism based on the resolvent operator and Monte-Carlo wave functions. We demonstrate that

the exact results obtained from this formalism are not in accordance with the results obtained from a non-Markovian master equation obtained by applying only the Born approximation thus demonstrating the invalidity of the Born approximation.
In chapter 6, we investigate an atomic Dicke system coupled to a Fano-profile density of modes. Introducing two pseudo-modes, a Markovian master equation can be derived for the atoms+pseudo-modes. One of the modes can be adiabatically eliminated and effectively we then have an atomic Dicke system coupled to a harmonic oscillator and both systems coupled to the same flat continuum. Studying the dynamics, we find that following the superradiant regime, a meta-stable state is reached for the atomic system. The decay of the meta-stable state is non-exponential and we derive an analytical expression for the decay based on perturbation theory and analytical expressions for trapping states identified by the Monte-Carlo wave function method. Further, we investigate mean-value equations of motion for the operators of the system and discuss different decorrelation approximations of the operator expectation values.
Appendix A contains a comment to a recent paper [9] by Tran Quang and Sajeev John in which they suggest to use dressed-state Monte-Carlo wave functions as a general technique to solve problems with more than one excitation in the structured reservoir. In this comment we argue that their approach violates the physical principles underlying the Monte-Carlo wavefunction method and that their approach produces unphysical results.
The resolvent operator is a strong tool for deriving analytical expressions for wave functions in Laplace space and it is used extensively in this thesis. In appendix B we review the definition and some of the analytical properties of the resolvent operator.
Finally, in appendix C, a thesis resumé for the university yearbook has been included.

Chapter II

Photonic Crystals

In subsequent chapters we discuss various aspects of the dynamics obtained for atoms experiencing the strongly modified radiation reservoir inside a photonic crystal. Photonic crystals are, however, interesting objects in themselves and constitute a very active field of research. The purpose of this chapter is to present some of the major findings related to photonic crystals as well as introduce a number of concepts which will be employed in subsequent chapters.
In section 2.2, we give a brief outline of the theory underlying photonic crystals. In a scalar approximation to the electromagnetic field, an analytical expression is found for the dispersion relation which exhibits gaps in energy. In section 2.3, we present different configurations providing a complete band gap. In section 2.4, different schemes for the construction of photonic crystals are shown and finally in section 2.5, we discuss various applications of these crystals.

2.1 Introduction

Progress in the understanding of semiconductors allows nowadays a detailed tailoring of the electronic properties of a material to suit specific needs. This has led to a wide range of new ceramics and alloys supporting technological breakthroughs with profound impact like the transistor or superconducting materials.
A similar impact can be expected if we learn to control the *optical* properties of a material. In optical devices, a major source of noise is spontaneous emission which is caused by the coupling of the material to the zero-point fluctuations of the electromagnetic vacuum field. If the density of modes of the electromagnetic field could be suppressed, devices with higher efficiencies could be obtained.
To see how such a control can be obtained, it is useful to draw an analogy to solid state physics. It is well-known that the periodic spatial modulation of the electronic potential in the bulk of a material results in Bragg scattering of the electrons and thus leads to a band structure in energy. If the lattice potential is sufficiently strong, a complete gap in energy may open extending in all directions.

In 1987, it was suggested by Yablonovitch [10] and John [11] that indeed a band structure can also be obtained for the electromagnetic field. To promote such a band structure they suggested as a host, a low-loss dielectric in which a periodically varying dielectric constant plays the role of the periodic potential. If the dielectric index contrast (i.e. the magnitude of the modulation) is sufficiently large, a complete band gap may arise thus prohibiting the propagation of the electromagnetic field for any polarization and spatial direction for a range of frequencies.
The suggestion by Yablonovitch and John prompted an extensive research theoretically as well as experimentally. Early theoretical works [12, 13] employing scalar equations for the electromagnetic field failed to reproduce the experimental results and agreement was first obtained when the vectorial nature of the electromagnetic field was taken into account [14]. In 1990, the search for a complete band gap succeeded when Ho, Chan and Soukoulis [15] reported the existence of a complete band gap in the configuration consisting of spheres embedded in a medium of different dielectric constant. This was followed by the first experimental observation in 1991 of a complete band gap for microwave radiation by E. Yablonovitch in a slightly different configuration which has become known as Yablonovite [16].
Since 1991, one goal of the theoretical research in photonic crystals has been to determine the crystal structure providing the largest possible band gap for the smallest possible refractive index contrast and on the experimental side the aim has been to push the gap center frequency towards wavelengths in the (near-)optical domain [17, 18, 19, 20, 21].
Other studies have focused on the various applications of photonic crystals. We know from solid state physics, that the introduction of a defect in an otherwise perfect crystal may provide for instance a localized electronic state with an energy in the gap. Recent research has investigated the effect of defects in a photonic crystal and it is found that the introduction of a point defect in the bulk of an otherwise perfect crystal may lead to a localized mode of the electromagnetic field which can thus serve as a very high Q-cavity. A linear defect may act as a waveguide and in a later section we shall see that light may propagate efficiently even in waveguides exhibiting sharp bends.

2.2 The Maxwell equations

The study of photonic crystals merges solid state physics with electromagnetism. The terminology used in the field of photonic crystals is rooted in solid state physics and when discussing the phenomena arising in these novel structures we also draw heavily on analogies to solid state physics but the underlying object we want to describe is the electromagnetic field. The natural starting point for an analysis of photonic crystals is therefore the Maxwell equations. We shall restrict ourselves to dielectric materials in which there are no free charges or

currents and in that case the Maxwell equations read (in CGS units)

$$\nabla \cdot \mathbf{B} = 0 \tag{2.1}$$
$$\nabla \cdot \mathbf{D} = 0 \tag{2.2}$$
$$\nabla \times \mathbf{E} + \frac{1}{c}\frac{\partial \mathbf{B}}{\partial t} = 0 \tag{2.3}$$
$$\nabla \times \mathbf{H} - \frac{1}{c}\frac{\partial \mathbf{D}}{\partial t} = 0 \tag{2.4}$$

where $\mathbf{E}$ and $\mathbf{H}$ are the macroscopic electric and magnetic fields and $\mathbf{D}$ and $\mathbf{B}$ are the displacement and magnetic induction fields, respectively.
The components of $\mathbf{D}$ can quite generally be expressed as a power series in $\mathbf{E}$

$$D_i = \sum_j \epsilon_{ij} E_j + \sum_{jk} \kappa_{ijk} E_j E_k + O(E^3) \tag{2.5}$$

For moderate field intensities and in the materials of interest, it is a good approximation to retain only the linear term in this expansion. We assume that the dielectric is macroscopic and isotropic so that $\mathbf{E}(\mathbf{r},\omega)$ is related to $\mathbf{D}(\mathbf{r},\omega)$ by a scalar dielectric function $\varepsilon(\mathbf{r})$ which is assumed to be constant within the frequency range of interest. For a low-loss dielectric we can treat $\varepsilon(\mathbf{r})$ as a real quantity. Finally, for many dielectric materials of interest, the magnetic susceptibility is close to unity and we may thus take $\mathbf{B} = \mathbf{H}$. Since we are looking for the eigenmodes of the system, we take the fields in a harmonic form $\mathbf{H}(\mathbf{r},t) = \mathbf{H}(\mathbf{r})e^{-i\omega t}$ and $\mathbf{E}(\mathbf{r},t) = \mathbf{E}(\mathbf{r})e^{-i\omega t}$. With these approximations and the harmonic form of the fields, the Maxwell equations read

$$\nabla \cdot \mathbf{H} = 0 \tag{2.6}$$
$$\nabla \cdot [\varepsilon(\mathbf{r})\mathbf{E}(\mathbf{r},t)] = 0 \tag{2.7}$$
$$\nabla \times \mathbf{E} - \frac{i\omega}{c}\mathbf{H} = 0 \tag{2.8}$$
$$\nabla \times \mathbf{H} + \frac{i\omega}{c}\varepsilon(\mathbf{r})\mathbf{E} = 0 \tag{2.9}$$

The two divergence equations imply that the electromagnetic field in the medium is purely transverse. Dividing (2.9) by $\varepsilon(\mathbf{r})$ and taking the curl, we find the following closed expression for $\mathbf{H}$

$$\Theta\mathbf{H} = \left(\frac{\omega}{c}\right)^2 \mathbf{H} \tag{2.10}$$

where the operator Θ is given by

$$\Theta = \nabla \times \frac{1}{\varepsilon(\mathbf{r})}\nabla \times \tag{2.11}$$

Eq. (2.10) has the form of an eigenvalue problem and one particularly appealing feature of this equation is the fact that the operator Θ is hermitian. This is

also the main reason for focusing on the magnetic rather than the electric field: A closed eigenvalue equation can be derived for the electric field as well but the operator in that case is not hermitian which complicates the solution of the problem.
To promote the creation of a band structure for the electromagnetic field, we introduce a modulation of the dielectric constant $\varepsilon(\mathbf{r})$ which is assumed periodic with lattice vector $\mathbf{R}$ i.e. $\varepsilon(\mathbf{r}) = \varepsilon(\mathbf{r}+\mathbf{R})$. The eigenfunctions of $\mathbf{H}$ then satisfy Floquet's theorem and they can thus be expanded as

$$\mathbf{H}(\mathbf{r}) = \sum_{\mathbf{G}} \mathbf{H}_{\mathbf{G}} e^{i(\mathbf{k}+\mathbf{G})\cdot\mathbf{r}} \tag{2.12}$$

where $\mathbf{k}$ is a fixed wave vector, $\mathbf{G}$ a reciprocal lattice vector and $\mathbf{H}_{\mathbf{G}}$ denote the Fourier coefficients of $\mathbf{H}(\mathbf{r})$ given by

$$\mathbf{H}_{\mathbf{G}} = \frac{1}{V_{\text{cell}}} \int_{\text{cell}} d\mathbf{r} \mathbf{H}(\mathbf{r}) e^{-i\mathbf{G}\cdot\mathbf{r}} \tag{2.13}$$

where the integration is over the Wigner-Seitz unit cell of volume V_{cell}.
Substituting (2.12) into (2.10) finally yields an infinite dimensional matrix equation

$$(\mathbf{k}+\mathbf{G}) \times \sum_{\mathbf{G}'} \eta_{\mathbf{G}\mathbf{G}'} (\mathbf{k}+\mathbf{G}') \times \mathbf{H}_{\mathbf{G}'} + \left(\frac{\omega}{c}\right)^2 \mathbf{H}_{\mathbf{G}} = 0 \tag{2.14}$$

where

$$\eta_{\mathbf{G}\mathbf{G}'} = \frac{1}{V_{\text{cell}}} \int_{\text{cell}} d\mathbf{r} e^{-i(\mathbf{G}-\mathbf{G}')\cdot\mathbf{r}} \varepsilon^{-1}(\mathbf{r}) \tag{2.15}$$

By truncating the infinite series in Eq. (2.14), the resulting finite matrix can be diagonalized using standard numerical methods to obtain the eigenfunctions and eigenenergies. This is an involved task but a number of conclusions can be reached without solving Eq. (2.14).
By a variational calculation it is straightforward to show that the eigenstate of Eq. (2.10) with the lowest frequency also minimizes the energy functional

$$E(\mathbf{H}) = \frac{\langle \mathbf{H}, \Theta\mathbf{H} \rangle}{2\langle \mathbf{H}, \mathbf{H} \rangle} \tag{2.16}$$

where the inner product $\langle ., . \rangle$ is defined by

$$\langle \mathbf{H}, \mathbf{G} \rangle = \int d\mathbf{r} \mathbf{H}^* \mathbf{G} \tag{2.17}$$

But

$$\begin{aligned} E(\mathbf{H}) = \frac{1}{2\langle \mathbf{H}, \mathbf{H} \rangle} \langle \mathbf{H}, \Theta\mathbf{H} \rangle &= \frac{1}{2\langle \mathbf{H}, \mathbf{H} \rangle} \int d\mathbf{r} \frac{1}{\varepsilon(\mathbf{r})} |\nabla \times \mathbf{H}|^2 \\ &= \frac{1}{2\langle \mathbf{H}, \mathbf{H} \rangle} \int d\mathbf{r} \frac{1}{\varepsilon(\mathbf{r})} |\frac{\omega}{c}\mathbf{D}|^2 \end{aligned} \tag{2.18}$$

The energy functional is thus minimized when the displacement field **D** is localized in the regions of high dielectric constant.
It is worth noting that even when $\varepsilon(\mathbf{r})$ is separable e.g. $\varepsilon(\mathbf{r}) = \varepsilon(x)\varepsilon(y)\varepsilon(z)$, the eigenfunctions of Eq. (2.10) are not since the differential operator Θ in Eq. (2.10) mixes different spatial directions.
A second important point is that no fundamental length can be constructed from the constants entering the equation of motion for the fields. This means that eigenfunctions found at one wavelength after a proper rescaling also are eigenfunctions at any other wavelength which implies that a specific photonic crystal structure can be investigated with microwaves where such a crystal is much easier to fabricate and the properties of such a structure are then exactly the same when the crystal is designed for optical light.
The larger the dielectric (or refractive) index contrast is, the easier it is to create a full 3D photonic band gap. However, the dielectric constants obtainable at optical wavelengths dictate an upper limit for the index contrast. The largest practical refractive index is that of the common semiconductors silicon and GaAs, with a refractive index n of 3.6 and a dielectric constant of $n^2 = 13$.

2.2.1 A photonic band gap in the scalar approximation.

It is instructive to neglect the vectorial nature of the electromagnetic field and assume scalar waves instead. This serves two purposes: first, it yields a problem for which an analytical expression can be found for the dispersion relation which exhibits gaps in energy and secondly, aspects of this solution will play a major role in our later studies of the response of atoms coupled near-resonantly to a photonic band gap.
In the scalar approximation, the equation of motion for the electromagnetic field reads

$$-\nabla^2\psi + V\psi = \left(\frac{\omega}{c}\right)^2\psi \tag{2.19}$$

where the potential V is given by

$$V(x) = -\left(\frac{\omega}{c}\right)^2 \sum_{m=-\infty}^{\infty} \varepsilon(x - mL) \tag{2.20}$$

and

$$\varepsilon(x) = \begin{cases} n^2 - 1, & |x| < a \\ 0, & \text{otherwise} \end{cases} \tag{2.21}$$

where n is the refractive index of the scatterer, a its radius, and $2a + b = L$ where b is the distance between scatterers and L is the size of the unit cell.
If we restrict ourselves to one period of the potential, the wave function can be written as

$$\psi(x) = \begin{cases} Ae^{ikx} + Be^{-ikx} & x < -a \\ Ce^{igx} + De^{-igx} & -a \le x \le a \\ Ee^{ikx} + Fe^{-ikx} & x > a \end{cases} \tag{2.22}$$

where $k = \omega/c$ and $g = n\omega/c$. Relations between the coefficients $A, .., F$ can be determined as follows. Since the potential remains finite, the wave function ψ and its first derivative should be continuous at $x = -a$ and $x = a$. This imposes constraints between the coefficients A, B, E, F which after some algebra can be formulated in matrix form

$$\begin{pmatrix} A \\ B \end{pmatrix} = \frac{1}{2} \begin{pmatrix} e^{2ika}(2\cos 2ga - ip\sin 2ga) & iq\sin 2ga \\ -iq\sin 2ga & e^{-2ika}(2\cos 2ga + ip\sin 2ga) \end{pmatrix} \begin{pmatrix} E \\ F \end{pmatrix} \quad (2.23)$$

where $p = k/g + g/k$ and $q = k/g - g/k$.
The eigenfunction ψ further has to satisfy the Floquet theorem i.e.

$$\psi(x + L) = e^{i\chi L}\psi(x) \quad (2.24)$$

where L is the lattice period and χ is a suitable wavevector. Imposing this condition we find

$$\begin{pmatrix} E \\ F \end{pmatrix} = \begin{pmatrix} Ae^{i\chi L - ikL} \\ Be^{i\chi L + ikL} \end{pmatrix} \quad (2.25)$$

Combining Eqs. (2.23) and (2.25) and $b = L - 2a$ leads after some algebra to the relation

$$\cos\chi L = \cos(2na\omega/c)\cos(b\omega/c) - \frac{n^2+1}{2n}\sin(2na\omega/c)\sin(b\omega/c) \quad (2.26)$$

which for the special case $b = 2na$ can be solved to yield the dispersion relation

$$\omega_k = \frac{c}{4na}\arccos\Big[\frac{4n\cos(kL) + (1-n)^2}{(1+n)^2}\Big] \quad (2.27)$$

Gaps are found at $k = m\pi/L$ for odd integer values of m. The center frequency of the lowest gap is $\omega_0 = (\pi c/L)(1+n)/2n$ and the width is

$$\Delta\omega = 2\frac{c(1+n)}{2nL}\Big(\pi - \arccos\Big[\Big[\frac{4n\cos(kL) + (1-n)^2}{(1+n)^2}\Big]\Big) \quad (2.28)$$

which for $n = 1.082$ yields a gap-midgap ratio of $\frac{\Delta\omega}{\omega_0} = 0.05$.
For frequencies close to the upper edge of the gap, the dispersion relation can be approximated by the effective mass dispersion relation

$$\omega_k \simeq \omega_e + A(k - k_0)^2 \quad (2.29)$$

where k_0 is the wave-vector corresponding to the band edge frequency ω_e and A is given by

$$A = \frac{-cL^2}{2a(1+n)^2}\frac{1}{\sin(4na\omega_e/c)} \quad (2.30)$$

containing constants pertaining to the structure of the crystal.
Eq. (2.27) was derived by neglecting the vectorial nature of the electromagnetic field. Experiments investigating the band structure of photonic crystals have shown that this approximation is too crude and to obtain agreement with experiments the vectorial nature of the electromagnetic field has to be taken into account. For our purposes; namely the investigation of atoms coupled to the electromagnetic field inside a photonic crystal, this is not a major concern since it will be shown that the atoms are sensitive only to the local form of the dispersion relation i.e. the quadratic expression in Eq. (2.29) and this is a valid local approximation for many realistic band structures as well. In the following chapters, Eq. (2.29) is thus applied to the study of one or more atoms coupled near-resonantly to the edge of a photonic band gap.

2.3 Experimental and theoretical results.

An important issue in the search for a photonic band gap material is to determine the best crystal structure. In order to address this issue, we now focus on the Brillouin zone (reciprocal lattice). The band gaps corresponding to different symmetry points of the Brillouin zone have to overlap in order to form a full 3D band gap. This is more likely to happen the closer to unity the ratio is between the closest and most distant symmetry point of the Brillouin zone – Or in other words: To promote the creation of a complete band gap, the Brillouin zone should be as sphere-like as possible. The most sphere-like structure among common crystals is the fcc-structure depicted in Fig. 2.1. The distance from the center of the Brillouin zone to the W-point (most distant symmetry) is about 29% larger than the distance to the L point (closest symmetry point).
A large number of fcc-structures have been investigated experimentally as well as theoretically to determine whether they possess a complete band gap. In 1990 this search succeeded when Ho, Chan and Soukoulis [15] showed that the fcc structure depicted in Fig. 2.2 consisting of spheres embedded in a medium with a contrasting dielectric constant yields a complete band gap when the refractive index contrast is sufficiently large and the radius of the spheres is chosen appropriately.
The band structure of the lattice of air spheres is shown in Fig. 2.3. A full gap is found between the second and third band with a gap-midgap ratio of 0.29 when the radius of the spheres is chosen to be $0.325a$ where a is the lattice constant. With this choice, 81% of the volume of the photonic crystal consists of air and the spheres of the structure are overlapping.
Experimentally, the first complete band gap was found in a different configuration in which a dielectric medium is drilled along three of the axes of the diamond lattice as illustrated in Fig. 2.4. This structure has been termed Yablonovite after its discoverer E. Yablonovitch. The band structure of Yablonovite is depicted in Fig. 2.5. When the radius of the holes is chosen to be $0.234a$ (a lattice constant), the crystal has a band gap between the second and third band with a gap-midgap ratio of 0.19.

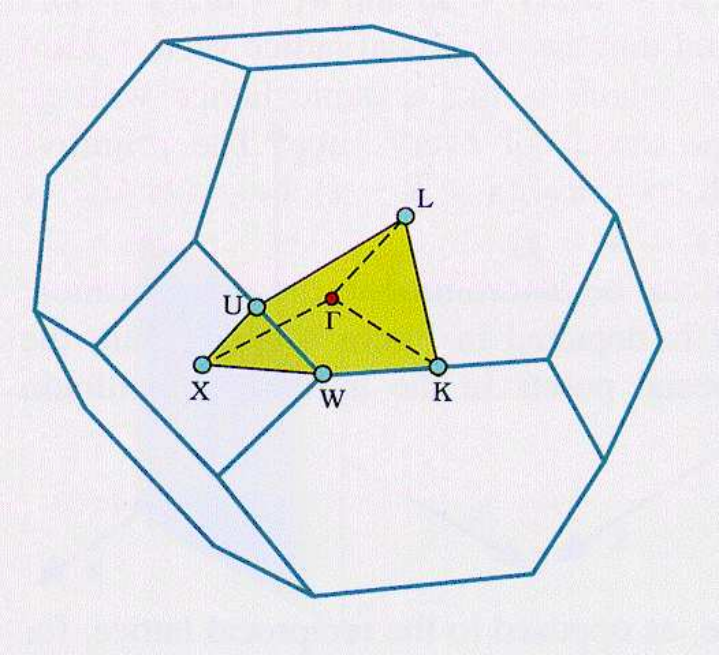

Figure 2.1: The Brillouin zone for a fcc crystal. The irreducible part of the Brillouin zone is colored [22]

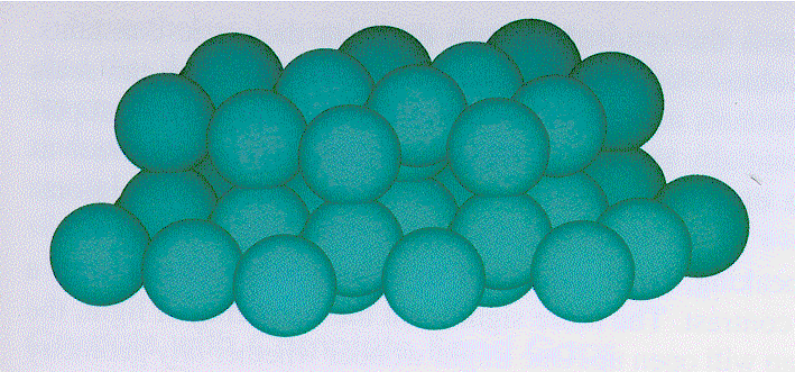

Figure 2.2: Arrangement of dielectric spheres providing a photonic band gap [22].

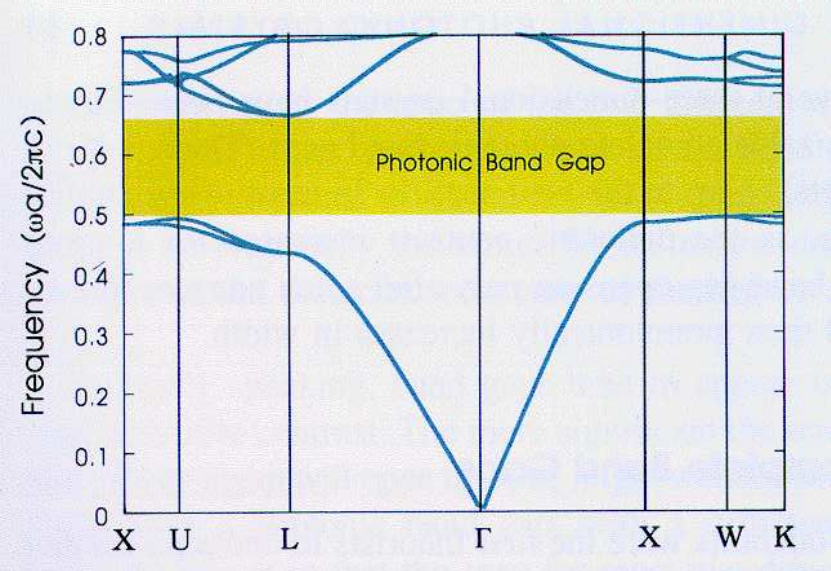

Figure 2.3: The band structure of the arrangement of air spheres. A full band gap exists between 2. and 3. band with a gap-midgap ratio of 0.29 [22]

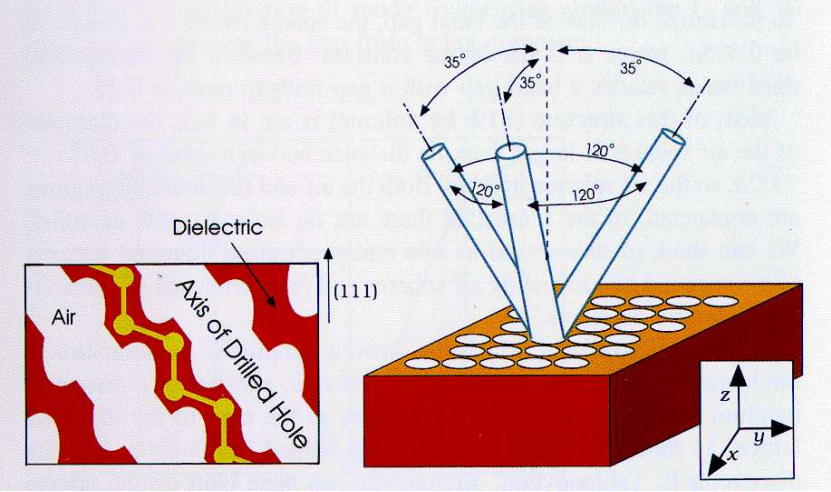

Figure 2.4: The construction of Yablonovite [22]

In Eq. (2.18) we found that the energy functional is minimized when the displacement field is localized in regions of high dielectric constant. The bands above and below the gap can thus be characterized by where their field pattern is located. In fact, the energy of the modes corresponding to the bands just below a gap, is located in regions of high dielectric constant. The energy of the modes just above a gap is correspondingly localized in the regions of low dielectric constant. Since regions of low dielectric constant typically are air regions, these bands are known as *air bands*. The bands just below the gap are correspondingly referred to as *dielectric bands*.
Although the characterization of a photonic crystal evades simple analytical approaches, a rule of thumb is that different regions of the photonic crystal containing the same material should be connected. This rule of thumb can be understood by recalling the vectorial nature of the electromagnetic field: In Eq. (2.18) it was shown that the field energy is minimized if the field pattern is localized in regions of high dielectric constant. If different regions of high dielectric constant are not connected, then field lines corresponding to a mode in the dielectric band have to penetrate air regions in the photonic crystal in order for the field lines to remain continuous. This leads to a higher energy of the mode thus preventing a band gap from opening. A connected crystal on the other hand allows the field lines of low-energy modes to connect neighboring regions of high dielectric constant through narrow "veins" of dielectric material without penetrating air regions of low dielectric constant.

2.4 Construction

The construction of a photonic crystal with a complete photonic band gap at optical wavelengths is an involved process since the periodic structure of the crystal has to be at approximately the same length scale as the wavelength of the light that should experience a band gap. As methods of creating a photonic crystal it has often been suggested to use "subtractive methods" in the sense that starting from a dielectric block, material is gradually removed in order to eventually obtain the desired crystal structure. Following this idea, photonic crystals have been fabricated in the microwave regime by manually drilling the large number of holes necessary to produce a photonic crystal. Since, however, the size of the holes reflects the wavelength of the radiation for which we want a band gap, it is evident that the method of drilling holes becomes inapplicable for near-optical wavelengths. Instead ion etching has been proposed and in some cases applied as a means of creating a photonic crystal since holes with a diameter of optical light can be created in a controlled fashion using this technique. The drawback of this method is, however, that the holes may not be too deep since in that case irregularities may occur in the etching process. Another disadvantage of the subtractive methods is that defects essential for different applications can only be precisely implemented in layers a few unit cells from the surface of the crystal.
A different approach to creating photonic crystals for short wavelength radia-

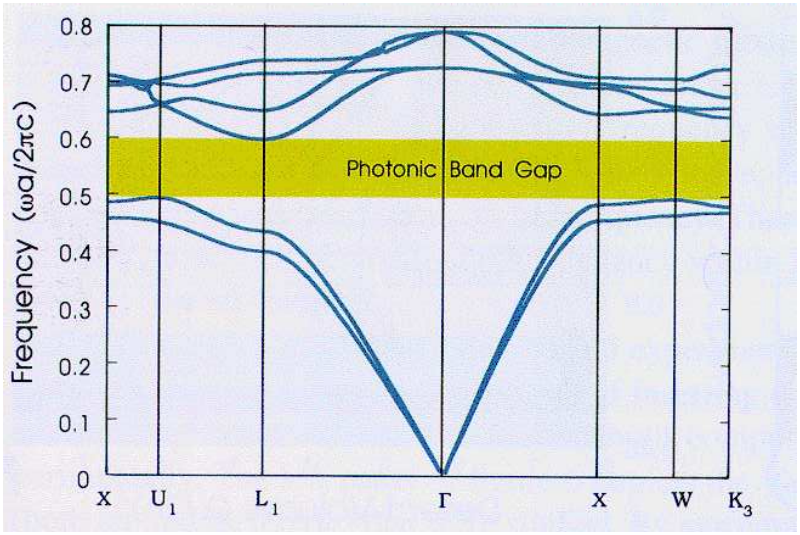

Figure 2.5: The band structure of Yablonovite. A full gap exists between 2. and 3 band with a gap-midgap ratio of 0.19 when the holes are $0.234a$ [22]

tion has been invoked by Stuke and collaborators. In a recent paper [23], they reported the construction of a photonic crystal by means of laser-induced chemical vapor deposition (LCVD) from the gas phase. In this approach [24], two weak orthogonal laser beams are overlapped in a reaction chamber containing trimethylamine alane [TMAA, $AlH_3N(CH_3)_3$] and a fair amount of oxygene. At the intersection point of the two lasers, the energy absorbed in the gas is sufficient to cause deposition directly from the gas phase whereas each of the two laser beams alone are sufficiently weak to cause negligible deposition. Moving the intersection point of the two lasers along the desired trajectory at a speed comparable to the deposition rate of aluminium $(\approx 60\mu m/s)$, complicated structures can be built directly in free space.
Since the crystal is built by deposition, it is straightforward to incorporate defects serving as waveguides or localized cavity modes in the periodic structure.
An example of a photonic crystal created by LCVD is shown in Fig. 2.6. The periodic structure consists of 15 rows of perpendicularly arranged aluminium oxide rods 40μm in diameter, with a 133μm periodicity and rod lengths of 3000μm. This structure was shown to possess a transmission minimum for radiation with a wavelength of 75μm as shown in Fig. 2.7. Since the crystal consists of only a few layers, no gap was found but the transmission was observed to drop as the number of layers in the crystal increased as we would expect. As a demonstration of the flexibility of their technique, Stuke and collaborators have constructed other structures exhibiting band gaps [24].

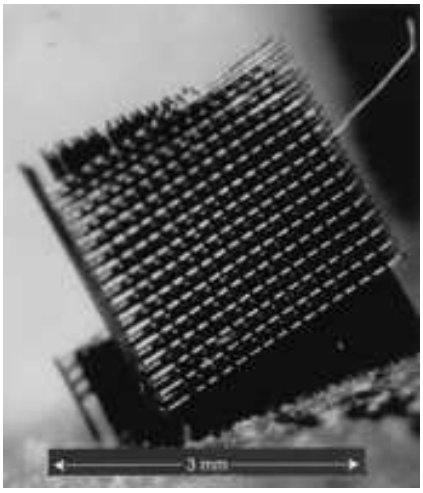

Figure 2.6: A photonic crystal created by LCVD [25].

2.5 Applications

The most characteristic feature of photonic crystals is their ability to strongly modify the propagational properties the electromagnetic field at certain frequencies due to their perfect periodicity and for this reason, they have been the subject of intense interest in recent years.
Different applications of photonic crystals rely, however, on breaking this perfect periodicity by introducing various defects in the crystal and we shall now discuss some of these possible applications.
In the microwave regime, superconducting cavities with very high Q-value have been constructed allowing the implementation of a whole range of experiments probing the interaction of light and matter like for instance the demonstration of Rabi-oscillations of an atom with a near-resonant cavity mode and the construction of the one- and two-photon micromasers [26, 27, 28]. For shorter wavelengths, however, the metallic mirrors become lossy thus preventing the construction of a high Q cavity in the optical domain. If the attempts to construct a photonic crystal in the optical domain succeed, the introduction of a proper point defect in the bulk of such a crystal would yield a localized mode or cavity with a very high Q-value. A point defect is introduced by removing or adding material at a site in the bulk of the crystal. The frequency and geometry of the localized mode can be tuned by varying the amount of material added or removed as shown in Fig. 2.8.
In Fig. 2.9, the localized field existing around a defect is plotted. The localized field has the form of a torus. The magnetic field lines flow around the inside of the torus while the displacement field circulates around the magnetic field on

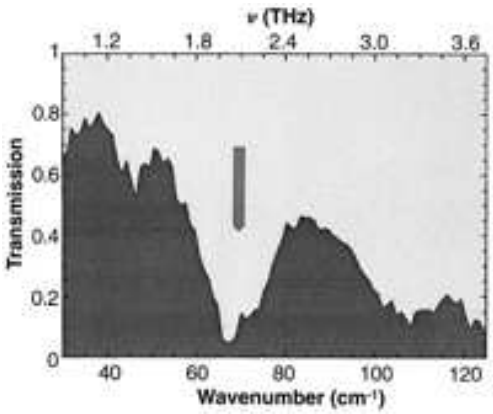

Figure 2.7: Transmission as a function of frequency [25].

the surface of the torus.
A linear instead of a point defect provides a waveguide which allows a strong control of the propagational properties of light. The optical fiber which is the conventional waveguide relies on total internal reflection as the mechanism to trap the light propagating in the fiber. Bending a fiber changes the internal reflection angle and thus leads to light leaking out of the side of the fiber. The trapping mechanism in a photonic crystal is different so what happens to a pulse propagating in a waveguide with sharp bends? This question was addressed by Joannopoulos and coworkers recently [22, 29, 30]. The setup they considered is depicted in Fig. 2.10 and consists of a photonic crystal which is formed by a regular grid of dielectric rods. The resulting crystal has a band gap for light propagating in the plane perpendicular to the rods and thus possesses a 2D band gap. Removing from this grid a row of rods forms a waveguide as shown in Fig. 2.10 and the corresponding band structure for this setup is shown in Fig. 2.11. The dark regions denote freely propagating modes and the light region the band gap. The existence of the path in the crystal introduces a guided mode with frequency in the band gap. Resonant light introduced in the waveguide therefore has to propagate along the waveguide. The path depicted in Fig. 2.10 has a 90° bend which for an optical fiber would yield a power transmission for a dielectric waveguide of around 30%. For the photonic crystal, 98% of the power of the light that goes in in one end comes out the other end even though the radius of curvature of the bend is less than the wavelength of the light.

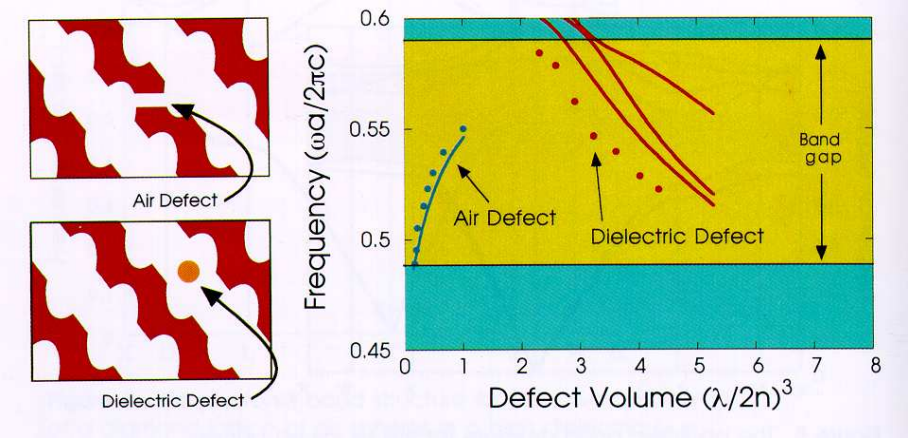

Figure 2.8: A defect is introduced in the bulk of the crystal by removing or adding dielectric material. The right-hand graph shows the frequency of the defect as a function of defect volume [22].

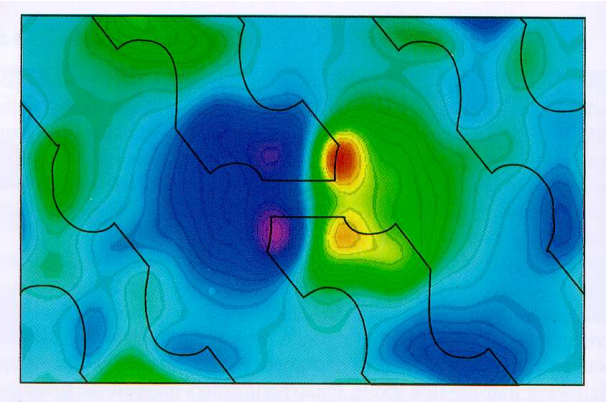

Figure 2.9: View of the localized magnetic field near an air defect in Yablonovite [22].

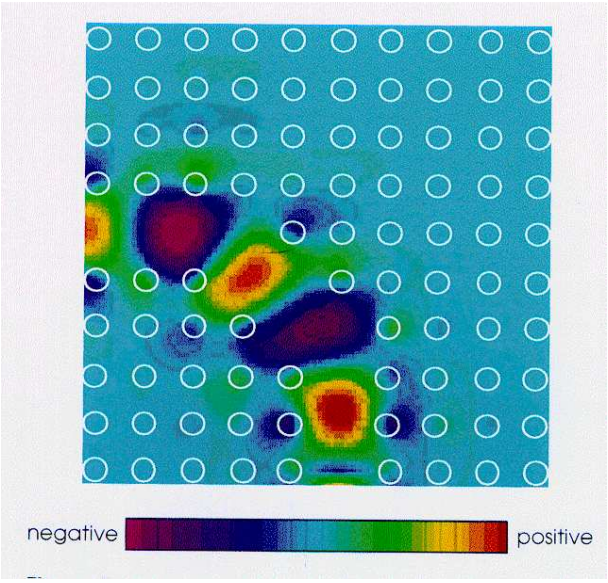

Figure 2.10: The displacement field of a TM mode propagating along a path carved in a square lattice of dielectric rods. Light is propagating from the bottom [22].

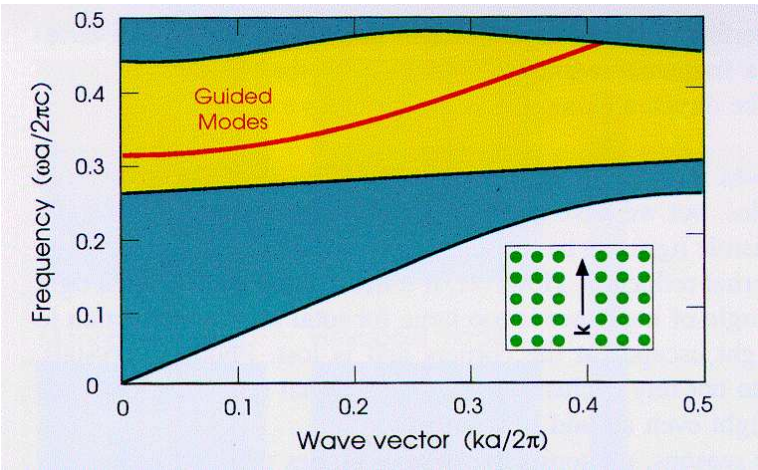

Figure 2.11: The projected band structure of TM modes for the waveguide. The dark regions contain the continuum of extended crystal states. The light colored region is the band gap and the line is the band of guided modes that propagate along the waveguide [22] .

Chapter III

Atom-Atom interaction at the edge of a photonic band gap

The interaction of two closely spaced atoms through the narrow band of strongly coupled modes at the edge of a photonic band gap is investigated. The resonant dipole-dipole interaction (RDDI) is strongly modified for atomic transition frequencies in the vicinity of the band gap edge, but we show that an analytical approximation to the RDDI agrees very well with the exact RDDI obtained by numerical integration using the exact dispersion relation. Having established the value of the RDDI, we can derive the amplitudes for the two atoms without resorting to the pole-approximation which is necessary due to the strongly modified mode structure in the dielectric host. For a wide range of parameters we find beating and population trapping in the long time limit. The distribution of population in the photonic continuum is investigated in the long time limit in the case of one and two atoms. It is found to be strongly asymmetric and to exhibit a strong signature of the unusual mode structure in the material at the band gap edge.

3.1 Introduction

The behavior of a two-level atom in a modified radiation reservoir, such as a high quality cavity, has become the standard testing ground for novel effects of quantum electrodynamics (QED) and has revealed a number of striking features. For instance, the spontaneous exponential decay of an excited atomic state in free space, traditionally thought of as an inherent property of the atom, can be enhanced or suppressed by enclosing the atom in a near-resonant cavity, depending on the magnitude of the atomic lifetime in vacuum relative to the lifetime of the photons in the cavity mode.
The recent emergence of materials with photonic band gaps has given rise to a new direction of inquiry; namely the behaviour of atomic decay inside such materials. By conception and construction, the periodic modulation of the dielectric constant in these materials leads to a strongly modified mode structure

such that photonic modes do not exist for a continuous range of frequencies that can be much larger than a typical atomic linewidth.
For an atom with transition frequency in the band gap and located inside the dielectric host, this may lead to a total inhibition of spontaneous decay [10], which in turn yields a so-called photon-atom bound state [31, 32] in which the radiation remains localized at the atom. For atomic transition frequencies closer to the band gap edge, the rapidly varying density of modes leads to a splitting of the atomic level, which in the time domain yields the rather unusual phenomenon of an oscillatory spontaneous decay [32, 33, 34, 35].
In parallel and independent developments, the issue of the modification of atomic radiative behaviour under atom-atom resonant dipole-dipole interaction has been receiving renewed attention. Beginning with the pioneering Dicke paper on superradiance [36, 37], the interaction of two closely spaced atoms sharing a photon in open space has been addressed in numerous studies, with the prediction of interesting effects such as atomic level shifts due to RDDI, oscillatory photon exchange and squeezing of two-atom resonance fluorescence. And rather recently a natural generalization of these phenomena has been addressed; namely the study of the RDDI of closely spaced atoms inside a near resonant perfect cavity [38]. The results predict a rather strong competition between RDDI and the atom-cavity coupling in the limit of small interatomic separations such that these two couplings become comparable in magnitude.
These developments point to two further levels of generalization. First, the interplay between RDDI and atom-cavity coupling in an open (lossy) cavity and second the same interplay with the cavity replaced by a photonic band gap environment. It is precisely these generalizations that we have undertaken in this chapter thus extending recent work [1]. We have thus addressed the problem of two identical two-level atoms with a transition frequency in the vicinity of the band gap edge and interacting through the narrow band of strongly coupled modes. This gives rise to many new effects and since it is important to distinguish the effects stemming from the modified mode-structure from those coming from the interatomic interaction, we have contrasted the results with known results for atoms in free space as well as two atoms coupled to a lossy cavity which we have obtained here.
The dynamics of a collection of two-level atoms with transition frequencies far inside the gap has been investigated by S. John and T. Quang [39]. In that case, the spontaneous decay is strongly suppressed but the RDDI between the atoms remains strong.
In addition to the theoretical interest in these questions, technological developments are making them accessible to experiment. Although the appropriate photonic band gap materials are not yet available in the optical regime, effects stemming from atom-atom coupling in an open cavity have already been observed [40].

This chapter is organized as follows: In the next section we present the model. In section 3.3, we calculate the couplings entering the equations of motion,

which allows us to solve these equations in section 3.4. The inversion is performed in section 3.5 and the dynamics is investigated in time-domain in section 3.6. In section 3.7, we calculate the distribution of population in the photonic continuum in the long time limit.

3.2 The Model

We consider two two-level atoms situated at different locations $\mathbf{R}_A, \mathbf{R}_B$ in the vacuum part of the crystal. Taking $\hbar = 1$, the Hamiltonian for the problem under consideration reads

$$H = H_0 + V \tag{3.1}$$

with

$$H_0 = \omega_A \sigma_A^z + \omega_B \sigma_B^z + \sum_{\mathbf{k}} \omega_{\mathbf{k}} a_{\mathbf{k}}^\dagger a_{\mathbf{k}} \tag{3.2}$$

neglecting the zero-point energy of the field modes, and

$$\begin{aligned} V = & i \sum_{\mathbf{k}} g_{\mathbf{k}} \left[a_{\mathbf{k}} e^{i\mathbf{k}\cdot\mathbf{R}_A} \sigma_A^+ - a_{\mathbf{k}}^\dagger e^{-i\mathbf{k}\cdot\mathbf{R}_A} \sigma_A^- \right] \\ & + i \sum_{\mathbf{k}} g_{\mathbf{k}} \left[a_{\mathbf{k}} e^{i\mathbf{k}\cdot\mathbf{R}_B} \sigma_B^+ - a_{\mathbf{k}}^\dagger e^{-i\mathbf{k}\cdot\mathbf{R}_B} \sigma_B^- \right] \end{aligned} \tag{3.3}$$

which is the ordinary interaction Hamiltonian in the rotating wave approximation where $\sigma^+, \sigma^-, \sigma^z$ are the atomic operators and $a_{\mathbf{k}}^\dagger, a_{\mathbf{k}}$ are the creation and annihilation operators of the vacuum modes, respectively, and the dependence on the atomic positions $\mathbf{R}_A, \mathbf{R}_B$ is shown explicitly.
The interaction term Eq. (3.3) should be expanded in terms of the modefunctions for the crystal. The expansion in terms of plane waves basically neglects the local structure of the crystal. However, the overall effect of the crystal structure on the vacuum field is taken into account through a modified dispersion relation for the electromagnetic field.
The coupling constant in Eq. 3.3) is given by

$$g_{\mathbf{k}} = \sqrt{\frac{\omega_{\mathbf{k}}}{2\varepsilon_0 V}} \mathbf{e}_{\mathbf{k}} \cdot \mathbf{d}_{ij} \tag{3.4}$$

Here $\mathbf{d}_{ij}$ is the atomic dipole moment, V the quantization volume, $\mathbf{e}_{\mathbf{k}}$ the polarization vector and $\omega_{\mathbf{k}}$ the photon energy.
The relevant states of the problem are

$$\begin{aligned} a &= |e_A, g_B, 0\rangle \\ b &= |g_A, e_B, 0\rangle \\ c &= |g_A, g_B, 1_{\mathbf{k}\mathbf{e}_l}\rangle \end{aligned} \tag{3.5}$$

where $g_{A(B)}, e_{A(B)}$ denote lower and upper states of the atoms $A(B)$, respectively, and the states c represent the photonic continuum.
As a means of deriving the appropriate equations for the atom-field dynamics non-perturbatively, we employ the resolvent operator[41],

$$G(z) = \frac{1}{z - H} \tag{3.6}$$

which is the Laplace-transform of the time-evolution operator, with z being the complex transform variable and H the full Hamiltonian of the system. This formalism, in terms of the wave functions instead of the density operator, is applicable here since we have no incoherent pumping of the system under consideration and we do not perform a trace over the vacuum field modes.

With the system initially in state a, the matrix elements of the resolvent operator read

$$\begin{aligned}
(z - \omega_a)G_{aa} &= 1 + \sum_c V_{ac}G_{ca} \\
(z - \omega_b)G_{ba} &= \sum_c V_{bc}G_{ca} \\
(z - \omega_c)G_{ca} &= V_{cb}G_{ba} + V_{ca}G_{aa}
\end{aligned}$$

Eliminating the continuum amplitude G_{ca}, we find the two coupled algebraic equations

$$(z - \omega_a)G_{aa} = 1 + \sum_c \frac{|V_{ac}|^2}{z - \omega_c}G_{aa} + \sum_c \frac{V_{ac}V_{cb}}{z - \omega_c}G_{ba} \tag{3.7}$$

$$(z - \omega_b)G_{ba} = \sum_c \frac{|V_{bc}|^2}{z - \omega_c}G_{ba} + \sum_c \frac{V_{bc}V_{ca}}{z - \omega_c}G_{aa} \tag{3.8}$$

containing several couplings, one of which is

$$\sum_c \frac{|V_{ac}|^2}{z - \omega_c} \tag{3.9}$$

describing the emission of a photon by atom A followed by a propagation of all the modes, before the photon is eventually reabsorbed by atom A.
Up to this point we have made no approximations specific to a band gap material and the two equations above could therefore as well describe two atoms in the vacuum of free space. The propagation of photons in a band gap material is strongly modified and it is therefore natural to expect a modification of the couplings, which will indeed be the case, as we show in the next section. But before proceeding to this issue, let us for instructive purposes investigate the cases of two atoms first in vacuum and second in an open cavity.

3.2.1 Atom-Atom interaction in free space vacuum

In this case we can perform the usual pole-approximation in the couplings which consists in replacing the Laplace variable z by the atomic transition frequency ω_A. The justification for performing this approximation is that the free space continuum(vacuum) is flat and changing the Laplace variable z around ω_A does not change the value of the coupling significantly. In the pole-approximation the couplings yield

$$\sum_c \frac{|V_{ac}|^2}{z-\omega_c} \simeq \Delta - i\Gamma \tag{3.10}$$

$$\sum_c \frac{|V_{bc}|^2}{z-\omega_c} \simeq \Delta - i\Gamma \tag{3.11}$$

$$\sum_c \frac{V_{ac}V_{cb}}{z-\omega_c} \simeq M_{ab} \tag{3.12}$$

assuming identical atoms and thus identical shifts and widths. The dipole-dipole matrix element M_{ab} is in general complex and diverges when the interatomic distance R goes to zero. This formal divergence stems from the fact that our model does not allow for molecule formation as the atoms approach each other and for our purposes, we do not need to allow for that case.
Inserting these quantities in the equations for the resolvent operator and writing these in matrix form, we find

$$\begin{bmatrix} z-\tilde{\omega}+i\Gamma & -M_{ab} \\ -M_{ba} & z-\tilde{\omega}+i\Gamma \end{bmatrix} \begin{bmatrix} G_{aa} \\ G_{ba} \end{bmatrix} = \begin{bmatrix} 1 \\ 0 \end{bmatrix} \tag{3.13}$$

where the shift has been absorbed in $\tilde{\omega}$.
The eigenvalues which are easily found as

$$z_\pm = \tilde{\omega} - i\Gamma \pm M_{ab} \tag{3.14}$$

lead to a damped sinusoidal dynamics in the time-domain. Whether the damping or the sinusoidal behaviour is dominant depends on the strength of M_{ab}, which in turn is determined by the atomic configuration and separation. In the long time limit and for finite separations there is no population trapping.

3.2.2 Atom-Atom interaction in a cavity

The equations (3.7) and (3.8) are easily extended to accomodate the presence of an open cavity

$$\begin{aligned}(z-\omega_a)G_{aa} &= 1+\sum_c \frac{|V_{ac}|^2}{z-\omega_c}G_{aa} + \sum_c \frac{V_{ac}V_{cb}}{z-\omega_c}G_{ba} \\ &\quad + \frac{|V_{ad}|^2}{z-\tilde{\omega}_d+i\kappa}G_{aa} + \frac{V_{ad}V_{db}}{z-\tilde{\omega}_d+i\kappa}G_{ba}\end{aligned} \tag{3.15}$$

$$(z-\omega_b)G_{ba} = \sum_c \frac{|V_{bc}|^2}{z-\omega_c}G_{ba} + \sum_c \frac{V_{bc}V_{ca}}{z-\omega_c}G_{aa} + \frac{|V_{bd}|^2}{z-\tilde{\omega}_d+i\kappa}G_{ba} + \frac{V_{bd}V_{da}}{z-\tilde{\omega}_d+i\kappa}G_{aa} \quad (3.16)$$

where V_{ad}, V_{bd} are the dipole-mode couplings of atom $A(B)$ respectively, $\tilde{\omega}_d$ is the resonance frequency of the cavity shifted due to the coupling to a reservoir, and κ the cavity decay width. These equations show that the presence of the cavity can be thought of as a Lorentzian superimposed on the flat background of vacuum modes.
Since the summations in the couplings are over the flat continuum (vacuum), we perform the pole-approximation as in Eqs. (3.10-3.12) and bring the equations to the matrix form

$$\begin{bmatrix} z-\tilde{\omega}+i\Gamma-\frac{|V_{ad}|^2}{z-\tilde{\omega}_d+i\kappa} & -M_{ab}-\frac{V_{ad}V_{db}}{z-\tilde{\omega}_d+i\kappa} \\ -M_{ba}-\frac{V_{bd}V_{da}}{z-\tilde{\omega}_d+i\kappa} & z-\tilde{\omega}+i\Gamma-\frac{|V_{bd}|^2}{z-\tilde{\omega}_d+i\kappa} \end{bmatrix} \begin{bmatrix} G_{aa} \\ G_{ba} \end{bmatrix} = \begin{bmatrix} 1 \\ 0 \end{bmatrix} \quad (3.17)$$

The motion of the coupled system is determined by the poles of the resolvent operator which are the roots of the characteristic polynomial.
In general, all three roots are complex and thus contain dissipative terms. This means that in the long time limit $t \gg \Gamma^{-1}, \kappa^{-1}$, there will be no population trapping as opposed to two atoms located in a photonic band gap material which is the case we treat in the rest of this chapter.

3.3 Calculation of the couplings

As a model for the photonic band gap material, we consider the isotropic crystal introduced by John [42], for which the dispersion relation is given by Eq. (2.27). In the following we choose the refractive index $n = 1.082$, which yields a gap center frequency $\omega_0 = \frac{\pi c}{L}\frac{1+n}{2n}$ and a relative gap width $\Delta\omega/\omega_0 = 0.05$. At (near-)optical frequencies, this gap is much larger than any typical atomic coupling and the influence of the lower band gap edge on the atomic dynamics can therefore be neglected for atomic transition frequencies in the vicinity of the upper band edge. For photonic frequencies close to the band edge, the dispersion relation Eq. (2.27) can be approximated by the effective mass dispersion relation Eq. (2.29)[42] which we shall use in the following.
In this section we address the calculation of the couplings

$$\sum_c \frac{V_{mc}V_{cn}}{z-\omega_c} \quad (3.18)$$

with $m, n \in \{a, b\}$ which when using the interaction Hamiltonian Eq. (3.3) can be written more explicitly as

$$\sum_c \frac{V_{mc}V_{cn}}{z-\omega_c} = \sum_{\mathbf{k},i,j,l} \frac{\omega_{\mathbf{k}}}{2\varepsilon_0 V} \frac{(e^{(l)}_{\mathbf{k}i} d^m_{egi}) e^{(l)}_{\mathbf{k}j} d^n_{gej}}{z-\omega_c} e^{i\mathbf{k}\cdot\mathbf{R}} \quad (3.19)$$

with $\mathbf{R} = \mathbf{R}_m - \mathbf{R}_n$ the relative distance between the two atoms if $m \neq n$, $i, j \in \{x, y, z\}$ and we have introduced a summation over polarization (index l) in the first equation. It is easily shown that the summation over polarization vectors yields

$$\sum_{l=1,2} e^{(l)}_{\mathbf{k}i} e^{(l)}_{\mathbf{k}j} = \delta_{ij} - \hat{k}_i \hat{k}_j \tag{3.20}$$

where $\hat{k} = (\sin\theta\cos\phi, \sin\theta\sin\phi, \cos\theta)$. Inserting this relation in the expression above and turning the summation over $\mathbf{k}$ into an integral, the relation reads

$$\sum_c \frac{V_{mc}V_{cn}}{z - \omega_c} = \frac{1}{(2\pi)^3} \sum_{ij} \int d^3k (\delta_{ij} - \hat{k}_i\hat{k}_j) \frac{\omega_{\mathbf{k}}}{2\varepsilon_0} \frac{d^m_{egi} d^n_{gej}}{z - \omega_{\mathbf{k}}} e^{i\mathbf{k}\cdot\mathbf{R}} \tag{3.21}$$

Since we have assumed an isotropic dispersion relation which contains no angular dependence, the angular integral can thus be performed.
The general result reads

$$\sum_c \frac{V_{mc}V_{cn}}{z - \omega_c} = \frac{1}{2\pi^2} \frac{1}{2\varepsilon_0} \sum_i \int dk k^2 \omega_k \tau_{ii}(k, R) \frac{d^m_{egi} d^n_{gei}}{z - \omega_k} \tag{3.22}$$

with

$$\begin{aligned} \tau_{ii}(k, R) = &\left[\frac{\sin kR}{kR} + \frac{\cos kR}{(kR)^2} - \frac{\sin kR}{(kR)^3}\right] \delta_{ix} \\ &+ \left[\frac{\sin kR}{kR} + \frac{\cos kR}{(kR)^2} - \frac{\sin kR}{(kR)^3}\right] \delta_{iy} \\ &+ \left[-\frac{2\cos kR}{(kR)^2} + \frac{2\sin kR}{(kR)^3}\right] \delta_{iz} \end{aligned} \tag{3.23}$$

where we have taken the z-axis along the interatomic separation axis.
The steps leading to Eq. (3.22) are standard and well-known. For $m \neq n$, Eq. (3.22) yields the RDDI between two neighbouring atoms and for $m = n$ the effective coupling of an atom with the reservoir. In that case $R = 0$.
For two atoms in free space, the free space dispersion relation $\omega_k = ck$ applies and the integral Eq. (3.22) can be evaluated by contour methods yielding the matrix element M_{ab} of Eqs. (3.14) and (3.17). In the present context, the dispersion relation Eq. (2.27) is rather complicated and the integral Eq. (3.22) has to be performed numerically.
The question of major interest here is, whether we can replace the variable z by the atomic transition energy ω_A in Eq. (3.22). This requires that the integral as a function of z is slowly varying. Calculations by John [42] and Kweon[43] have shown that for atomic transition frequencies in the gap far from the edge, the value of the dipole-dipole matrix element approaches that of vacuum i.e. for two closely spaced atoms with transition frequencies in the gap, the virtual

photons exchanged are of such energy that the atoms do not experience the existence of the gap. It is, however, not evident whether this also holds for atomic transition frequencies at the edge of the gap. To explore the sensitivity of the value of the integral on z, we have performed a careful numerical investigation of the coupling Eq. (3.22) using the exact dispersion relation Eq. (2.27) for the crystal and have indeed found that the value Eq. (3.22) assumes in the vicinity of the band edge is sensitively dependent on z and as a result we cannot replace z by ω_A.
Before proceeding to the numerical results, we present an approximate analytical calculation of the coupling.

The complex Laplace variable z can in this context be written $z = x + i\eta$, where η is a small positive quantity. Using the identity

$$\frac{1}{x+i\eta} \stackrel{\eta\to 0}{=} \mathcal{P}\frac{1}{x} - i\pi\delta(x) \tag{3.24}$$

where $\mathcal{P}$ denotes principal value part, in the integral Eq. (3.22) and leaving out for the moment the multiplicative coefficients yields

$$\begin{aligned}&\int dk k^2 \omega_k \tau_{ii}(k,R)\frac{1}{z-\omega_k}\\ &= \mathcal{P}\int dk k^2 \omega_k \tau_{ii}(k,R)\frac{1}{x-\omega_k} - i\pi\int dk k^2 \omega_k \tau_{ii}(k,R)\delta(x-\omega_k)\end{aligned} \tag{3.25}$$

For $m \neq n$, we denote the first part of Eq. (3.25) by V_{mn} and this gives rise to the divergent part of the dipole-dipole interaction, diverging for small interatomic distances as $\frac{1}{R^3}$. By numerical integration of this quantity, we have established that it is to a very good approximation given by the real part of the RDDI obtained for two atoms in free space.
For $m = n$ the principal value part gives rise to the Lamb shift of the excited atomic states. We absorb this energy shift in the eigenenergies of the excited atomic states.
To evaluate the second integral of Eq. (3.25), we apply the effective mass approximation Eq. (2.29). Inserting this expression in the integral Eq. (3.25) yields

$$\int dk k^2 \omega_k \tau_{ii}(k,R)\delta(x-\omega_k) \simeq k_+^2 \omega_{k_+} \tau_{ii}(k_+,R)\frac{1}{2\sqrt{x-\omega_e}\sqrt{A}} \tag{3.26}$$

where $k_+ = k_0 + \sqrt{\frac{x-\omega_e}{A}}$.
For atomic transition frequencies at the edge of the gap $\omega_A \simeq \omega_e$, the contribution $\sqrt{\frac{x-\omega_e}{A}}$ will be negligible since the resolvent operator has a pole at $x \simeq \omega_A \simeq \omega_e$. Neglecting $\sqrt{\frac{x-\omega_e}{A}}$ compared to k_0, we thus find the simpler expression

$$\int dk k^2 \omega_k \tau_{ii}(k,R)\delta(x-\omega_k) \simeq k_0^2 \omega_e \tau_{ii}(k_0,R)\frac{1}{2\sqrt{x-\omega_e}\sqrt{A}} \tag{3.27}$$

which applies to the case of $m = n$ as well as $m \neq n$.
For notational convenience, we define

$$C_M = \sum_i \frac{1}{4\pi\epsilon_0} \frac{d^m_{egi} d^n_{gei}}{2\sqrt{A}} k_0^2 \omega_e \tau_{ii}(k_0, R) \tag{3.28}$$

for $m \neq n$ and

$$\begin{aligned} C_n &= \sum_i \frac{1}{4\pi\epsilon_0} \frac{|d^n_{egi}|^2}{2\sqrt{A}} k_0^2 \omega_e \tau_{ii}(k_0, R=0) \\ &= \sum_i \frac{1}{4\pi\epsilon_0} \frac{|d^n_{egi}|^2}{2\sqrt{A}} k_0^2 \omega_e \frac{2}{3} \end{aligned} \tag{3.29}$$

for $m = n$.
In the Σ configuration for instance, i.e. the atomic dipoles parallel and aligned perpendicular to the interatomic separation axis, C_M reads

$$C_M = \frac{\omega_e}{4\pi\epsilon_0} \frac{d^m_{eg} d^n_{ge}}{2\sqrt{A}} \left[\frac{k_0 \sin k_0 R}{R} + \frac{\cos k_0 R}{R^2} - \frac{\sin k_0 R}{k_0 R^3} \right] \tag{3.30}$$

Collecting the terms, we find

$$\sum_c \frac{|V_{ac}|^2}{z - \omega_c} = \frac{-iC_a}{\sqrt{z - \omega_e}} \tag{3.31}$$

where the Lamb shift part of the coupling has been absorbed in the atomic eigenenergies and

$$\sum_c \frac{V_{ac} V_{cb}}{z - \omega_c} = V_{ab} + \frac{-iC_M}{\sqrt{z - \omega_e}} \tag{3.32}$$

where V_{ab} is the principal value part of the RDDI-integral in Eq. (3.25). We note that the RDDI Eq. (3.32) has a term diverging as $z \to \omega_e$. For atomic transition frequencies outside the gap i.e. $z > \omega_e$, this yields an imaginary contribution to the interatomic coupling. For atomic transition frequencies in the gap i.e. $z < \omega_e$, the argument of the square root changes sign and the square root term and thus the whole interatomic coupling becomes purely real.
As has been noted in the literature [42], the occurence of the square root terms in Eqs. (3.32) and (3.31) corresponds to a density of states given by

$$\rho(\omega) = \frac{V}{(2\pi)^3} \frac{k_0^2}{2\sqrt{A}} \frac{1}{\sqrt{\omega - \omega_e}} \Theta(\omega - \omega_e) \tag{3.33}$$

where $\Theta(\omega - \omega_e)$ is the Heaviside step-function.
In the following, we assume V_{ab} and C_M to be real quantities which is not a restriction, since this can be achieved by a proper phase-transformation of the

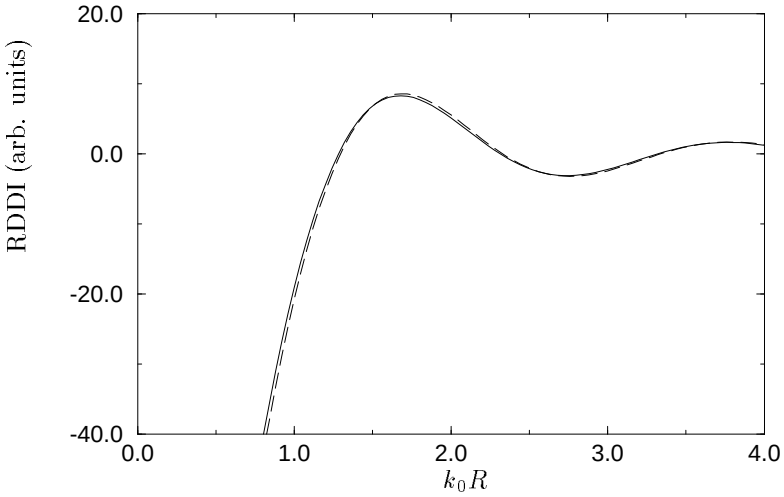

Figure 3.1: RDDI as a function of the interatomic distance R for atoms in the Σ configuration with $z = 0.998\omega_e$. The solid line is the numerical solution of (3.22) and the dotted curve Eq. (3.32).

interaction Hamiltonian turning the dipole-moments into real quantities.
To check the validity of the effective mass approximation in calculating the RDDI, we present the results obtained from Eq. (3.32) and by numerical integration of Eq. (3.22).

In Fig. 3.1, we compare the results obtained by numerical integration of the exact expression for the coupling Eq. (3.22) with the approximate analytical result Eq. (3.32) obtained in the effective mass approximation as a function of the interatomic separation with $z = 0.998\omega_e$. As the real part of the RDDI of Eq. (3.32) we have used the coupling obtained for two atoms in vacuum.
There is indeed a very good agreement. For this choice of parameters, $z < \omega_e$ which yields a negative argument in the square root part of Eq. (3.32) and the coupling is thus purely real.

In Fig. 3.2, we plot the coupling with $z = 1.002\omega_e$. Again we find a very good agreement between the exact expression Eq. (3.22) and the approximate expression Eq. (3.32).
We have tested the sensitivity of Eq. (3.22) on z by calculating the coupling for various values of z in the vicinity of ω_e and the dependence on z as given by the approximate expression in Eq. (3.32) has been confirmed. We have thus shown that the RDDI given by Eq. (3.22) can be replaced by the more explicit expression Eq. (3.32), where V_{ab} is the real part of the dipole-dipole coupling for two atoms in the vacuum of free space.

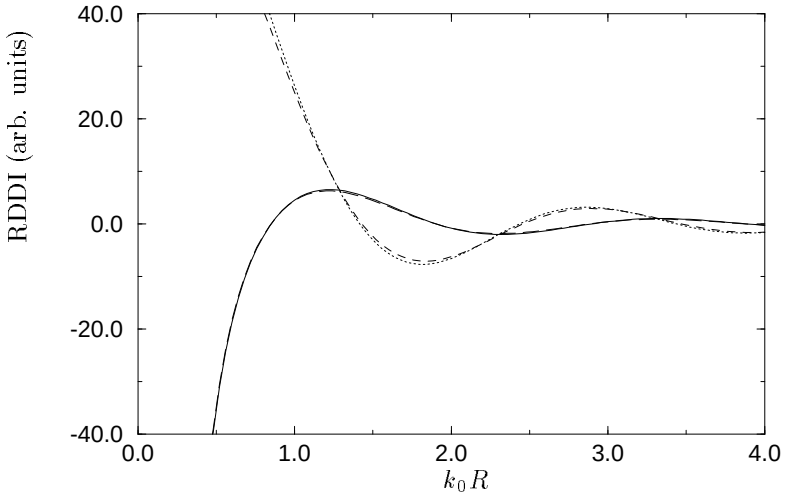

Figure 3.2: RDDI as a function of the interatomic distance R for atoms in the Σ configuration with $z = 1.002\omega_e$. The solid and long-dashed lines are the numerical computations of (3.22) and (3.32) respectively. The dotted and dashed lines are the imaginary parts of (3.22) and (3.32) respectively.

3.4 Revisiting the resolvent operator equations

Using Eqs. (3.31) and (3.32) in the equation for the resolvent matrix elements, we find

$$\begin{aligned}(z-\omega_a)G_{aa} &= 1 + V_{ab}G_{ba} + \frac{-iC_a}{\sqrt{z-\omega_e}}G_{aa} + \frac{-iC_M}{\sqrt{z-\omega_e}}G_{ba} \\ (z-\omega_b)G_{ba} &= V_{ba}G_{aa} + \frac{-iC_b}{\sqrt{z-\omega_e}}G_{ba} + \frac{-iC_M}{\sqrt{z-\omega_e}}G_{aa}\end{aligned}$$

assuming as before that the matrix element C_M is real. The equations can be slightly simplified by multiplying both sides of the equations with $\sqrt{z-\omega_e}$ and transforming the Laplace variable z by $z - \omega_a \to z$ which corresponds to transforming to an interaction picture rotating at ω_a. We further assume $\omega_a = \omega_b$ and $C_a = C_b \equiv C$ i.e. the atoms are identical and define $\delta = \omega_a - \omega_e$. Writing the equations in matrix form finally yields

$$\begin{bmatrix} z\sqrt{z+\delta} + iC & -\sqrt{z+\delta}V_{ab} + iC_M \\ -V_{ba}\sqrt{z+\delta} + iC_M & z\sqrt{z+\delta} + iC \end{bmatrix} \begin{bmatrix} G_{aa} \\ G_{ba} \end{bmatrix} = \begin{bmatrix} \sqrt{z+\delta} \\ 0 \end{bmatrix} \quad (3.34)$$

Eliminating the continuum amplitude, we have obtained two coupled algebraic equations for two two-level atoms interacting through RDDI and through a

narrow band of strongly coupled modes. As opposed to standard treatments dealing with system-reservoir interactions, we have at no point performed a pole-approximation simply because the reservoir in our case is very far from being "flat". The peculiar features of the continuum are reflected by the square root terms appearing in the resolvent operator equations.
We can immediately identify the eigenstates of the matrix in Eq. (3.34) as the symmetric and antisymmetric product states defined by

$$\psi_{s(a)} = \frac{1}{\sqrt{2}} \left[|e_A g_B\rangle \pm |g_A e_B\rangle \right] \tag{3.35}$$

The symmetric product state ψ_s is a Dicke state and would for atoms in free space correspond to a super-radiant state. We shall, however, see that in a photonic band gap material we can actually have population trapping in this symmetric state.
In the study of the interactions of atoms with cavity modes, the dynamics of the systems under consideration is exclusively determined by the location of the poles of the resolvent operator in the complex plane. This is, however, not the full truth in this problem; On performing the inversion integral to obtain the time dependent amplitudes, there is a contribution coming from the cut in the complex plane (arising from the photonic continuum) which yields a non-negligible contribution to the dynamics of the system. But for the moment, we proceed as usual by finding the roots of the characteristic polynomial of the above equations. It reads

$$0 \quad = \quad \left[z\sqrt{z+\delta} + iC \right]^2 - \left[\sqrt{z+\delta} V_{ab} - iC_M \right]^2 \tag{3.36}$$

assuming that V_{ab} is real. To obtain a polynomial in z, we multiply by the conjugate which yields the characteristic polynomial

$$\begin{aligned} h(z) = \left[z^2(z+\delta) - C^2 - V_{ab}^2(z+\delta) + C_M^2 \right]^2 \\ +4(z+\delta) \left[Cz + C_M V_{ab} \right]^2 \end{aligned} \tag{3.37}$$

By multiplying the characteristic equation with its conjugate, we have of course introduced extra roots and thereby extra poles. These extra poles, however, do not contribute when we perform the inversion integral.
In general, the roots of Eq. (3.37) are complicated expressions and they read

$$z_1 \quad = \quad \frac{-\delta - 2V_{ab}}{3} + \frac{2^{\frac{1}{3}}(\delta - V_{ab})^2}{3B_-} + \frac{B_-}{3 \cdot 2^{\frac{1}{3}}} \tag{3.38}$$

$$z_2 \quad = \quad \frac{-\delta - 2V_{ab}}{3} - e^{i\pi/3} \frac{2^{\frac{1}{3}}(\delta - V_{ab})^2}{3B_-} - e^{-i\pi/3} \frac{B_-}{3 \cdot 2^{\frac{1}{3}}} \tag{3.39}$$

$$z_3 \quad = \quad \frac{-\delta - 2V_{ab}}{3} - e^{-i\pi/3} \frac{2^{\frac{1}{3}}(\delta - V_{ab})^2}{3B_-} - e^{i\pi/3} \frac{B_-}{3 \cdot 2^{\frac{1}{3}}} \tag{3.40}$$

$$z_4 = \frac{-\delta + 2V_{ab}}{3} + \frac{2^{\frac{1}{3}}(\delta + V_{ab})^2}{3B_+} + \frac{B_+}{3 \cdot 2^{\frac{1}{3}}} \tag{3.41}$$

$$z_5 = \frac{-\delta + 2V_{ab}}{3} - e^{i\pi/3}\frac{2^{\frac{1}{3}}(\delta + V_{ab})^2}{3B_+} - e^{-i\pi/3}\frac{B_+}{3 \cdot 2^{\frac{1}{3}}} \tag{3.42}$$

$$z_6 = \frac{-\delta + 2V_{ab}}{3} - e^{-i\pi/3}\frac{2^{\frac{1}{3}}(\delta + V_{ab})^2}{3B_+} - e^{i\pi/3}\frac{B_+}{3 \cdot 2^{\frac{1}{3}}} \tag{3.43}$$

where the following abbreviations have been introduced

$$B_- = (A_- + \sqrt{A_-^2 - 4(\delta - V_{ab})^6})^{\frac{1}{3}} \tag{3.44}$$

$$B_+ = (A_+ + \sqrt{A_+^2 - 4(\delta + V_{ab})^6})^{\frac{1}{3}} \tag{3.45}$$

and

$$\begin{aligned} A_- &= 2(V_{ab} - \delta)^3 - 27(C - C_M)^2 \\ A_+ &= -2(V_{ab} + \delta)^3 - 27(C + C_M)^2 \end{aligned} \tag{3.46}$$

It is easily seen that the six roots can be viewed as being the roots of two different third order polynomials. One triplet of eigenvalues corresponds to the symmetric product state, and the other triplet to the anti-symmetric product state Eq. (3.35).

We found in Eq. (3.34) coupled algebraic equations governing the motion of the system. Eliminating the amplitude G_{ba} we find for G_{aa}

$$\begin{aligned} G_{aa} = \frac{z(z+\delta) + iC\sqrt{z+\delta}}{h(z)} \big[&(z^2 - V_{ba}^2)(z+\delta) + C_M^2 \\ &-C^2 - 2i\sqrt{z+\delta}(Cz + C_M V_{ab})\big] \end{aligned} \tag{3.47}$$

and for G_{ba}

$$\begin{aligned} G_{ba} = \frac{V_{ba}(z+\delta) - iC_M\sqrt{z+\delta}}{h(z)} \big[&(z^2 - V_{ba}^2)(z+\delta) + C_M^2 \\ &-C^2 - 2i\sqrt{z+\delta}(Cz + C_M V_{ab})\big] \end{aligned} \tag{3.48}$$

where $h(z)$ is the characteristic polynomial of Eq. (3.37). As is evident from Eqs. (3.47) and (3.48), the expressions for the amplitudes contain square root terms. This means that the amplitudes have a branch cut in the complex plane and we must therefore be very careful when performing the inversion. We take the branch cut along the negative imaginary axis thereby defining the first Riemann sheet to be $\theta \in]-\pi/2 : 3\pi/2[$.
We could discuss the behaviour of the system in different regimes in terms of the location of the eigenvalues in the complex plane. As we mentioned above,

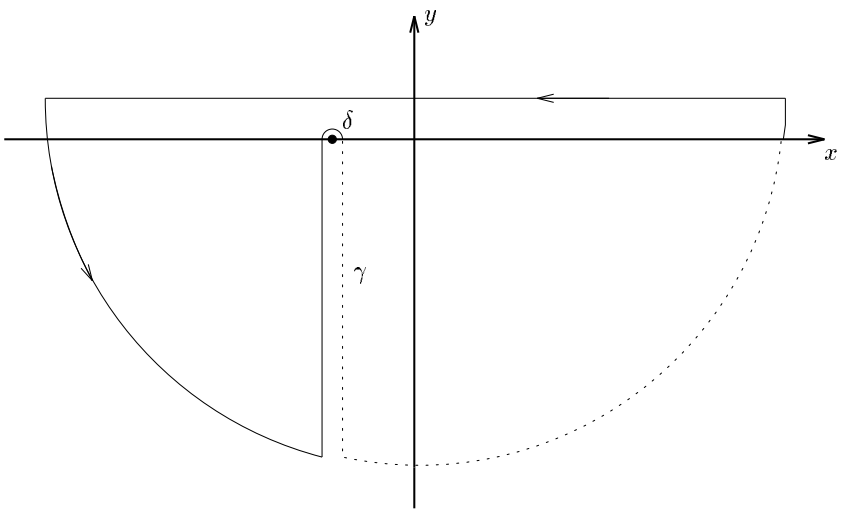

Figure 3.3: The contour used to invert the amplitudes to time domain.

however, there is a non-negligible contribution to the inversion integral which stems from the photonic continuum and which cannot be discussed in terms of eigenvalues. In order to see the precise behaviour of the system, we therefore perform the inversion integral and investigate the system in time domain.

3.5 The inversion

The inversion integral reads

$$\mathcal{U}(t) = \frac{1}{2\pi i}\int_{\infty+i\epsilon}^{-\infty+i\epsilon} dz G(z) e^{-izt} \tag{3.49}$$

where ϵ is an infinitesimal small positive quantity. To evaluate the integral, we close the contour with a semi-circle in the lower half of the complex plane as depicted in Fig. 3.3 and use the residue theorem. When the radius of the semi-circle goes to infinity, this part of the contour does not contribute. Since the functions to invert have a branch cut, we have to do a detour around the branching point. This detour, denoted γ does contribute.
Applying the residue theorem, we find

$$\mathcal{U}_k(t) = \sum_j (z - z_j) G_{ka}(z) e^{-izt}|_{z=z_j} - \frac{1}{2\pi i}\int_\gamma dz e^{-izt}\sqrt{z+\delta}\, p_k(z) \tag{3.50}$$

with $k = \{a, b\}$ and since all poles are simple. For higher order poles, the residues are more complicated. The sum over j is a sum over all poles that do

not have a positive imaginary part since those poles fall outside the integration contour. The function $p_k(z)$ introduced in the last integral is the part of the expressions for G_{aa} and G_{ba} containing the square root terms, thus

$$\begin{aligned} p_a(z) &= i\frac{(z+\delta)(-Cz^2 - CV_{ba}^2 - 2C_M V_{ba} z) + C(C_M^2 - C^2)}{h(z)} \\ p_b(z) &= -i\frac{C_M\left[(z^2+V_{ba}^2)(z+\delta) + C_M^2 - C^2\right] + 2V_{ba}(z+\delta)Cz}{h(z)} \end{aligned} \quad (3.51)$$

Let us look at the detour integral along the path γ

$$\begin{aligned} \int_\gamma dz e^{-izt}\sqrt{z+\delta}p_k(z) &= \int_\infty^0 dy e^{i\frac{3\pi}{2}} e^{-iye^{i3\pi/2}t} e^{i\delta t}\sqrt{e^{i\frac{3\pi}{2}}y}p_k(ye^{i\frac{3\pi}{2}} - \delta) \\ &+ \int_0^\infty dy e^{-i\frac{\pi}{2}} e^{-iye^{-i\pi/2}t} e^{i\delta t}\sqrt{e^{-i\frac{\pi}{2}}y}p_k(ye^{-i\frac{\pi}{2}} - \delta) \\ &= 2ie^{i\frac{3\pi}{4}}\int_0^\infty dy e^{-yt+i\delta t}\sqrt{y}p_k(-iy-\delta) \end{aligned} \quad (3.52)$$

with $k \in \{a, b\}$ and $y = z + \delta$.
With the normalization of $2\pi i$, the detour part thus reads

$$\frac{1}{2\pi i}\int_\gamma dz e^{-izt}\sqrt{z+\delta}p_k(z) = \frac{e^{i\frac{3\pi}{4}}}{\pi}\int_0^\infty dy e^{-yt+i\delta t}\sqrt{y}p_k(-iy-\delta) \quad (3.53)$$

The integral cannot be computed analytically (except for certain limits) but is easily computed numerically. The influence of the integrals can, however, be found in the long time limit. In that case only the lowest order in z contributes to the integrals, and we thus find

$$\begin{aligned} \frac{1}{2\pi i}\int_\gamma dz e^{-izt}\sqrt{z+\delta}p_a(z) &\simeq \frac{e^{i\frac{3\pi}{4}}}{\pi}\int_0^\infty dy e^{-yt+i\delta t}\sqrt{y}p_a(0) \\ &= \frac{e^{i\frac{3\pi}{4}+i\delta t}}{\pi}p_a(0)\frac{\Gamma(3/2)}{t^{\frac{3}{2}}} \end{aligned} \quad (3.54)$$

In the long time limit, the detour-integral thus contributes as $t^{-\frac{3}{2}}$. A similar behaviour is found for the other detour-integral.
The prefactor $p_a(0)$ in Eq. (3.54) determines the influence of the detour-integral on the total wave function. By examining the expression for $p_k(z)$, one finds $p_k(0) \propto \delta^{-1}$ for large detunings. The influence of the detour-integral therefore becomes negligible when the atomic transition frequency is detuned far from the band gap edge in which case the atomic evolution becomes exponential (positive detuning) or the decay is inhibited (negative detuning).
The behaviour of the system resembles the departure from exponential decay for an atom in free space due to corrections to the pole-approximation [44]. We recall, however, that in our problem the photon continuum is strongly modified compared to the free space case, and the pole-approximation does not provide a valid starting point for our calculation.

3.6 The wave functions in time domain

Having established the influence of the detour integral, we investigate the system in different limits in the time domain.

3.6.1 One atom

If the interatomic separation is very large, we have $C_M \sim V_{ab} \sim 0$ and the problem reduces to the one-atom problem already treated in the literature [32, 33]. In that case the characteristic polynomial Eq. (3.37) simplifies to

$$0 = \left[z^2(z+\delta) + C^2\right]^2 \tag{3.55}$$

which seems to indicate that this one-atom system has three poles that are all of order two. The expression for G_{aa} does, however, simplify and we find

$$G_{aa} = \frac{z(z+\delta) - i\sqrt{z+\delta}C}{z^2(z+\delta) + C^2} \tag{3.56}$$

which is the expression also derived by John and Quang [32] and Kofman *et al* [33]. This expression has three poles, of which only two contribute since the third pole has a positive imaginary part and thus falls outside the inversion contour. Of the two remaining poles, one has an imaginary part and thus gives rise to a transient, dissipative dynamics, whereas the second pole is purely real and thus corresponds to a stable, non-decaying state of the system. In the transient regime, both poles will contribute to the dynamics which gives rise to beating, which is indeed a rather unusual phenomenon in spontaneous decay.
For an atomic transition frequency at the band edge ($\delta = 0$), the roots are

$$\begin{aligned} z_1 &= -C^{\frac{2}{3}} \\ z_2 &= e^{i\frac{\pi}{3}}C^{\frac{2}{3}} \\ z_3 &= e^{-i\frac{\pi}{3}}C^{\frac{2}{3}} \end{aligned} \tag{3.57}$$

In the long time limit, only the real root contributes and the atomic population is then given by

$$|\mathcal{U}_{aa}(t)|^2 \sim \left|\frac{z_1^2 - iC\sqrt{z_1}}{(z_1 - z_2)(z_1 - z_3)}\right|^2 = \frac{4}{9} \tag{3.58}$$

which means that a considerable part of the population is bound on the atom in the long time limit. This is what has been referred to as a "bound photon-atom state" in the literature [31, 32]. For atomic transition frequencies in the gap, the population trapping can be close to 1 as is evident from Fig. 3.4, where we have plotted the atomic population as a function of time for different detunings with respect to the band gap edge.
Spontaneous emission is taking place on a fast timescale roughly given by $C^{-2/3}$

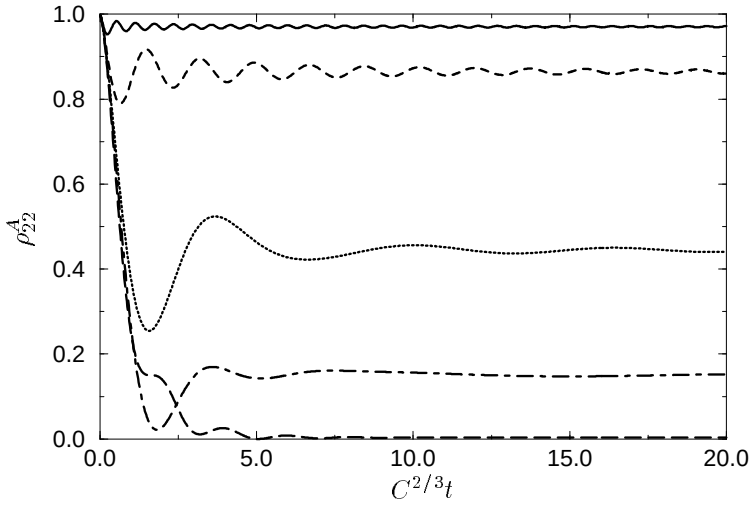

Figure 3.4: The time evolution of the excited state population as a function of time for different detunings: $\delta = -10C^{2/3}$ (solid line), $\delta = -3C^{2/3}$ (dashed line), $\delta = 0$ (dotted line), $\delta = C^{2/3}$ (dashed-dotted line) and $\delta = 3C^{2/3}$ (long-dashed line)

and in this transient regime, part of the atomic population is lost. On a longer timescale, the population remains almost constant but we see a slight oscillation which stems from the beating between the stable, non-decaying state and the detour-integral. Physically, this effect stems from the emitted photon which is reflected in the dielectric host and thus oscillates back and reexcites the atom. Even for atomic transition frequencies outside the gap ($\delta > 0$), we find a significant population trapping as has been noted in the literature [32, 33].

3.6.2 Two atoms at the band edge ($\delta = 0$)

At the band edge $\delta = 0$ and for negligible dipole-dipole coupling $V_{ab} \simeq 0$, the roots of the characteristic polynomial are the following

$$z_1 = e^{i\pi/3}(C + C_M)^{\frac{2}{3}} \quad (3.59)$$

$$z_2 = e^{-i\pi/3}(C + C_M)^{\frac{2}{3}} \quad (3.60)$$

$$z_3 = -(C + C_M)^{\frac{2}{3}} \quad (3.61)$$

$$z_4 = e^{i\pi/3}(C - C_M)^{\frac{2}{3}} \quad (3.62)$$

$$z_5 = e^{-i\pi/3}(C - C_M)^{\frac{2}{3}} \quad (3.63)$$

$$z_6 = -(C - C_M)^{\frac{2}{3}} \quad (3.64)$$

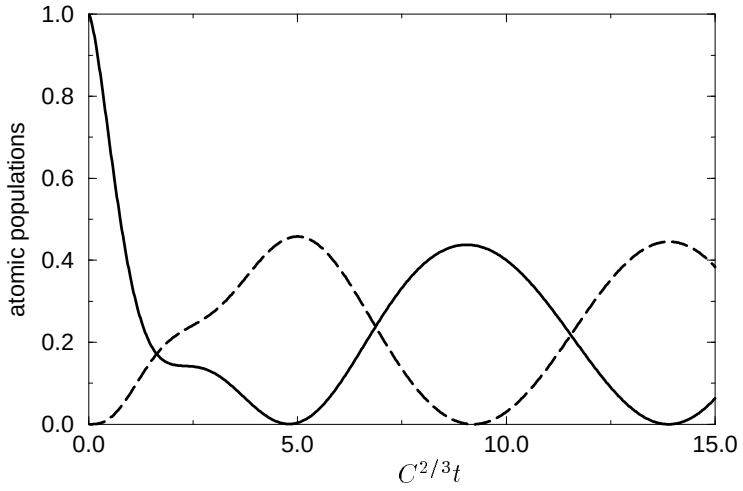

Figure 3.5: The time evolution of the excited state populations as a function of time for atomic transition frequencies at the band edge ($\delta = 0$). The solid line is the population of the initially excited atom A and the dashed line is for atom B. $C_M/C = \frac{1}{2}, V_{ab} = 0$

Two of these roots are real; namely $z = -(C + C_M)^{\frac{2}{3}}$ and $z = -(C - C_M)^{\frac{2}{3}}$ and by inserting these in the equation for the characteristic polynomial Eq. (3.36), it is easily confirmed that these roots are also roots in the orignal polynomial. That the roots are real means that they correspond to stable, non-decaying states of the coupled system. The existence of two such stable states implies that the system has no steady state in the conventional sense of the word, since in the long time limit, the system will beat between these two non-decaying states. On the other hand, if the system is viewed in the basis of the symmetric- and anti-symmetric product states, it is found to have a steady state.
Of the four remaining roots, two will not contribute since they have a positive imaginary part and thus fall outside the integration contour and the two remaining roots will give rise to a transient, damped behaviour.
Now, one of the real poles corresponding to a stable state is actually the eigenvalue of the symmetric product state. We thus find the surprising result that the symmetric product state which in free space is super-radiant in the photonic band gap can be a partially stable non-decaying state.
In Fig. 3.5, we have plotted the atomic populations as a function of time. From the figure, we identify an initial transient regime in which part of the population is lost. On a longer timescale, the remaining population is exchanged between the atoms in an oscillatory, non-dissipative manner. This is also a rather sur-

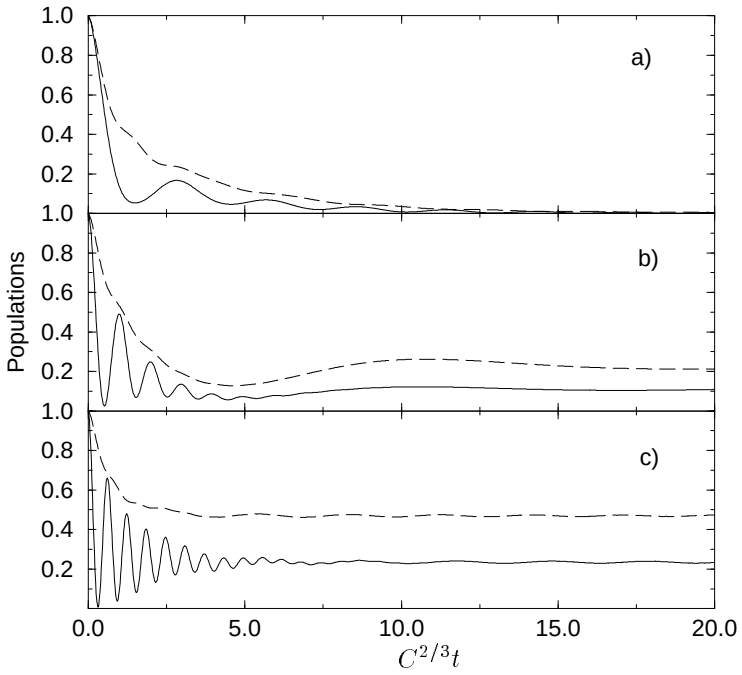

Figure 3.6: The excited state populations as a function of time for $\delta = 3, C = 1$, $C_M = 0.8$ and different values of V_{ab}. The solid line is the population in the excited state of atom A. The dashed line is the sum of the populations in the excited states of atom A and B. *a)* $V_{ab} = 1$. *b)* $V_{ab} = 3$.*c)* $V_{ab} = 5$.

prising result: In the study of atoms coupled to cavities, we typically see beating (Rabi-oscillations) when the Rabi-frequency exceeds the decay width and the Rabi-oscillation is then a transient phenomena, which is eventually damped out. In the present problem, dissipation only acts in a transient regime, after which it is effectively turned off and then only the coherent oscillation of the remaining excitation between the two atoms persists. Physically, this part of the excitation is protected against dissipation, since it corresponds to a photon with energy in the gap, tunneling between the two atoms.

3.6.3 Small interatomic separation.

When the interatomic separation becomes very small i.e. $R \ll \lambda$, the real part of the dipole-dipole interaction (V_{ab}) becomes the dominant part of the interaction. We investigate this regime for different detunings. In Fig. 3.6, we plot the population in the excited state of the initially excited atom A and the total population of atom A and B as a function of time for different values of V_{ab}

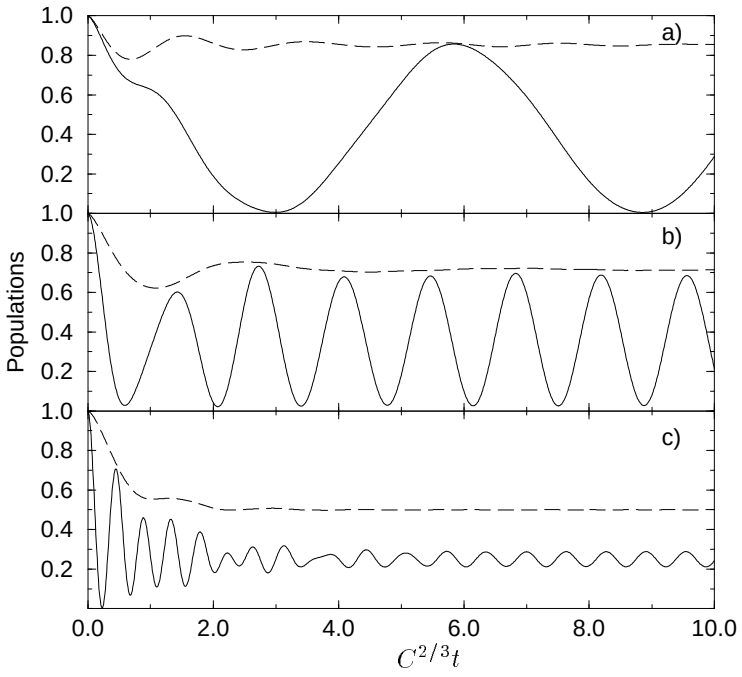

Figure 3.7: The excited state populations as a function of time for $\delta = -3$, $C = 1$, $C_M = 0.8$ and different values of V_{ab}. The solid line is the population in the excited state of atom A. The dashed line is the sum of the populations in the excited states of atom A and B. *a)* $V_{ab} = 1$, *b)* $V_{ab} = 3$ and *c)* $V_{ab} = 7$.

with $\delta = 3$. With this choice of parameters, the atomic transition frequencies are tuned outside the gap into the allowed part of the spectrum. For a relatively weak RDDI ($V_{ab} = 1$), the atomic population is lost in the long time limit as is evident from the figure. For a slightly stronger RDDI ($V_{ab} = 3$), the coupling between the two atoms is now comparable to the detuning from the band gap edge and the splitting of the atomic levels due to the coupling is hence strong enough to move part of the atomic level into the gap where it is protected from dissipation. We therefore find a non-negligible population trapping for this choice of parameters. This becomes even more apparent for an even stronger coupling ($V_{ab} = 5$), in which case close to 50 percent of the initial excitation remains bound on the two atoms in the long time limit.
The reverse case is illustrated in Fig. 3.7, where again the atomic population on atom A and the sum of the atomic populations are plotted for $\delta = -3$ and various values of V_{ab}.

For a relatively weak RDDI ($V_{ab} = 1$), there is a significant population trapping in the long time limit. As the RDDI is becoming comparable to the

detuning from the band gap edge, the population-trapping is decreased since the level splitting is now large enough to move part of the atomic levels into the allowed part of the spectrum.

3.7 The photonic population distribution

In the literature, different quantities have been employed as a measure of the spectrum [45]. For an atom in free space, the spectrum is the distribution of population in the continuum modes in the long time limit. In the present case, however, an initially excited atom with a transition frequency close to the edge of the gap with a certain probability evolves into a photon-atom bound state which is a superposition of atomic excited state in the presence of no photon and atomic ground state with a superposition of one-photon states. The superposition of photonic states yields a wavepacket in real space which is well localized around the atom. A detector located outside the large crystal does not detect the localized photonic wavepacket but only the fluorescent light lost in the initial transient regime of the atomic evolution. The distribution of population in the photonic continuum does therefore not coincide with the spectrum we would measure with a detector located outside the crystal. Kofman and coworkers have investigated the spectrum of one atom in a photonic band gap material [33].
In this section we investigate the distribution of population in the continuum in the long time limit.

3.7.1 One atom

The one-photon part of the field in the time domain is given by

$$|\psi\rangle = \sum_{\mathbf{k}l} \mathcal{U}_{ca}(t)|\mathbf{k}l\rangle \tag{3.65}$$

where the summation is over all continuum states and $\mathcal{U}_{ca}$ is the amplitude for the continuum mode c with frequency $\omega_c = \omega_a + \Delta$, obtained by inverting the expression

$$G_{ca} = \frac{V_{ca}G_{aa}}{z-\Delta} \tag{3.66}$$

where G_{aa} is the one-atom amplitude given by Eq. (3.56).
In the long time limit, only the roots with no imaginary(dissipative) part contribute to the dynamics in time domain of the continuum mode. Assuming that the atomic transition frequency is at the band gap edge ($\delta = 0$), there are two poles contributing: One is the free evolution of the mode at frequency ω and the other pole at $-C^{2/3}$ stems from the non-decaying photon-atom bound state.
In this case, the population in the mode is

$$|\mathcal{U}_{ca}(t)|^2 = \frac{|V_{ca}|^2}{(\Delta + C^{2/3})^2}\left[\frac{\Delta^4 + C^2\Delta}{(\Delta^2 + C^{4/3} - \Delta C^{2/3})^2}\right.$$

$$+\frac{4}{9}-\frac{4}{3}\frac{\Delta^2}{\Delta^2+C^{4/3}-\Delta C^{2/3}}\cos(\Delta t+C^{2/3}t) +\frac{4}{3}\frac{C\sqrt{\Delta}}{\Delta^2+C^{4/3}-\Delta C^{2/3}}\sin(\Delta t+C^{2/3}t)\Bigg] \quad (3.67)$$

Eq. (3.67) contains an implicit dependence on the orientation of the atomic dipole in space. We perform an integration of Eq. (3.67) over the angular part. Furthermore we perform a time average over the period $2\pi/(\Delta+C^{2/3})$ in order to eliminate the time dependent terms.
In the long time limit, the frequency distribution is therefore given by the angular integrated, stationary terms of Eq. (3.67)

$$\begin{aligned} S(\omega) &= \rho(\omega)\sum_{l=1,2}\int d\Omega|\mathcal{U}_{ca}|^2 \\ &= \frac{\Theta(\omega-\omega_e)}{\pi\sqrt{\omega-\omega_e}}\frac{C}{(\Delta+C^{2/3})^2}\left[\frac{\Delta^4+C^2\Delta}{(\Delta^2+C^{4/3}-\Delta C^{2/3})^2}+\frac{4}{9}\right] \end{aligned} \quad (3.68)$$

where $\omega=\omega_a+\Delta=\omega_e+\Delta$ since $\delta=0$ and the density of states $\rho(\omega)$ is given by Eq. (3.33).
Eq. (3.68) does indeed yield a rather unusual distribution of population quite different from the usual Lorentzian form obtained for a two-level atom in free space as can also be seen from Fig. 3.8, where we have plotted the frequency distribution as a function of ω.
The coupled system consisting of "atom+reservoir" has a pole at $\exp(-i\pi/3)C^{2/3}$ and we would thus expect the population distribution to have a peak at $\frac{1}{2}C^{2/3}$. The density of modes does, however, strongly suppress radiation at this wavelength and instead the photon emission close to the band gap edge ($\Delta\approx 0$) is strongly amplified.
We calculate the population in the continuum modes in the long time limit, which is given by

$$\int_0^\infty d\omega S(\omega)=\frac{5}{9} \quad (3.69)$$

To obtain this result, the integral has been performed numerically. In the long time limit, we therefore find that the atomic excited state population given by Eq. (3.58) and the population in the photonic continuum add up to one as should be the case.

3.7.2 Two atoms

When the couplings between the two atoms cannot be neglected, the general expression for the continuum amplitude in frequency domain reads

$$G_{ca}=\frac{1}{z-\omega_c}\left[V_{ca}G_{aa}+V_{cb}G_{ba}\right] \quad (3.70)$$

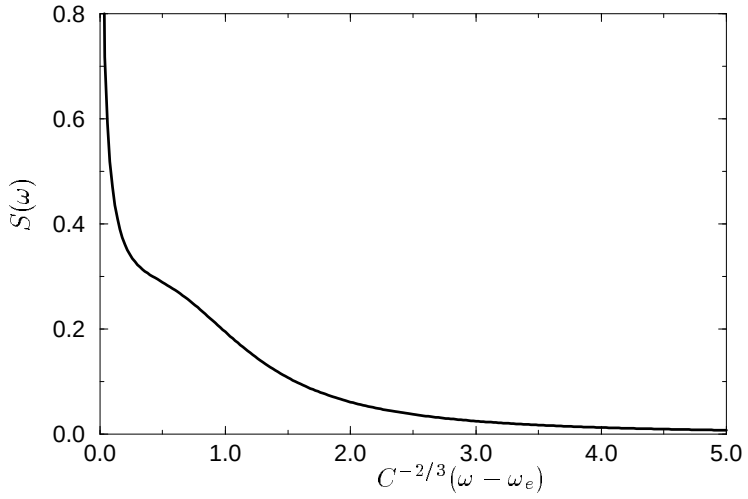

Figure 3.8: The photonic population distribution for one atom in a photonic band gap with transition frequency at the band gap edge ($\delta = 0$).

Let us consider the simpler case of $V_{ab} = \delta = 0$. The roots of the system are then given by Eqs. (3.59-3.64) and the expression for the continuum amplitude reads

$$G_{ca} = \frac{1}{z-\omega_c}\frac{1}{h(z)}\left[V_{ca}(z^2 + iC\sqrt{z}) - iV_{cb}C_M\sqrt{z}\right] \left[z^3 + C_M^2 - C^2 - 2iC\sqrt{z}z\right] \tag{3.71}$$

while the stable roots of the system are given by Eq. (3.61) and Eq. (3.64). In the long time limit, these roots and the root $z = \omega$ contribute. As before, we transform the amplitude to the time domain keeping only the contribution from real roots, taking absolute square and leaving out terms depending on frequency. In the end, we obtain for the angular integrated continuum population

$$\begin{aligned} S(\omega) &= \rho(\omega)\sum_{l=1,2}\int d\Omega|\mathcal{U}_{ca}(t)|^2 \\ &= \frac{\Theta(\omega-\omega_e)}{\pi\sqrt{\omega-\omega_e}}\frac{C\Delta}{h(\Delta)^2}\left[\Delta^3 + C^2 - C_M^2\right]\left[(\Delta^3 + C_M^2 - C^2)^2 + 4\Delta^3C^2\right] \\ &+ \frac{\Theta(\omega-\omega_e)}{\pi\sqrt{\omega-\omega_e}}\frac{32C^2C_M^2}{9\tilde{h}^2}\left[\frac{C-C_M}{((C-C_M)^{2/3}+\Delta)^2} + \frac{C+C_M}{((C+C_M)^{2/3}+\Delta)^2}\right] \end{aligned} \tag{3.72}$$

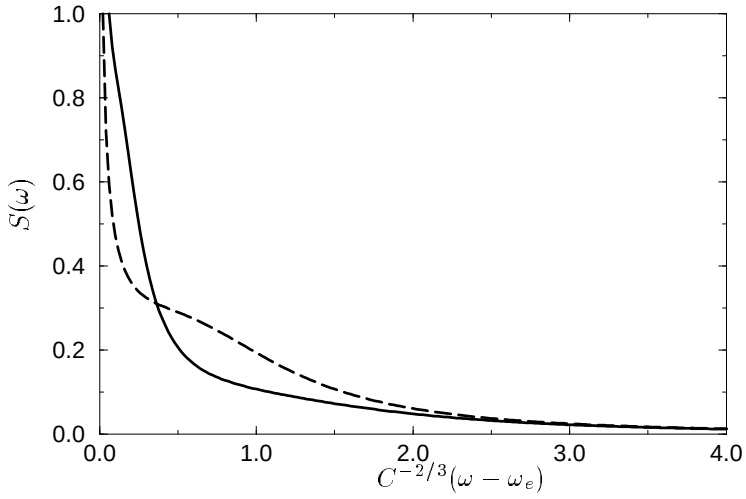

Figure 3.9: The photonic population distribution for two atoms in a photonic band gap with transition frequencies at the band gap edge ($\delta = 0$) and $V_{ab} = 0$. The solid line is for $C_M/C = 0.9$ and the long-dashed line is for $C_M/C = 0.1$

where we have defined

$$\tilde{h} = \left[(C - C_M)^{4/3} + (C + C_M)^{4/3} - (C^2 - C_M^2)^{2/3}\right] \left[(C + C_M)^{2/3} - (C - C_M)^{2/3}\right] \tag{3.73}$$

The population distribution Eq. (3.72) has been plotted in Fig. 3.9. From the figure, we find that the population distribution has a "shoulder" which vanishes when $C \sim C_M$. The reason for this becomes apparent by investigating the eigenvalues of the coupled system. The coupled system fluoresces at the energies $\frac{1}{2}(C - C_M)^{2/3}$ and $\frac{1}{2}(C + C_M)^{2/3}$. The shoulder in the population distribution thus stems from the fluorescence at the energy $\frac{1}{2}(C - C_M)^{2/3}$, which coincides with the band gap edge when $C \sim C_M$, in which case the shoulder disappears. As in the case of one atom, we have by numerical integration of the population distribution over ω, made sure that the population in the continuum modes and the atomic excited state population add up to one.

3.8 Summary

In this chapter we have presented a model calculation for two atoms with transition frequencies near the edge of a photonic band gap and interacting through

the narrow band of strongly coupled modes.
We addressed the problem using the resolvent operator formalism by means of which, the wave functions of the system are obtained in Laplace space.
Eliminating the field mode amplitudes from the equations of motion, we obtained two coupled, algebraic equations for the amplitudes of the two atoms coupled through second order expressions involving summations over the continuum states. One of these couplings is the RDDI between the two neighbouring atoms. We presented an analytical calculation of the RDDI and showed that it agrees very well with a numerical integration of the RDDI using the exact dispersion relation for the dielectric host.
With the analytical expressions for the couplings, the set of equations for the two atoms was solved and we investigated the amplitudes of the two atoms in the time domain. Although the atoms are coupled to a dissipative environment, we found population trapping and beating in the long time limit for a wide range of parameters.
We have also calculated the photonic population distributions for one and two atoms, respectively, and found that the location of the peaks of the distributions is mainly determined by the mode structure and not as is usually the case, by the location of the poles of the coupled system in the complex plane. Furthermore we found, not surprisingly, that the mode structure acts as a frequency filter and effectively cuts off frequencies in the photon distribution below the band edge.

Chapter IV

Strongly non-Lorentzian emission spectra in a radiative cascade

We investigate the spectrum for an atomic ladder system where one transition is coupled near-resonantly to the edge of a photonic band gap and the other transition is coupled to a flat background of radiation modes. The corresponding emission spectra are strongly non-Lorentzian.

4.1 Introduction

The interaction of simple atomic systems with strongly modified radiation reservoirs is a topic of much current interest [1]-[5],[32, 33], [46]-[56], motivated in part by the prospect of a new class of phenomena in quantum optics predicted in connection with the novel and unusual properties of PBG materials [10, 11] and in part by the intrinsic interest in new types of effects not amenable to standard techniques. One such effect was identified in the last chapter; namely for an atom located inside a photonic band gap material and with a transition frequency in the photonic band gap, the spontaneous decay is strongly modified to the extent of being turned off for atomic transition frequencies sufficiently far inside the band gap resulting in a "photon-atom bound state" [31] reflecting the fact that a photonic wavepacket remains localized at the site of the atom. But this very property of localization due to the perfect reflectivity of the inside of the PBG material, makes its direct observation difficult since the photon does not leave the material.
It is then necessary to explore arrangements through which the probing of these features is possible. Such arrangements, intended to probe the strong coupling of two systems and most notably atom and radiation, are a major domain of interest in quantum optics. They acquire, however, a qualitatively different level of complexity when applied to non-standard reservoirs. It is the purpose of this chapter to present an arrangement for the probing of a photon-atom bound state through the well-known three-level ladder system and to show the unusual behavior it exhibits in this context. Related to the work presented here is the

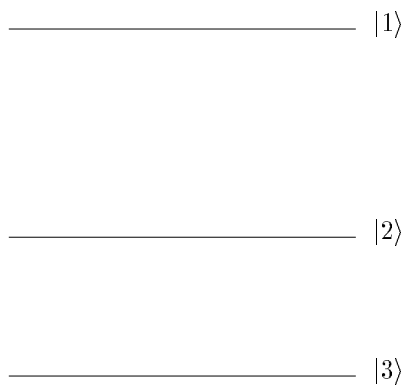

Figure 4.1: The atomic level scheme

paper of John and Quang [32] in which they investigate the emission spectrum of a Lambda system where one transition is coupled to the edge of a PBG and the other to a flat background of radiation modes.
The system considered in this chapter is depicted in Fig. 4.1 and it represents three atomic states capable of cascade dipole transitions $|1\rangle \rightarrow |2\rangle \rightarrow |3\rangle$ and is assumed to be initially in state $|1\rangle$. The transition frequencies of the two transitions are assumed to be very different which means that the transitions are effectively coupled to independent reservoirs. One transition is coupled to a flat background of radiation modes yielding the usual exponential decay while the other is coupled near-resonantly to the edge of a photonic band gap and thus experiences a rapidly varying density of modes. We investigate the case where the upper transition of the ladder is coupled to a PBG as well as the case where the lower transition is coupled to the unusual reservoir.
In free space, the spectrum for the photon emitted on the upper transition in the radiative cascade would be a Lorentzian with a width which is the sum of the decay widths of the two upper atomic levels. In other words: Observing only the first photon in a radiative cascade provides information about the lower level in the transition. In the present context, however, when the frequency of the lower transition is near the edge of the band gap, the respective levels are coupled to an unusual reservoir whose influence is reflected in the spectrum of the upper transition.

4.2 The system

We consider a three-level atom as depicted in Fig. 4.1, with the states $|1\rangle, |2\rangle, |3\rangle$. Neglecting the zero point energies of the field modes and performing the rotating wave approximation (RWA) for the interaction term, the Hamiltonian for this

system reads ($\hbar = 1$)

$$H = H_0 + V \tag{4.1}$$

with

$$H_0 = \omega_1\sigma_{11} + \omega_2\sigma_{22} + \sum_\alpha \omega_\alpha a_\alpha^\dagger a_\alpha + \sum_\alpha \omega_\alpha b_\alpha^\dagger b_\alpha \tag{4.2}$$

and

$$V = i\sum_\alpha g_\alpha(a_\alpha^\dagger\sigma_{21} - a_\alpha\sigma_{12}) + i\sum_\alpha g_\alpha(b_\alpha^\dagger\sigma_{32} - b_\alpha\sigma_{23}) \tag{4.3}$$

where $a, a^\dagger (b, b^\dagger)$ are the creation and annihilation operators of the two reservoirs and the atomic operators are given by $\sigma_{ij} = |i\rangle\langle j|$ with $i, j \in \{1, 2, 3\}$.
We denote by $D(\omega_\lambda)$ and $D(\omega_\gamma)$ the spectral response of the upper and lower transition, respectively. As we noted in the paragraph after Eq. (3.33), the effective mass dispersion relation Eq. (2.29) corresponds to a spectral response given by

$$D(\omega_\alpha) \equiv \int d\Omega_\alpha \rho(\omega_\alpha)|g_\alpha|^2 = \frac{C}{\pi}\frac{\Theta(\omega_\alpha - \omega_e)}{\sqrt{\omega_\alpha - \omega_e}} \tag{4.4}$$

where $C = d^2k_0^2\omega_e/(4\pi\epsilon_0\sqrt{A})$ is the effective coupling with d the atomic dipole moment and the integration in Eq. (4.4) runs over the 4π solid angle.
The relevant states for the system under consideration are

$$|a\rangle = |1, 0, 0\rangle \tag{4.5}$$
$$|b\rangle = |2, 1_\lambda, 0\rangle \tag{4.6}$$
$$|c\rangle = |3, 1_\lambda, 1_\gamma\rangle \tag{4.7}$$

where 1_γ and 1_λ denote photons in the two radiation reservoirs.

4.3 Spectrum

With the system initially in the state $|a\rangle$, the resolvent operator equations read

$$(z - \omega_a)G_{aa} = 1 + \sum_b V_{ab}G_{ba} \tag{4.8}$$

$$(z - \omega_b)G_{ba} = V_{ba}G_{aa} + \sum_c V_{bc}G_{ca} \tag{4.9}$$

$$(z - \omega_c)G_{ca} = V_{bc}G_{ba} \tag{4.10}$$

where $\omega_a = \omega_{13}$, $\omega_b = \omega_{21} + \omega_\lambda$ and $\omega_c = \omega_\lambda + \omega_\gamma$.
The total wavefunction $|\Psi(t)\rangle$ in time domain reads

$$|\Psi(t)\rangle = \mathcal{U}_{aa}(t)|a\rangle + \sum_\lambda \mathcal{U}_{ba}(t)|b\rangle + \sum_{\lambda,\gamma} \mathcal{U}_{ca}(t)|c\rangle \tag{4.11}$$

where the amplitudes $\mathcal{U}_{ia}(t)$ $(i \in \{a,b,c\})$ are obtained by performing the inversion integral

$$\mathcal{U}_{ia}(t) = \frac{1}{2\pi i}\int_{\infty+i\epsilon}^{-\infty+i\epsilon} G_{ia}(z)e^{-izt}dz \tag{4.12}$$

The quantity of interest is the emission spectrum which is the population in the reservoir mode ω_λ in the long time limit

$$S(\omega_\lambda) = \sum_i |\langle 1_\lambda, i|\Psi(t)\rangle|^2 \tag{4.13}$$

where i is short hand notation for all other quantum numbers.

4.3.1 Lower transition coupled to PBG

Let us consider first the case where the lower atomic transition $|2\rangle \rightarrow |3\rangle$ is coupled near-resonantly to the edge of the PBG.
Eliminating the continuum amplitude G_{ba} and G_{ca}, we find for G_{aa} and G_{ba}, respectively

$$(z-\omega_a)G_{aa} = 1 + \sum_b \frac{|V_{ba}|^2}{z-\omega_b}G_{aa} \tag{4.14}$$

$$(z-\omega_b)G_{ba} = V_{ba}G_{aa} + \sum_c \frac{|V_{bc}|^2}{z-\omega_c}G_{ba} \tag{4.15}$$

The continuum involved in the summation over b-states is assumed to be smooth which validates the usual Markov approximation

$$\sum_b \frac{|V_{ba}|^2}{z-\omega_b} = \Delta - i\Gamma/2 \tag{4.16}$$

The summation over c states is performed using the effective mass approximation Eq (2.29), which when turning the summation into an integral yields

$$\sum_c \frac{|V_{bc}|^2}{z-\omega_c} = \frac{-iC}{\sqrt{z-\omega_e-\omega_\lambda}} \tag{4.17}$$

Inserting these expressions for the coupling, we find for the amplitude G_{ba},

$$G_{ba} = \frac{V_{ba}}{z-\omega_a+i\Gamma/2}\frac{1}{z-\omega_b+\frac{iC}{\sqrt{z-\omega_e-\omega_\lambda}}} \tag{4.18}$$

which can be cast in the form

$$G_{ba} = \frac{V_{ba}\sqrt{z-\omega_e-\omega_\lambda}}{z-\omega_a+i\Gamma/2}\frac{(z-\omega_b)\sqrt{z-\omega_e-\omega_\lambda}-iC}{(z-z_+)(z-z_-)(z-z_0)}$$

where $z_\pm, z_0$ are the roots of the polynomial $(z-\omega_b)^2(z-\omega_e-\omega_\lambda)+C^2$ defined such that z_0 is the purely real root and z_+, z_- have a positive and negative imaginary part, respectively. For an atomic transition frequency ω_{23} far inside the band gap, all three roots are purely real.
Since $\omega_b = \omega_{23}+\omega_\lambda$, it is clear that all three roots contain a common factor ω_λ. For later convenience we introduce the roots $\bar{z}_{0,\pm}$ corresponding to an interaction picture rotating at ω_b i.e. $\bar{z}_{0,\pm} = z_{0,\pm} - \omega_b$.
When the amplitude G_{ba} is inverted to time domain, the pole z_+ does not contribute, the pole z_0 is purely real and thus corresponds to a stable state i.e. the photon-atom bound state and the pole z_- is complex and in time domain this leads to damping with a rate given by the imaginary part of the pole.
The expression for the continuum amplitude G_{ca} reads

$$G_{ca} = \frac{V_{cb}V_{ba}}{z-\omega_c}\frac{\sqrt{z-\omega_e-\omega_\lambda}}{z-\omega_a+i\Gamma/2}\frac{(z-\omega_b)\sqrt{z-\omega_e-\omega_\lambda}-iC}{(z-z_+)(z-z_-)(z-z_0)}$$

In time domain and in the long time limit, only the two non-dissipative poles contribute and the time-dependent amplitude $\mathcal{U}_{ca}(t)$ for the reservoir mode hence reads

$$\mathcal{U}_{ca}(t) = A\exp(-i\omega_c t) + B\exp(-iz_0 t) \tag{4.19}$$

where A, B are defined such that

$$V_{cb}V_{ba}A = (z-\omega_c)G_{ca}(z)|_{z=\omega_c} \tag{4.20}$$
$$V_{cb}V_{ba}B = (z-z_0)G_{ca}(z)|_{z=z_0} \tag{4.21}$$

The spectrum can now be calculated using Eq. (4.13) and since the rapidly varying terms A^*B and B^*A average out when we perform the integration over the photon frequency ω_γ, we find

$$S(\omega_\lambda) = \rho(\omega_\lambda)\int d\Omega_\lambda |\mathcal{U}_{ba}|^2 + D(\omega_\lambda)\int d\omega_\gamma D(\omega_\gamma)[|A|^2+|B|^2] \tag{4.22}$$

where the integration in the first term is over the solid angle Ω_λ and $D(\omega_\lambda)$ is the spectral response of the flat continuum coupled to the upper transition and $D(\omega_\gamma)$, the spectral response of the PBG continuum coupled to the lower transition.
We should stress that the term $\rho(\omega_\lambda)\int d\Omega_\lambda|\mathcal{U}_{ba}|^2$ does not appear in the expression for the spectrum for a ladder system in free space since in that case all the population is in the atomic ground state $|3\rangle$ in the long time limit [41].
The integral over the frequency ω_γ in Eq. (4.22) can not be calculated in the usual way applying the residue theorem due to the presence of the square root terms. Instead the integral is calculated numerically. The results are presented in Fig. 4.2.
Let us now discuss the form of the spectrum for different detunings $\delta_2 \equiv \omega_{23}-\omega_e$ with respect to the band gap edge.

For an atomic transition frequency far inside the gap ($\delta_2 \ll 0$), the system reduces to an effective two-level system since the transition $|2\rangle \to |3\rangle$ effectively becomes energetically forbidden and the population therefore remains in the state $|b\rangle$. This means that Eq. (4.22) simplifies to

$$S(\omega_\lambda) \simeq \rho(\omega_\lambda) \int d\Omega_\lambda |\mathcal{U}_{ba}|^2 = \frac{f}{(\omega_\lambda - \omega_{12} + \bar{z}_0)^2 + (\frac{\Gamma}{2})^2} \tag{4.23}$$

where

$$f = \left| \frac{\bar{z}_0 \sqrt{\bar{z}_0 + \delta_2} - iC}{(\bar{z}_0 - \bar{z}_+)(\bar{z}_0 - \bar{z}_-)} \sqrt{\bar{z}_0 + \delta_2} \right|^2 D(\omega_\lambda) \tag{4.24}$$

which has the form of a Lorentzian with a width Γ since the spectral response $D(\omega_\lambda)$ of the flat continuum is very slowly varying. In this case the spectrum thus reduces to that found for a two-level atom in free space vacuum.
For an atomic transition frequency far outside the gap i.e. $\delta_2 \gg 0$, the photon-atom bound state disappears i.e. $|\mathcal{U}_{ba}|^2 = 0$ and the dynamics on the transition $|2\rangle \to |3\rangle$ becomes that of normal exponential decay. We thus expect the spectrum to reduce to that of a ladder system in free space namely a Lorentzian with a linewidth which is the sum of the widths of the two upper levels.
We show now that this is actually the case. The expression for the spectrum Eq. (4.22) simplifies to

$$S(\omega_\lambda) \simeq \int d\omega_\gamma D(\omega_\lambda) D(\omega_\gamma) |A|^2 \tag{4.25}$$

where

$$|A|^2 = \frac{(\omega_\gamma - \omega_e)}{(\Delta_\gamma - \bar{z}_+)(\Delta_\gamma - \bar{z}_-)(\Delta_\gamma - \bar{z}_0)} \frac{1}{(\Delta_\gamma + \delta_\lambda)^2 + (\Gamma/2)^2} \tag{4.26}$$

where $\Delta_\gamma = \omega_\gamma - \omega_{23}$ and $\delta_\lambda = \omega_\lambda - \omega_{21}$. The main contributions to the integral come from the poles $\bar{z}_+$ and $\delta_\lambda + i\Gamma/2$. We can thus approximate the integral by

$$\int d\omega_\gamma D(\omega_\gamma) |A|^2 \simeq \int_{-\infty}^{\infty} d\omega_\gamma \frac{C\sqrt{\delta_2}}{\delta_2 \pi} \frac{1}{(\Delta_\gamma - \bar{z}_+)(\Delta_\gamma - \bar{z}_-)} \frac{1}{(\Delta_\gamma + \delta_\lambda)^2 + \Gamma^2/4} \tag{4.27}$$

This integral can be calculated using the residue theorem yielding

$$S(\omega) \sim \frac{1}{(\omega - \omega_{12} + \bar{z}_r)^2 + (\Gamma + \bar{z}_i)^2/4} \tag{4.28}$$

where $\bar{z}_i = \mathrm{Im}(\bar{z}_+)$ and $\bar{z}_r = \mathrm{Re}(\bar{z}_+)$.
For an atomic transition frequency far outside the gap i.e. $\delta_2 \gg 0$, the spectrum is thus Lorentzian with a width given by the sum of the widths of the levels $|1\rangle$ and $|2\rangle$ and a center frequency given by $\omega_{12} - \bar{z}_r$.

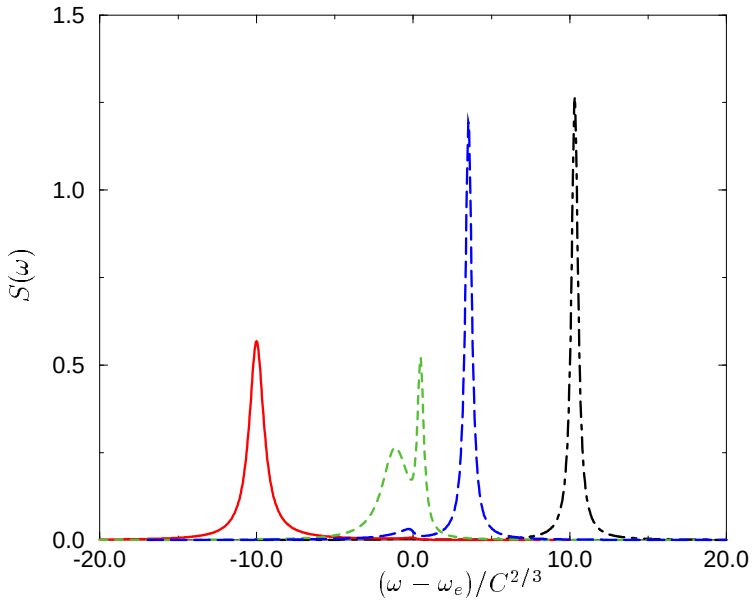

Figure 4.2: The spectrum for the first photon in the radiative cascade is plotted as a function of photon frequency for different detunings $\delta_2 = \omega_{23} - \omega_e$ with respect to the band gap edge $\delta_2 = 10$ (solid line), $\delta_2 = 1$ (dotted line), $\delta_2 = -1$ (long-dashed line) and $\delta_2 = -10$ (dot-dashed line)

When the transition frequency ω_{23} is in the vicinity of the band gap edge, the narrow band of strongly coupled modes leads to a splitting of the atomic level. One part of the atomic level is moved into the band gap where it is protected from dissipation and the other part is moved into the allowed part of the spectrum where it can decay freely. The upper level can therefore decay to two different levels and the spectrum consequently acquires two peaks as is also clearly seen in Fig. 4.2. The splitting of the two peaks is a direct measure of the strength of the coupling of the lower transition to the photonic band gap.

4.3.2 Upper transition coupled to PBG

We now investigate the case where the upper atomic transition $|1\rangle \rightarrow |2\rangle$ is coupled near-resonantly to the edge of a photonic band gap and the lower transition is coupled to a flat background of radiation modes yielding a width Γ for the state b.
Eliminating as before the continuum amplitudes, we then find the expression

for the upper state amplitude G_{aa}

$$G_{aa} = \frac{1}{z - \omega_a + \frac{iC}{\sqrt{z-\omega_e-\omega_{23}+i\Gamma/2}}} \tag{4.29}$$

where the width Γ of the state b now enters in the expression for G_{aa}. The decay of the state b means that there is no longer a photon-atom bound state since any population fed into state b decays to state c. It could be said that, in some sense the photon-atom bound state becomes metastable. In the long time limit, all the population must therefore be found in state c for which the amplitude reads

$$G_{ca} = \frac{V_{cb}}{z-\omega_c}\frac{V_{bc}}{z-\omega_b+i\Gamma/2}\frac{1}{z - \omega_a + \frac{iC}{\sqrt{z-\omega_e-\omega_{23}+i\Gamma/2}}} \tag{4.30}$$

This expression depends on ω_λ since $\omega_c = \omega_\lambda + \omega_\gamma$.
In the long time limit only the pole $z = \omega_c$ contributes and the amplitude $\mathcal{U}_{ca}(t)$ then reads

$$\mathcal{U}_{ca} = \frac{V_{cb}V_{ba}}{\omega_c-\omega_b+i\Gamma/2}\frac{e^{-i\omega_c t}}{\omega_c - \omega_a + \frac{iC}{\sqrt{\omega_c-\omega_e-\omega_{23}+i\Gamma/2}}} \tag{4.31}$$

The spectrum for the first photon is then readily calculated using Eq. (4.13) and the results are presented in Fig. 4.3. For atomic transition frequencies far outside the gap ($\omega_{12} - \omega_e \gg 0$), the spectrum approaches a Lorentzian. For transition frequencies closer to the band gap edge, the spectrum acquires a divergent tail which becomes increasingly pronounced for atomic transition frequencies inside the gap. This is indeed an unusual effect in an emission spectrum.

4.4 Summary

We have analyzed the emission spectra for a radiative cascade in which the upper or lower atomic transition is coupled near-resonantly to the edge of a photonic band gap. When the atomic transition frequency is tuned far outside the gap, we find the usual Lorentzian spectrum. For atomic transition frequencies in the vicinity of the band gap edge, the spectrum becomes strongly non-Lorentzian and can thus be used to experimentally probe features of the interaction of simple atomic systems with the strongly modified radiation reservoirs inside a photonic band gap.

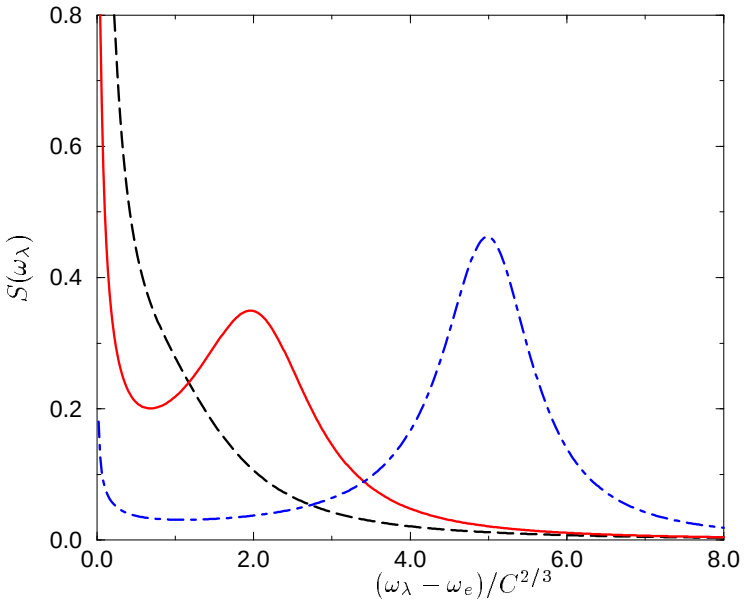

Figure 4.3: The spectrum for the first photon in the radiative cascade is plotted as a function of photon frequency for different detunings $\delta = \omega_{12} - \omega_e$ with respect to the band gap edge $\delta = 0$ (dashed line), $\delta = 2$ (solid line), $\delta = 5$ (dot-dashed line)

Chapter V

Fluorescence into flat and structured radiation continua: An atomic density matrix without a master equation

We investigate an atomic Λ-system with one transition coupled to a laser field and a flat continuum of vacuum modes and the other transition coupled to field modes near the edge of a photonic band gap. The system requires simultaneous treatment of Markovian and non-Markovian dissipation processes, and to treat the system dynamics, we propose a formalism based on the resolvent operator and Monte-Carlo wavefunctions. We demonstrate that the exact results obtained from this formalism are not in accordance with the results obtained from a non-Markovian master equation obtained by applying only the Born approximation thus demonstrating the invalidity of the Born approximation. Finally, we present results relevant to the experimental characterization of a structured continuum.

5.1 Introduction

With the advent of PBG materials and dispersive media, the mode structure of the electromagnetic field can be tailored in a controllable fashion providing for instance band gaps or defect modes of various forms [10, 11]. The rapidly varying mode structure in the radiation reservoir invalidates the Born-Markov approximations normally employed for a simple quantum system like an atom when this is located inside a PBG-material with transition frequency near the edge of the gap. The reservoir degrees of freedom are thus not easily eliminated to derive a master equation for the reduced system dynamics. The main body [32, 33, 1, 2] of theoretical works on atomic interactions within PBG materials has therefore addressed the unitary dynamics in terms of the complete atom(s)+field wavefunctions.
In this chapter, we address a Λ-system with one laser-driven transition experiencing a flat vacuum without structure and the frequency of the other transition

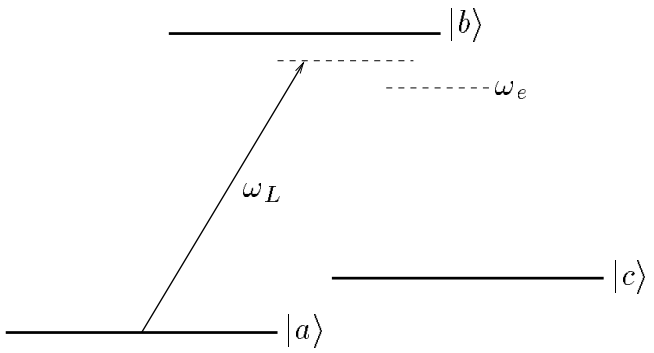

Figure 5.1: Level scheme

near the edge of a PBG. A unitary wavefunction dynamics is incompatible with the treatment of the atomic fluorescence on the "free"-space transition, and we must seek a way to apply the simple Markovian properties of this process in the solution of the complete problem. A formulation in terms of Monte-Carlo wave functions (MCWF) turns out to be particularly useful for this purpose. This method then also suggests itself as a means of solving other problems emerging in the overlapping domain of quantum optics, semiconductors and nano-structures where dissipation of Markovian and non-Markovian character may co-exist. Furthermore, our work establishes an application of the MCWF treatment which goes beyond its conventional correspondence with Born-Markov master equations.
The Λ-system is interesting from an experimental point of view since atoms may be present in their ground state in the dielectric host, and the dynamics of the interaction with the field modes in the vicinity of the gap may be studied when the laser excitation on the "free"-space transition is turned on. In partial analogy with the shelving scheme technique we note that the fluorescence signal on the "free"-space transition may serve as to probe details of the interaction between the atom and the field modes in the PBG material.

5.2 The model

We consider a three-level atom with two lower levels $|a\rangle$ and $|c\rangle$ coupled by the electric dipole coupling to a common excited level $|b\rangle$, see Fig. 5.1. On the $|a\rangle \leftrightarrow |b\rangle$ transition we apply a laser field, and the atom may decay by spontaneous emission due to the coupling to a flat radiation reservoir. The transition $|b\rangle \rightarrow |c\rangle$ is accompanied by the emission of a photon with frequency in the vicinity of the photonic band gap edge, and this atomic transition is significantly modified by the presence of the dielectric host.

Neglecting the zero-point energies of the field modes, and setting the atomic energy levels to the values 0, $\hbar\omega_b$ and $\hbar\omega_c$ respectively, we write the Hamiltonian for the system ($\hbar = 1$)

$$H = H_0 + V \tag{5.1}$$

where

$$H_0 = \omega_b\sigma_{bb} + \omega_c\sigma_{cc} + \sum_\lambda \omega_\lambda a_\lambda^\dagger a_\lambda + \sum_\lambda \omega_\lambda b_\lambda^\dagger b_\lambda \tag{5.2}$$

where the interaction term in the rotating wave approximation is given by

$$\begin{aligned} V &= V_R + V_{pbg} + V_L & (5.3)\\ &= i\sum_\lambda g_\lambda(a_\lambda^\dagger\sigma_{ab} - a_\lambda\sigma_{ba}) + i\sum_\lambda g_\lambda(b_\lambda^\dagger\sigma_{cb} - b_\lambda\sigma_{bc}) \\ &\quad + ig_L(\sigma_{ba}e^{-i\omega_L t} - \sigma_{ab}e^{i\omega_L t}) & (5.4)\end{aligned}$$

where V_R and V_{pbg} denote the couplings to the flat and the PBG-reservoirs, respectively and V_L is the laser coupling, σ_{ij} denote atomic dyadic operators $|i\rangle\langle j|$ with $i, j \in \{a, b, c\}$; a_λ, b_λ are the field annihilation operators of the flat vacuum and PBG vacuum, respectively, and the laser field is represented by a semiclassical c-number field. We assume that the coupling to the flat continuum may be treated by perturbation theory in the usual way, *i.e.* an energy shift (Lamb shift) and a decay rate γ may be attributed to the excited state $|b\rangle$. The Lamb shift is assumed incorporated in the atomic energy ω_b in Eq. (5.1), and the decay rate describes an incoherent transition mechanism by which atoms in the excited state $|b\rangle$ decay to the ground state $|a\rangle$. We shall incorporate the decay mechanism by an effective non-hermitian Hamiltonian H_{eff}

$$\begin{aligned} H_{\text{eff}} &= \omega_b\sigma_{bb} + \omega_c\sigma_{cc} + \sum_\lambda \omega_\lambda b_\lambda^\dagger b_\lambda + i\sum_\lambda g_\lambda(b_\lambda^\dagger\sigma_{cb} - b_\lambda\sigma_{bc}) \\ &\quad + ig_L(\sigma_{ba}e^{-i\omega_L t} - \sigma_{ab}e^{i\omega_L t}) - \frac{i\gamma}{2}\sigma_{bb} & (5.5)\end{aligned}$$

In the next section, we identify the wave function evolution governed by this Hamiltonian, and next, by appealing to the Monte Carlo wave function formalism we shall obtain the exact evolution of the atomic system. In section 5.4, we derive a non-Markovian master equation applying only the Born approximation and compare the resulting dynamics to the exact dynamics obtained from the Monte-Carlo wave function treatment.

5.3 Monte-Carlo wave functions

With the system initially in the lower state a, the resolvent operator equations read

$$(z - 0)G_{aa}(z) = 1 + V_{ab}G_{ba}(z + \omega_L)$$

$$
\begin{aligned}
(z-\omega_\lambda)G_{c_\lambda a}(z) &= V_{c_\lambda b}G_{ba}(z) \qquad (5.6)\\
(z-\omega_b+\frac{i\gamma}{2})G_{ba}(z) &= V_{ba}G_{aa}(z-\omega_L)+\sum_\lambda V_{bc_\lambda}G_{c_\lambda a}(z)
\end{aligned}
$$

where $V_{ab}=g_L$ and the amplitudes $G_{c_\lambda a}(z)$ pertain to the PBG-continuum states $|c\rangle\otimes|1_\lambda\rangle$. Using Eq. (2.29) in the summation over continuum modes and turning the summation into an integral, we get

$$
(z-\omega_b+i\gamma/2)G_{ba}(z)=V_{ba}G_{aa}(z-\omega_L)-\frac{iC}{\sqrt{z-\omega_e-\omega_{ca}}}G_{ba}(z),
$$

where the effective dipole coupling to the mode structure is given by $C=d^2k_0^2\omega_e/(4\pi\varepsilon_0\sqrt{A})$ [2], with d the atomic dipole moment on the $b\leftrightarrow c$ transition. Solving these coupled, algebraic equations for G_{aa} and G_{ba}, we find

$$
\begin{aligned}
G_{aa}(z) &= \frac{(z-\omega_b+i\gamma/2)+iC/\sqrt{z-\omega_e-\omega_{ca}}}{(z-\omega_L)[(z-\omega_b+i\gamma/2)+iC/\sqrt{z-\omega_e-\omega_{ca}}]-|V_{ab}|^2} \qquad (5.7)\\
G_{ba}(z) &= \frac{V_{ba}}{(z-\omega_L)[(z-\omega_b+i\gamma/2)+iC/\sqrt{z-\omega_e-\omega_{ca}}]-|V_{ba}|^2} \qquad (5.8)
\end{aligned}
$$

The dynamics of the system is obtained by inverting the amplitudes to time domain by means of the inversion integral for the time evolution operator. Due to the high order of the polynomial of z in the denominator and the presence of the square root terms in Eqs. (5.7) and (5.8), it is not easy to apply the residue theorem and thus to obtain the amplitudes in time domain analytically. Instead we compute the two inversion integrals numerically. This integration is straightforward, and the calculation yields for example the populations of the initial ground state $|a\rangle$ and of the excited atomic state $|b\rangle$ as functions of time, $\pi_a^0(t)=|\mathcal{U}_{aa}(t)|^2$, $\pi_b^0(t)=|\mathcal{U}_{ba}(t)|^2$. We keep track of the norm $P(t)$ of the wave function, noting that it changes only due to the imaginary part of the excited state energy, and hence

$$
\frac{\partial P}{\partial t}|_{loss}=-\gamma\pi_b^0(t) \qquad (5.9)
$$

which in integrated form reads

$$
P(t)=1-\gamma\int_0^t dt'\pi_b^0(t'), \qquad (5.10)
$$

In Fig. 5.2 we show an example of the relevant time dependent quantities $P(t)$, $\pi_a^0(t)$ and $\pi_b^0(t)$. From the figure, it is evident that the populations in the states $|a\rangle$ and $|b\rangle$ approach zero after a transient evolution. There is, however, a substantial part of the population ($P(\infty)\sim 20\%$) which is not lost by fluorescence on the free-space transition. This population is transferred to the atomic state $|c\rangle$ associated with the PBG-continuum, and at any time we have $\pi_c^0(t)=P(t)-\pi_a^0(t)-\pi_b^0(t)$.

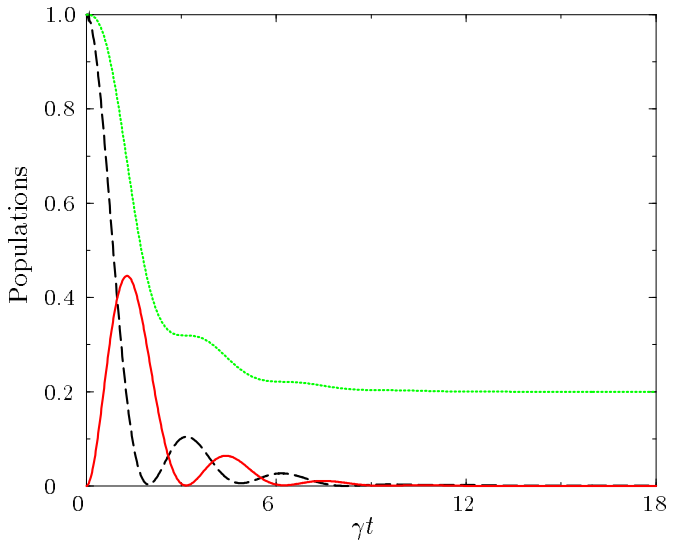

Figure 5.2: The populations $\pi_a^0(t)$ (dashed line), $\pi_b^0(t)$ (solid line) and the norm $P(t)$ (dotted line) are plotted as functions of time. The parameters chosen are: $C^{2/3} = \gamma/3, V_{ab} = \gamma, \omega_e = \omega_b$.

The spontaneous decay on the $|b\rangle \rightarrow |a\rangle$ transition was treated only as a loss mechanism for the excited state amplitude, but the atoms are incoherently fed back in the ground state $|a\rangle$, and from here they are re-excited by the laser. In a density matrix formulation, when tracing over the resulting different photon number states of the flat reservoir, the elimination of the PBG-modes would be exceedingly difficult, if possible at all.
It has been shown that dissipative problems in quantum mechanics may be solved by stochastic wave function equations as an alternative to master equations [57, 58, 59, 60, 61]. In the "quantum jump" scheme, one propagates state vectors according to a non-hermitian Hamiltonian, and at certain instants of time, chosen according to a random process, this propagation is interrupted by quantum jump projections of the state vectors (see [62] for a recent review). In the formulations of the method so far, the continuously propagated state vector is described as the solution of a Schrödinger equation, but, the atomic populations $\pi_i^0(t)$ identified after elimination of the PBG reservoir above may be applied just as well for the construction of the atomic density matrix.
The function $P(t)$ is the norm of the no-jump state vector [60] and consequently the probability that a photon has not been registered in the flat reservoir at time

t.
The ensemble averaged populations can be found by solution of integral equations: The population of an atomic state $\overline{\pi}_i(t)$ is a sum of a term representing the population given that the atom has not decayed and a term representing the population given that the latest jump occurred at time t',

$$\overline{\pi}_i(t) = \pi_i^0(t) + \int_0^t dt' \gamma \overline{\pi}_b(t') \pi_i^0(t-t'). \tag{5.11}$$

Note that $\pi_i^0(t-t') = \pi_i^0(t-t')/P(t-t') \cdot P(t-t')$ provides the given normalized population with the appropiate no-jump weight-factor. Eq.(5.11) must be solved for $\overline{\pi}_b(t)$ first, *e.g.* by a Laplace transform: $\overline{\pi}_b(z) = \pi_b^0(z)/(1-\gamma\pi_b^0(z))$, and one may subsequently obtain the other populations (see also [63]).
The populations can of course also be found by simulations. In a single trajectory one considers the normalized populations $\pi_i(t) = \pi_i^0(t)/P(t)$ (and other density matrix elements if necessary), until a jump occurs when $P(t)$ equals a random number ε chosen uniformly on the interval betwen zero and unity. The quantum jump puts the atom in the state $|a\rangle$, and from here the evolution starts over again. In Fig. 5.3, we plot $\overline{\pi}_a(t)$ and $\overline{\pi}_b(t)$ obtained by an average of 10^4 stochastic wave functions for the same parameters as used in Fig. 5.2.

Let us comment on the atomic dynamics obtained in Fig. 5.3. After an initial transient evolution, the populations $\overline{\pi}_{a,b}(t)$ approach zero in a non-exponential way. The fluorescence signal on the $|b\rangle \to |a\rangle$ transition thus vanishes as opposed to the case of a two-level atom in free space. In the simulations we note that no jump will occur if the random number ε is smaller than $P(\infty)$. When this value is non-zero, each realization only exhibits a limited number of jumps since eventually the value chosen for ε will be smaller than $P(\infty)$. The probability of having exactly k photon emissions (jumps) in a given simulated trajectory is $(1-P(\infty))^k P(\infty)$, and the mean number of photons $\bar{n}$ emitted per atom is thus

$$\bar{n} = \sum_{k=0}^{\infty} kP(\infty)(1-P(\infty))^k = P(\infty)^{-1} - 1 \tag{5.12}$$

$P(\infty)$ can be calculated in the following way: The amplitude $\mathcal{U}_{c_\lambda a}(t)$ is the inverse Laplace transform of

$$G_{c_\lambda a} = V_{c_\lambda b} G_{ba}/(z-\omega_\lambda) \tag{5.13}$$

In the long time-limit only the pole $z = \omega_\lambda$ contributes and the Residue Theorem can thus be applied to the inversion integral for $G_{c_\lambda a}$ to yield

$$\mathcal{U}_{c_\lambda a}(t) = V_{c_\lambda b} G_{ba}(\omega_\lambda) e^{-i\omega_\lambda t} \tag{5.14}$$

and since $P(\infty) = \pi_c^0(\infty)$ we find

$$P(\infty) = \sum_\lambda |V_{c_\lambda b} G_{ba}(\omega_\lambda)|^2$$

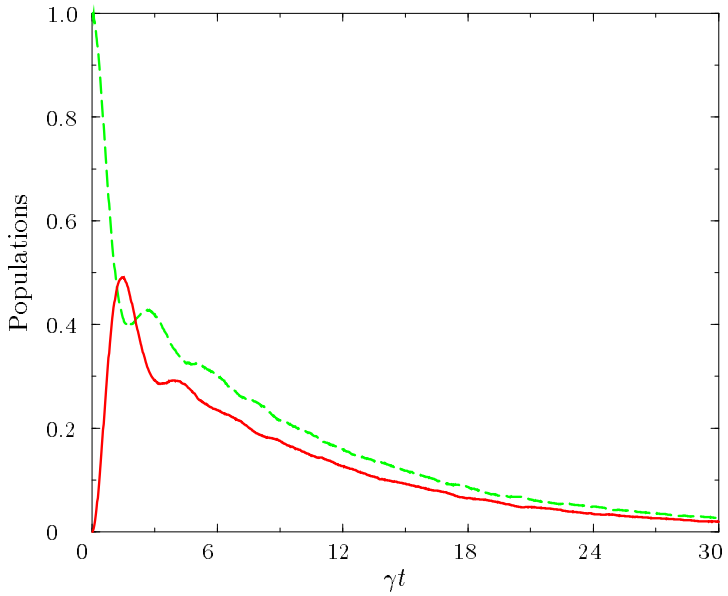

Figure 5.3: The populations $\overline{\pi}_a(t)$ (dashed line) and $\overline{\pi}_b(t)$ (solid line) are plotted as functions of time. The parameters chosen are the same as in Fig. 2. The curves are averaged over 10^4 trajectories.

The summation over modes can be turned into an integral, which is calculated numerically.
For a Λ-system in free space with a branching of the decay from the upper state, there will also be a finite number of fluorescence photons emitted on the laser driven transition, corresponding to $P(\infty) = \gamma'/(\gamma+\gamma')$ with γ, γ' being the decay rates of state $|b\rangle$ to the states $|a\rangle$ and $|c\rangle$ respectively, and the total number of fluorescence photons on the $|b\rangle \rightarrow |a\rangle$ transition is thus independent of the parameters of the driving field for a Λ-system in free space. This is different in our case, as seen in Fig. 5.4, where $P(\infty)$ and the mean number of fluorescence photons emitted on the free space transition are plotted as functions of the laser detuning from the PBG edge for different choices of the laser coupling. For a rather weak laser coupling, the transition to the atomic state $|c\rangle$ is a Raman-process which is strongly suppressed when the laser is tuned below the band gap edge since there are then no resonant PBG-modes for the Stokes photon. A stronger laser coupling leads to an Autler-Townes splitting of level $|b\rangle$ and population is then transferred to the PBG-continuum by a higher order process, removing the step-like character of $P(\infty)$. The fluorescence signal may hence

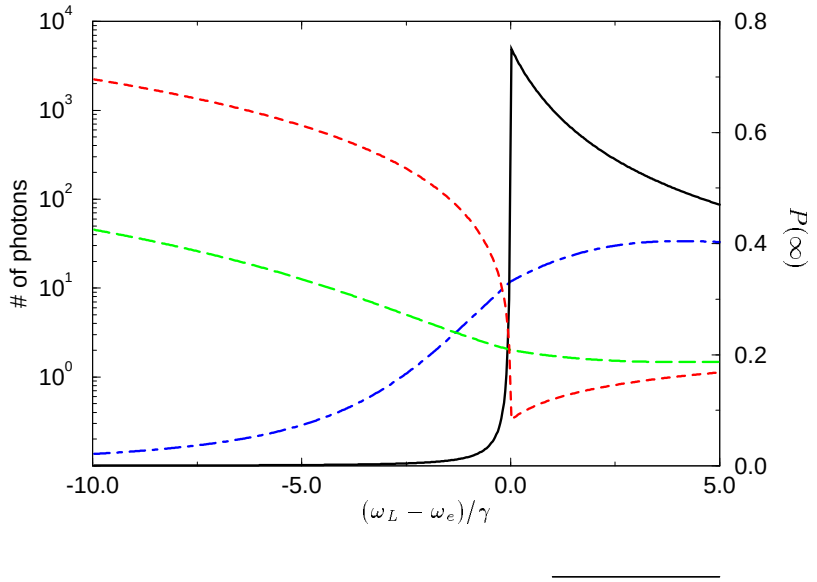

Figure 5.4: Solid line is $P(\infty)$ for $V_{ab} = \gamma/2$ and dashed line the number of fluorescence photons. The dot-dashed line is $P(\infty)$ for $V_{ab} = 3\gamma$ and the long-dashed line the number of fluorescence photons. The parameters chosen: $C^{2/3} = \gamma$, $\omega_b = \omega_e$

probe details of the PBG structure.

5.4 A master equation in the Born-approximation

We just presented an exact treatment of the problem by means of a mixture of resolvent operator and Monte-Carlo wave function techniques. A more conventional approach is to derive a reduced master equation (ME) governing only the motion of the atomic system. To this end we have to apply the Born-approximation to the density operator for the system consisting of Λ-system+PBG-reservoir in order to eliminate the PBG-reservoir.
In this section the derivation of the non-Markovian master equation for the Λ-system is presented, employing only the Born approximation and the resulting dynamics obtained from propagation of the master equation is compared to the exact results obtained using the methods described in the previous secton.
The density operator ρ_T for the total system consisting of Λ-system+reservoirs

obeys the equation of motion

$$\frac{d}{dt}\rho_T = \frac{1}{i}[V(t), \rho_T(t)] \tag{5.15}$$

where V is the interaction term given by Eq. (5.4) and we have transformed to an interaction picture rotating at frequency ω_{ba} thus eliminating the free energies in H_0. By a formal integration of Eq. (5.15), we find

$$\begin{aligned}\frac{d}{dt}\rho_T &= \frac{1}{i}[V_L(t), \rho_T(t)] \\ &\quad + \frac{1}{i}[V_R(t) + V_{pbg}(t), \rho_T(0) + \frac{1}{i}\int_0^t dt'[V(t'), \rho_T(t')]]\end{aligned} \tag{5.16}$$

To proceed, we apply the Born-approximation which asserts that correlations between the atom and the reservoirs can be neglected i.e.

$$\rho_T(t) = \rho_A(t) \otimes \rho_{PBG} \otimes \rho_R \tag{5.17}$$

where $\rho(t)$ is the atomic density operator and ρ_R, ρ_{PBG} are the density operators for the flat and the PBG reservoirs, respectively. We further assume that the reservoirs are in thermal equilibrium i.e. all off-diagonal elements are zero and that there are no thermal photons in the reservoirs.
Following the usual steps [64, 41] we find the following equation of motion for the atomic density operator ρ.

$$\begin{aligned}\frac{d}{dt}\rho &= \frac{1}{i}[V_L(t), \rho] + \frac{\gamma}{2}[2\sigma_{ba}\rho\sigma_{ab} - \sigma_{bb}\rho - \rho\sigma_{bb}] \\ &+ \sum_\lambda g_\lambda^2 \int_0^t dt' e^{i\Delta_\lambda(t-t')}[\sigma_{cb}\rho(t')\sigma_{bc} - \rho(t')\sigma_{bb}] \\ &+ \sum_\lambda g_\lambda^2 \int_0^t dt' e^{-i\Delta_\lambda(t-t')}[\sigma_{cb}\rho(t')\sigma_{bc} - \sigma_{bb}\rho(t')]\end{aligned} \tag{5.18}$$

where the Markov-approximation has been applied to the flat reservoir thus yielding the well-known Lindblad form for the spontaneous decay. The remaining summation over modes is a summation over the PBG-continuum. This summation can be performed using Eq. (3.31)

$$\sum_\lambda g_\lambda^2 e^{i\Delta_\lambda(t-t')} = \frac{C e^{i(\omega_e - \omega_{bc})(t-t') + i\pi/4}}{\sqrt{\pi}\sqrt{t-t'}} \tag{5.19}$$

Inserting the expressions for the coupling to the PBG-continuum, we finally find the equation of motion for the reduced density operator [49]

$$\frac{d}{dt}\rho = \frac{1}{i}[V_L(t), \rho] + \frac{\gamma}{2}[2\sigma_{ba}\rho\sigma_{ab} - \sigma_{bb}\rho - \rho\sigma_{bb}]$$

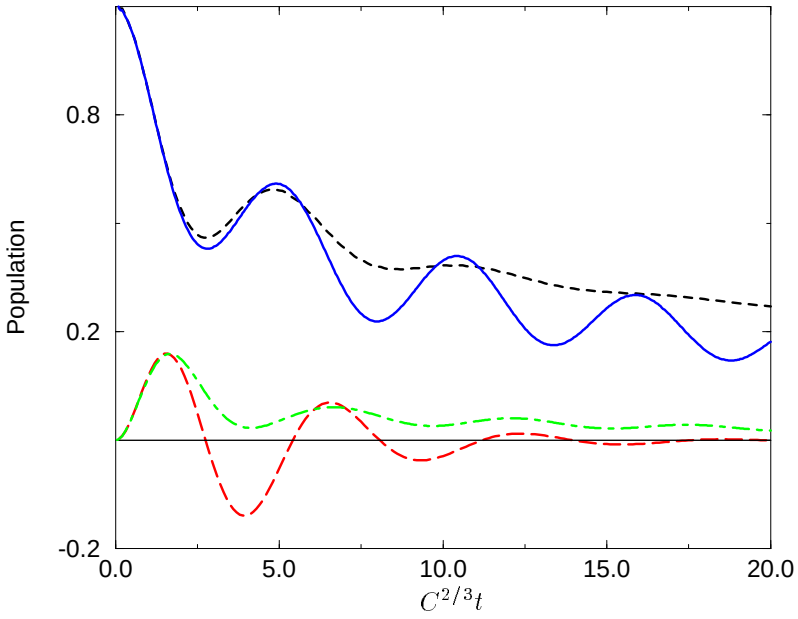

Figure 5.5: The populations in state a and b are plotted as functions of time. The solid (dashed) line is the population in state a obtained by MCWF (the Born-ME). The dot-dashed (long-dashed) curve is the population in state b obtained by MCWF (Born-ME). The parameters chosen are $\delta_{bL} = \delta_{be} = 0$, $V_{ab}/C^{2/3} = 1/2$, $\gamma/C^{2/3} = 0.1$.

$$+\int_0^t dt' \frac{Ce^{i\delta_{bc}(t-t')-i\pi/4}}{\sqrt{\pi}\sqrt{t-t'}}[\sigma_{cb}\rho(t')\sigma_{bc} - \rho(t')\sigma_{bb}]$$
$$+\int_0^t dt' \frac{Ce^{-i\delta_{bc}(t-t')+i\pi/4}}{\sqrt{\pi}\sqrt{t-t'}}[\sigma_{cb}\rho(t')\sigma_{bc} - \sigma_{bb}\rho(t')] \qquad (5.20)$$

where $V_L(t) = ig_L(\sigma_{ba}e^{-i(\omega_L-\omega_{ba})t} - \sigma_{ab}e^{i(\omega_L-\omega_{ba})t})$ and $\delta_{bc} = \omega_{bc} - \omega_e$.
The non-Markovian nature of the master equation i.e. the convolution integral complicates a direct propagation in time domain. Transforming the equation to Laplace space, the convolution turns in to a direct product and by projecting the density operator on the atomic states, closed analytical expressions for the various populations and coherences can be derived and the expression for the

upper state population reads

$$\rho_{bb}(z) = \frac{1}{z}\frac{V_{ab}^2(\alpha_1+\alpha_2)}{z+i\gamma+\beta-V_{ab}^2[2+\beta/z](\alpha_1+\alpha_2)} \tag{5.21}$$

with

$$\begin{aligned}
\beta &= \frac{iC}{\sqrt{z+\delta_{be}}} - \frac{C}{\sqrt{z-\delta_{be}}} \\
\alpha_1 &= \frac{1}{z+\delta_{bL}+i\gamma/2-\frac{C}{\sqrt{z-\Delta}}} \\
\alpha_2 &= \frac{1}{z-\delta_{bL}+i\gamma/2+i\frac{C}{\sqrt{z+\Delta}}}
\end{aligned}$$

and for the lower state

$$\rho_{aa}(s) = 1/z - (1+\beta/z)\rho_{bb}(s) \tag{5.22}$$

and the detunings are given by $\delta_{bL} = \omega_{ba} - \omega_L$, $\delta_{be} = \omega_{bc} - \omega_e$ and $\Delta = \delta_{be} - \delta_{bL}$. The expressions are inverted to time domain by numerically evaluating the Laplace inversion integral. In Fig. 5.5, we plot the populations in state a and b as functions of time obtained by inverting Eqs. (5.21) and (5.22) to time domain. The agreement is rather poor and in particular we find the pathological effect of negative values for the probability of being in the upper state b. In Fig. 5.6, we plot the population in state a as a function of time when the laser is resonant with the upper state b which is detuned inside the photonic band gap. In this case we find a better agreement between the exact MCWF-treatment and Eqs. (5.22) but still the ME does not get the oscillation period and amplitudes completely right. For larger detunings from the band gap edge or stronger laser couplings, the atomic levels are removed even further from the band gap edge into the flat part of the continuum. This will of course increase the validity of the ME. It is, however, also the regime where an ordinary Born-Markov master equation becomes valid. For many purposes, the interesting domain is, however, for atomic transition frequencies in the vicinity of the band gap and for laser couplings that do not exceed the PBG coupling and in that case, the Born approximation is invalidated.

5.5 Conclusions

In this chapter we investigated the dynamics of an atomic lambda-system with one transition coupled to a laser field and a flat continuum of vacuum modes and the other transition coupled to field modes near the edge of a photonic band gap. A reduced non-Markovian master equation was derived applying *only* the Born-approximation.

In parallel we solved the dynamics exactly using a technique involving the resolvent operator and Monte-Carlo wave functions. Comparing the resulting

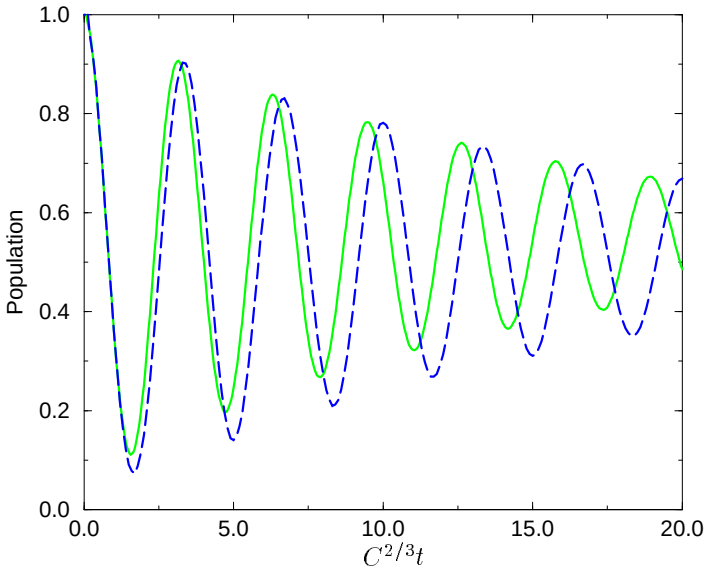

Figure 5.6: The population in state a is plotted as function as time. The solid curve is obtained by MCWF and the dashed curve is obtained by inversion of Eqs. (5.22). The parameters chosen are $\delta_{bL} = 0$, $\delta_{be}/C^{2/3} = -3$, $V_{ab} = C^{2/3}$ and $\gamma/C^{2/3} = 0.1$.

dynamics of the two approaches we found a very poor agreement of the non-Markovian master equation with the exact results thus invalidating the use of the Born-approximation.
The Born-approximation neglects correlations between the atom and the reservoir modes and it may therefore not be surprising that the Born-approximation is invalidated since an atom near-resonant with a photonic band gap edge may form a photon-atom bound state in which the correlations to the reservoir modes are essential.
In conclusion we have demonstrated a technique for the solution of a problem for which a Born-Markov master equation does not exist.
The specific form of the structured continuum is not essential for our approach, but it is important that only one photon states of the PBG-continuum appear (a possible slow decay from state $|c\rangle$ back to $|a\rangle$ can only be treated if we may assume that the photon in the PBG continuum escapes before the atom is re-excited to level $|b\rangle$). The simulations and the analytical expression Eq. (5.11) are simplified by the fact that all jumps put the atom in the same state. Our formalism, however, is perfectly capable of treating more general systems with

branching of the decay from state $|b\rangle$ to multiple states $|a_j\rangle$. This implies that the index a is replaced by the set of indices a_j with the corresponding enlargement of the set of equations (5.6) and (5.11). The no-jump evolution and the associated delay function, following a jump to a given level a_j, are then readily computed.

The MCWF technique has been applied to non-Markovian problems through the solution of Markovian master equations for enlarged model systems [65]. Our situation, however, is different, since without ever having a master equation we have, by recourse to conditioned wave function dynamics, been able to obtain the atomic density matrix. We anticipate that by combination of the ideas in ref. [65] and in this chapter a wide class of non-Markovian problems may become tractable.

Chapter VI

Superradiance in a structured radiation reservoir

An atomic Dicke system is coupled to a photonic band gap continuum, which we model by a Fano-profile density of states. By introduction of two pseudo-modes, a markovian master equation can be derived governing only the degrees of freedom of the atoms+the two pseudo-modes. One of the modes can be adiabatically eliminated and effectively we then have an atomic Dicke system coupled to a harmonic oscillator and both systems coupled to the same flat continuum. We find that following the superradiant regime, a meta-stable state is reached for the atomic system. The decay of the meta-stable state is non-exponential and we derive an analytical expression for the decay based on perturbation theory and trapping states identified by the Monte-Carlo wavefunction method. Further, we investigate mean-value equations of motion for the operators of the system and discuss different decorrelation approximations of the operator expectation values.

6.1 Introduction

Recently, the interaction of one or more atoms with the strongly modified radiation reservoir inside a photonic band gap (PBG) material [11, 10] has attracted considerable attention [2, 3, 4, 32, 33, 55]. A common feature of these studies is the fact that only the zero- and one-photon parts of the reservoir Hilbert space were involved and consequently the atomic dynamics could be solved in terms of wave functions for the complete system atom(s)+field [2, 3, 4, 32, 33, 55]. In the more general case where several excitations of the structured continuum are involved, the wave function formalism becomes intractable due to multiple integrations over photonic continua. Ideally, we would then prefer a reduced master equation governing only the dynamics of the atoms. It does not, however, seem possible to derive a master equation since the Born-Markov approximations normally applied are invalid for atomic transition frequencies close to the edge of the band gap. The Markov approximation assuming a "flat" reservoir in the vicinity of the atomic transition frequency is obviously invalidated but also the Born approximation which assumes that correlations between the small quan-

tum system and the "large" reservoir are negligible, is no longer valid.
Since the standard methods thus fail, it is not evident how to treat a problem with multiple excitations in the structured continuum. In a recent paper [46], John and Quang studied superradiance[36, 37] in a PBG and to obtain a closed set of equations of motion for the atomic operator expectation values they proposed a mean-field Ansatz to the Heisenberg picture equations of motion for the atomic operators. In this way they could obtain a closed set of non-Markovian equations of motion for the atomic operators. However, since they could not obtain a master equation they could not assess the validity of the mean-field Ansatz.
In this chapter [5] we investigate an atomic Dicke system [36] coupled to a PBG which we model by a Fano-profile density of states. Although our model does not possess a full gap it nevertheless shares a number of features with a full band gap while at the same time it lends itself to definitive quantitative conclusions. Due to the analyticity of the density of states, we can apply methods proposed by Imamoglu [65, 66] and Garraway [67, 68], in which a finite number of pseudo-modes are introduced and treated on an equal footing with the atomic degrees of freedom, to obtain a Markovian master equation for the atoms+pseudo-modes and we can now study processes with multiple photon emissions into the radiation reservoir.
Our model allows us to perform a mean-field approximation to the equations of motion for the atomic operator expectation values and the resulting dynamics is compared to the exact results obtained by propagation of the master equation. In this way we can actually test the validity of the mean-field approximation. We further study the effects of the modified radiation reservoir on superradiance [46, 36, 37]. When the atomic transition frequency is tuned close to the minimum in the density of states, we find that following the superradiant emission, a meta-stable state is reached in which a significant part of the excitation remains bound at the site of the atoms. This state, then, is a slowly decaying photons-atoms bound state. The existence of such a state is in contrast to a Dicke system in free space, where the atoms lose all their excitation in a superradiant pulse to the modes of the reservoir. The decay of the meta-stable state is non-exponential and we derive an analytical expression for the decay based on perturbation theory and analytical expressions for trapping states identified by appealing to the Monte-Carlo wave function method.
This chapter is organized as follows: In section 6.2, we present the model and derive a master equation for the Dicke system interacting with two pseudo-modes. One of the modes can be adiabatically eliminated and effectively we then have a master equation for a Dicke system coupled to a pseudo-mode and both systems decaying to the same flat reservoir. In section 6.3, we present the dynamics of the system and find that a significant part of the excitation remains trapped after the superradiant regime. This is discussed in greater detail in section 6.4 and in section 6.5 we derive an analytical expression for the decay rate of the meta-stable state. In section 6.6, we derive mean-values (semi-classical) equations for the system and discuss various decorrelation approximations.

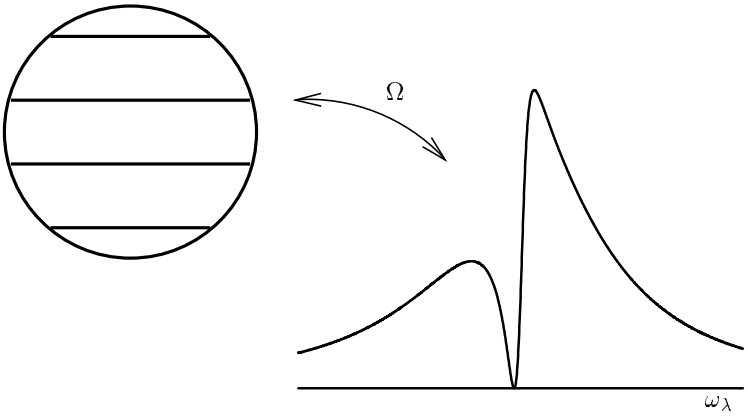

Figure 6.1: The atomic Dicke system (illustrated by the sphere) is coupled to a Fano-profile density of modes.

6.2 The model

We study the dynamics of one or several two-level atoms identically coupled to a structured radiation reservoir which we model as a Fano profile as illustrated in Fig. 6.1. The model Hamiltonian for the system reads in an interaction picture ($\hbar = 1$)

$$H_F = \omega_{21} J_z + \sum_\lambda \omega_\lambda a_\lambda^\dagger a_\lambda + \sum_\lambda g_\lambda (a_\lambda^\dagger J^- + a_\lambda J^+) \tag{6.1}$$

where $a_\lambda^\dagger, a_\lambda$ are the creation and annihilation operators of the reservoir mode λ with energy ω_λ and coupling constant

$$g_\lambda = \sqrt{\frac{\omega_\lambda}{2\varepsilon_0 V_q}} \mathbf{e}_\lambda \cdot \mathbf{d}_{12} \tag{6.2}$$

Here $\mathbf{d}_{12}$ is the atomic dipole moment, V_q the quantization volume and $\mathbf{e}_\lambda$ the polarization vector. The macroscopic atomic inversion and dipole operators J_z, J^+, J^- are defined by $J^+ = \sum_i |2\rangle_{ii}\langle 1|$, $J^- = \sum_i |1\rangle_{ii}\langle 2|$ and $J_z = \sum_i (|2\rangle_{ii}\langle 2| - |1\rangle_{ii}\langle 1|)$ where $|2\rangle_i, |1\rangle_i$ are the upper and lower levels of atom i, respectively and ω_{21} is the atomic transition frequency. The atomic operators obey the commutation relations of angular momenta: $[J^+, J^-] = 2J_z$, $[J_z, J^+] = J^+$ etc., and the atomic product state can thus be represented by the so-called Dicke states $|jm\rangle$, where $j = N/2$ with N being the number of atoms and $m \in [-j : j]$ is a measure of the number of atomic excitations.
The structure of the continuum enters through the summation over modes in

the interaction term. We model the structure of the continuum as a Fano profile and the density of states thus reads

$$\rho(\omega) = \frac{f}{(\omega-\omega_c)^2+(\kappa/2)^2}\frac{(q+\omega-\omega_c)^2}{(\omega-\omega_c)^2+(\gamma/2)^2}, \tag{6.3}$$

where γ and q are parameters describing the structure of the continuum. The Lorentzian of width κ ($\kappa \gg \gamma, q$) ensures that the density of states is normalizable such that

$$\int_{-\infty}^{\infty} d\omega\, \rho(\omega) = 2\pi \tag{6.4}$$

which determines the value of the normalization constant f

$$f = \frac{\gamma+\kappa}{4q^2/\gamma\kappa+1} \tag{6.5}$$

The density of states is zero at frequency $\omega = \omega_c - q$. Since the density of states is zero in a point and not in an interval, we expect aspects such as population trapping to be very sensitive with respect to the detuning from ω_c.
Strictly speaking, Eq. (6.3) does not represent a Fano-profile due to the presence of the extra Lorentzian but in the following calculations, we investigate the dynamics of the system in the limit $\kappa \gg \Omega, q, \gamma$ and effectively the atoms are then coupled to a radiation reservoir with a Fano-profile.

6.2.1 Pseudo-mode description

To derive a master equation we replace summations over modes by integrations

$$\sum g_\lambda^2 \to \frac{\Omega^2}{2\pi}\int d\omega\, \rho(\omega) \tag{6.6}$$

where Ω contains the atomic dipole and we apply the method developed by Imamoglu and Garraway [65, 67, 68] in which pseudo-modes are introduced to model the structures in the continuum. For a density of states which is normalizable and only contains poles in the lower half of the complex plane, the idea is to introduce a pseudo-mode associated with each pole. The poles of the density of states Eq. (6.3) located in the lower half of the complex plane are $\omega = \omega_c - i\gamma/2$ and $\omega = \omega_c - i\kappa/2$ and the coupling strengths between the atomic Dicke system and the pseudo-modes are determined by the formalism in Ref. [67]. The effect of the structured continuum on the atomic dynamics can thus be represented by two coupled pseudo-modes both coupled to the atoms. The system is described by the Hamiltonian

$$\begin{aligned} W &= \omega_{21}J_z + \omega_c a_1^\dagger a_1 + \omega_c a_2^\dagger a_2 \\ &\quad + V_{12}(a_2 a_1^\dagger + a_2^\dagger a_1) + g_2(J^+ a_2 + J^- a_2^\dagger) + g_1(a_1^\dagger J^- + a_1 J^+) \end{aligned} \tag{6.7}$$

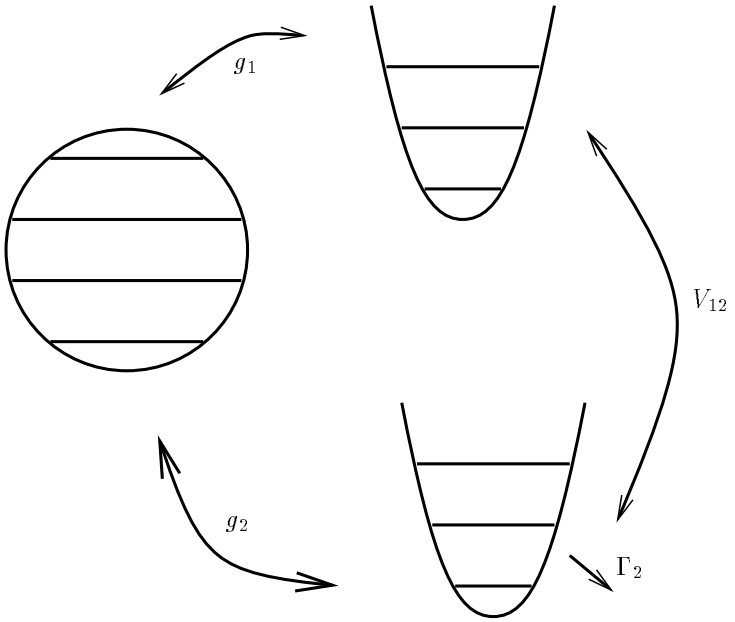

Figure 6.2: The radiation reservoir with a Fano-profile density of modes can be eliminated by introduction of two pseudo-modes coupled to the Dicke system as depicted above.

where

$$V_{12} = \sqrt{\gamma\kappa}/2 \tag{6.8}$$

$$g_1 = \Omega q\sqrt{\frac{1}{q^2+\gamma\kappa/4}} \tag{6.9}$$

$$g_2 = \frac{\Omega}{2}\sqrt{\frac{1}{q^2/\gamma\kappa+1/4}} \tag{6.10}$$

and is depicted in Fig. 6.2. The pseudo-mode 2 is damped, and the atoms (and the pseudo-mode 1) only experience dissipation via the coupling to this mode. The master equation for the coupled system reads

$$\dot{\rho} = \frac{1}{i}[W,\rho] + \frac{\Gamma_2}{2}[2a_2\rho a_2^\dagger - a_2^\dagger a_2\rho - \rho a_2^\dagger a_2] \tag{6.11}$$

where

$$\Gamma_2 = \kappa+\gamma \tag{6.12}$$

6.2.2 Adiabatic elimination of strongly damped mode

To ensure that the density of states is normalizable, we multiplied it with a Lorentzian of width κ. If κ is much larger than the other couplings Ω, γ, q entering the problem, the dynamics of the pseudo-mode 2 is strongly damped and the mode can be adiabatically eliminated. Consequently we need only consider the zero and one-photon components of mode 2. Retaining these components and tracing over mode 2, the following master equation is derived

$$\dot{\rho} = \frac{1}{i}[W', \rho] + \frac{2}{\Gamma}[2S^- \rho S^+ - S^+ S^- \rho - \rho S^+ S^-] \tag{6.13}$$

where

$$W' = \Delta J_z + g_1(a^\dagger J^- + a J^+) \tag{6.14}$$

and we have transformed the master equation to an interaction picture rotating at frequency ω_c. Thus $\Delta = \omega_{21} - \omega_c$ and we have introduced the operator S^- given by

$$S^- = V_{12} a + g_2 J^- \tag{6.15}$$

Effectively, the adiabatic elimination leaves us with an atomic system coupled to a harmonic oscillator and both systems coupled directly to the same flat reservoir.
Since we are left with a system with only one oscillator mode, the index 2 on the decay rate Γ has been omitted and the index 1 has been omitted on the annihilation and creation operators of the field mode.
Starting from a structured reservoir where the usual Born-Markov approximations are invalid, we have thus derived a master equation. In order to make this master equation Markovian, it was necessary to introduce two pseudo-modes. This is, however, a small complication compared to the benefits of having a Markovian instead of a non-Markovian master equation.

6.3 Dynamics

The dynamics of the coupled system consisting of Dicke states+pseudo-mode is obtained by propagation of the master equation Eq. (6.13) from which we can also determine the evolution of all operators of the system. An alternative but equivalent approach is to apply Monte-Carlo wave functions [58, 59, 57, 60, 62]. To this end we propagate the wave function $|\psi\rangle$ of the system using the effective non-hermitian Hamiltonian

$$H_{\text{eff}} = \Delta J_z + g_1(a^\dagger J^- + a J^+) - \frac{2i}{\Gamma} S^+ S^- \tag{6.16}$$

interrupted by quantum jumps with the jump operator $\sqrt{\frac{2}{\Gamma}} S^-$. The non-hermiticity of the effective Hamiltonian H_{eff} implies that the norm of the wave

function is not conserved, and the quantum jumps occur when $\|\psi\|^2 = \varepsilon$ where $\varepsilon \in [0:1]$ is chosen stochastically. In each jump event, the system loses an excitation and the post-jump wave function $|\psi\rangle$ is given by

$$|\psi\rangle \to S^-|\psi\rangle / \|S^-|\psi\rangle\| \tag{6.17}$$

The denominator ensures that the post-jump wave function is normalized and a new random value is chosen for ε which determines the occurence of the subsequent quantum jump. The results are averaged over a large number of independent realizations.

In the following, it will be convenient to refer to subspaces containing states with the same number of excitations. We refer to these subspaces as *layers* and to characterize the layers, we introduce the quantum number $k = m+n$ where m is a Dicke state atomic quantum number and n is the number of photons in the pseudo-mode. One layer thus consists of all product states $|m,n\rangle \equiv |jm\rangle \otimes |n\rangle$ for which $m+n$ assumes the same value. The effect of a jump is to move the dynamics of the system from layer k to layer $k-1$.

Between jumps the dynamics is determined by the effective Hamiltonian Eq. (6.16) and since it only couples states with the same number of excitations, only states within the same layer are coupled. If in addition the system be initially in a state with a specific number of excitations i.e. within one layer, the state of the system at any later instant is also restricted to just one layer. This means that at any instant of a simulation we only have to propagate wave function amplitudes corresponding to the number of states within a single layer. It also proves convenient to view the dynamics of the system from a wave function point of view when we discuss population trapping and dynamics in the long time limit.

We shall now present the evolution of the system determined by propagation of Monte-Carlo wave functions.

In Fig. 6.3, the atomic inversion is plotted as function of time for various values of the atomic detuning from the pseudo-mode frequency $\Delta = \omega_{21} - \omega_c$. From the figure we find that the short-time dynamics is superradiant for all detunings. When the detuning is large and positive (the dot-dashed) curve, we find a dynamics which resembles that of a superradiant system in free space. However, for smaller and negative detunings, the superradiant behavior is turned off before the Dicke system has lost all its excitation. For those detunings the Dicke system reaches a meta-stable state in which a significant part of the excitation remains bound at the atoms. In particular, we find that the detuning $\Delta = -\sqrt{2j+1}g_1$ yields a very slowly decaying state and we return in section 6.5 to a discussion of this result. For larger, negative detunings (the solid curve), the meta-stable state disappears again.

The atomic Dicke system is coupled to a Fano-profile density of modes. When the atomic system is tuned close to a minimum in the density of modes, the atomic decay must be suppressed since the atomic decay according to Wigner-Weisskopf theory is proportional to the local density of modes of the reservoir. This actually served as a motivation for studying this particular choice for the

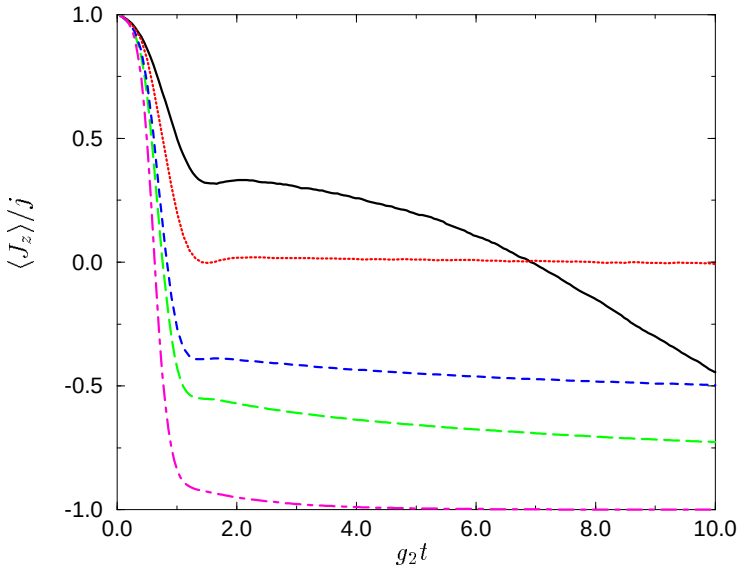

Figure 6.3: The atomic inversion $\langle J_z \rangle$ is plotted as function of time for various detunings $\Delta = \omega_{21} - \omega_c$. $\Delta = -4g_2$ (solid curve), $\Delta = -\sqrt{2j+1}g_1 (\approx -2.82 g_2)$ (dotted curve), $\Delta = -g_2$ (dashed curve), $\Delta = 0$ (long-dashed curve) and $\Delta = 4$ (dot-dashed curve). The parameters chosen are $g_1/g_2 = 0.2$, $V_{12}/g_2 = \sqrt{2j+1}$, $\Gamma/g_2 = 101$ and $j = 100$. The curves are obtained by simulation of the master equation and averaged over 100 trajectories.

density of modes.
We can also explain the meta-stable state in terms of the pseudo-mode picture: From the master equation Eq. (6.13), we find that the atoms and the pseudo-mode are coupled to the same flat reservoir (through the operator S^-). This implies interference because whenever we detect a photon emitted from this system, we can not tell whether this photon was emitted from the atoms or from the pseudo-mode. The photon in the continuum thus represents a final state reached through two different paths. In this picture, the meta-stable state is thus due to a quantum interference between the atoms and the pseudo-mode. The sensitive behavior of the inversion on the detuning has also been found for single atom dynamics in other models of PBG-reservoirs [32, 33, 67, 68, 69].

6.4 Population trapping

In the previous section, we presented numerical results for the dynamics of the system. For a wide range of parameters, we found that the system after a superradiant regime reaches a meta-stable state in which a significant part of the excitation remains bound at the atoms. This is a feature that our model shares with PBG models previously studied [32, 33, 46, 67, 68, 69].
We now address this behavior and in the next section we derive an analytical expression for the decay rate in the long-time limit. But as a first step, we show in this section the existence of a trapping state within each layer which is an exact eigenstate of the dissipative part of the Hamiltonian with eigenvalue zero. A non-trivial state $|k_0\rangle$ obeying $S^-|k_0\rangle = 0$ can be expanded in the product state basis, $|m,n\rangle$, as $|k_0\rangle = \sum_m c_m^k |m, k-m\rangle$ where k is the number of the layer and $n = k - m$, and we thus find

$$\begin{aligned} S^-|k_0\rangle &= \sum_m c_m^k \Big[V_{12}\sqrt{k-m}|m, k-m-1\rangle \\ &+ g_2 \sqrt{j(j+1)-m(m-1)}|m-1, k-m\rangle \Big] \end{aligned} \tag{6.18}$$

Coefficients of each state must vanish which provides the following recursive relation

$$0 = c_m^k V_{12}\sqrt{k-m} + c_{m+1}^k g_2 \sqrt{j(j+1)-m(m+1)} \tag{6.19}$$

from which the amplitudes of the trapping state can be determined.
Squaring the amplitudes of the recursion relation, we find

$$|c_{m+1}^k|^2 = \frac{V_{12}^2}{g_2^2}\frac{k-m}{j(j+1)-m(m+1)}|c_m^k|^2 \tag{6.20}$$

and we derive a closed expression for the population in the m'th level

$$|c_m^k|^2 = \left(\frac{V_{12}}{g_2}\right)^{2p} \frac{(k+j)!(2j-p)!}{(k+j-p)!2j!p!}|c_{-j}^k|^2 \tag{6.21}$$

where $p = m + j$ and where $|c_{-j}^k|^2$ serves as a normalization constant.

6.4.1 Analytical approximation to the atomic population distribution

Although Eq. (6.21) is exact, it is not very transparent. Instead, we shall derive a gaussian approximation to Eq. (6.21). If the population distribution has a symmetric peak at $m = \bar{m}$, the distribution must assume the same value in points located symmetrically around the peak. Under this assumption, we apply Eq. (6.20) for non-integer values of m and find $\bar{m}$ by solving the equation

$$1 = \frac{|c_{\bar{m}+1/2}^k|^2}{|c_{\bar{m}-1/2}^k|^2} = \frac{V_{12}^2}{g_2^2}\frac{k-\bar{m}-1/2}{j(j+1)-(\bar{m}-1/2)(\bar{m}+1/2)} \tag{6.22}$$

To ensure a comparable significance of the atomic and pseudo-mode contributions to S^-, we now assume a fixed relationship between V_{12} and g_2 namely $V_{12} = \sqrt{2j+1}g_2$. With this choice we obtain

$$\bar{m} = j + 1/2 - \sqrt{(2j+1)(j-k)} \tag{6.23}$$

We further assume that the population distribution can be approximated by a gaussian

$$|c_m^k|^2 \simeq \frac{1}{\sqrt{\pi}b} e^{-(m-\bar{m})^2/b^2} \tag{6.24}$$

The ratio of subsequent populations obtained from the gaussian approximation reads

$$\frac{|c_{m+1}^k|^2}{|c_m^k|^2} = e^{-(2(m-\bar{m})+1)/b^2} \simeq 1 - \frac{2(m-\bar{m})+1}{b^2} \tag{6.25}$$

for $m \simeq \bar{m}$.
Comparing this expression with the recursion relation Eq. (6.20), we identify the width as

$$\frac{1}{b^2} = \frac{1}{2}\left[\frac{1}{k-\bar{m}+1/2} - \frac{1}{j-\bar{m}+1/2} + \frac{1}{j+\bar{m}+1/2}\right] \tag{6.26}$$

In Fig. 6.4, we have plotted Eqs. (6.21) and (6.24) as functions of m for a fixed value of the number of excitations in order to estimate the validity of the gaussian approximation. A very good agreement is found. In the following, we use Eq. (6.24) with a width given by (6.26) and extend the integration limits to $\pm\infty$, when we calculate moments of the distribution. This is a valid approximation provided the number of excitations left in the system is not too low (> 10) because if that is the case, the tails of the distribution fall outside the allowed region of m values. We also note that the gaussian approximation does not work too well when the number of excitations approaches the number of atoms i.e. full excitation. In that case, the trapping state has most of the excitation on the atoms which means that the distribution can not be well approximated by a gaussian. When $k = j$, we find $\bar{m} = j + 1/2$ according to Eq. (6.23) which obviously is not a valid result. This is, however, not particularly worrying since the gaussian approximation to the exact distribution is very good in the domain of interest.

6.5 Decay rate in the long time limit

In this section we derive an analytical expression for the decay rate of the total number of excitations in the long time limit based on perturbation theory and the gaussian expression for the population distribution we found in the

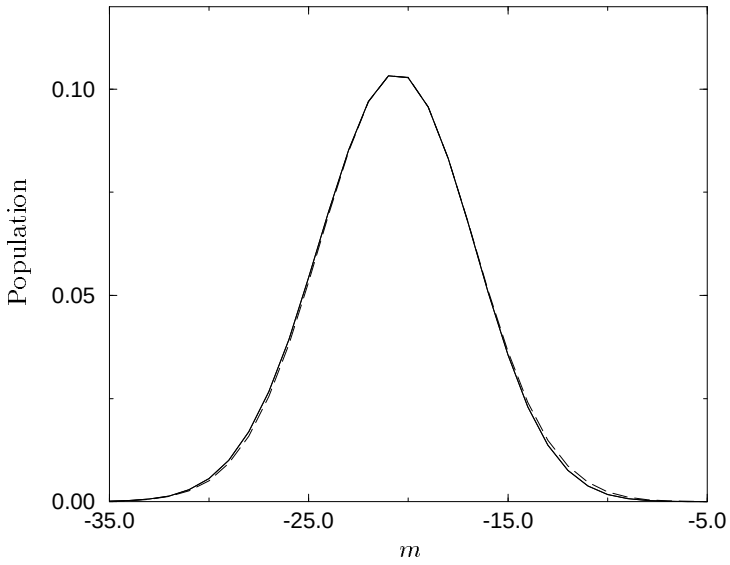

Figure 6.4: The exact atomic population (solid line) is plotted as a function of m. The dotted line is the gaussian approximation. The parameters chosen are $j = 50$, $k = 0$.

previous section. For that purpose, it proves convenient to rewrite the effective Hamiltonian as

$$H_{\text{eff}} = H_0 + V \tag{6.27}$$

with

$$H_0 = (R - \frac{2i}{\Gamma})S^+S^- - g_1\sqrt{2j+1}N_{ex} \tag{6.28}$$

$$V = \Delta J_z + \frac{g_1}{\sqrt{2j+1}}(j + J_z)^2 \tag{6.29}$$

where we have introduced the coupling parameter $R = \frac{g_1}{V_{12}g_2}$ and the operator $N_{ex} = J_z + a^\dagger a + j$ which is diagonal within each layer.
The trapping states given by Eq. (6.19) are exact eigenstates of the H_0 operator given by Eq. (6.28) and in particular eigenstates of the dissipative part of the Hamiltonian with eigenvalue zero. However, since the trapping states are not eigenstates of the operator V given by Eq. (6.29), this part of the Hamiltonian rotates the different components of the state at slightly different frequencies thereby destroying the trapping effect.

We note that when the system contains only a few excitations, V becomes negligible since then $(j + J_z)|jm\rangle \approx 0$.
In Fig. 6.3 we plotted the atomic inversion as a function of time and for the detuning $\Delta = -\sqrt{2j+1}g_1$ we found that the superradiant phase of the emission ceased at $\langle J_z\rangle \approx 0$ followed by an extraordinarily slow decay of the atomic inversion. We note that for this particular choice of the detuning, the linear terms in J_z in Eq. (6.29) are eliminated and the operator V hence only contains quadratic terms in J_z which give rise to a very small contribution when $\langle J_z\rangle \approx 0$.
We approximate the state of the system in the long time limit as a trapping state+a correction. Applying time independent perturbation theory, we find that the first order correction $|k_0^1\rangle$ to the population trapping state $|k_0\rangle$ is given by [70]

$$|k_0^1\rangle = \frac{\Phi}{E_0 - H_0} V|k_0\rangle \tag{6.30}$$

where Φ is a projection operator, projecting on all other states than the population trapping state.
The projection operator Φ can of course be expanded in any basis. However, since the exact population distribution is well approximated by a gaussian centered at $\bar{m}$, we choose to expand Φ in a basis of superposition states $|k_i\rangle$, $i \neq 0$, with amplitudes corresponding to eigenstates of a harmonic oscillator with position variable $x = m - \bar{m}$ for integer values of m. The amplitudes of the first excited state $|k_1\rangle$ of this fictitious oscillator for instance are then apart from a normalization factor given by $d_m = (m - \bar{m})c_m^k$ and the projection operator Φ can be expanded as $\Phi = \sum_{i=1}^{\infty} |k_i\rangle\langle k_i|$ where $|k_i\rangle$ is the i'th harmonic oscillator eigenstate centered at $\bar{m}$.
We are interested in the decay rate of the total number of excitations of the system, which is given by

$$\gamma_k = \frac{4}{\Gamma}\langle\psi|S^+S^-|\psi\rangle \tag{6.31}$$

where we take $|\psi\rangle = |k_0\rangle + |k_0^1\rangle$, and since $S^-|k_0\rangle = 0$, we find

$$\gamma_k = \frac{4}{\Gamma}\langle k_0^1|S^+S^-|k_0^1\rangle \tag{6.32}$$

The matrix element on the right hand side yields

$$\langle k_0^1|S^+S^-|k_0^1\rangle \quad = \quad \sum_i \left|\langle k_i|\frac{V}{E_0 - H_0}|k_0\rangle\right|^2 \langle k_i|S^+S^-|k_i\rangle \tag{6.33}$$

To calculate the matrix elements involved we use the gaussian approximation Eq. (6.24) to the exact distribution and extend the integration limits to $\pm\infty$. The resulting gaussian integrals are readily computed and finally, inserting all the matrix elements, we find that the dominant contribution to the decay rate

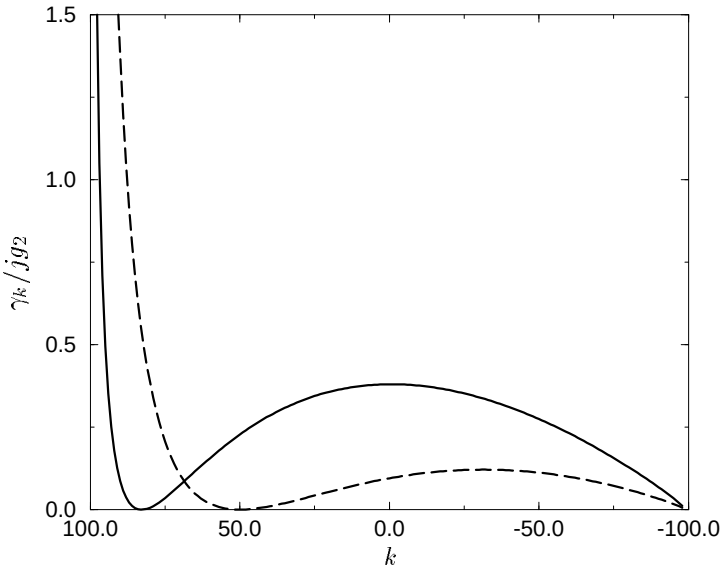

Figure 6.5: The decay rate γ_k for the total number of excitations is plotted in units of g_2 as a function of k for two different values of the detuning. The solid line has $\Delta = -4g_2$, and the long-dashed line has $\Delta = -\sqrt{2j+1}g_1 (\approx -2.82g_2)$. The parameters chosen are: $g_1/g_2 = 0.2$, $V_{12}/g_2 = \sqrt{2j+1}$, $\Gamma/g_2 = 101$ and $j = 100$.

γ_k comes from coupling to the state $|k_1\rangle$ i.e.

$$\begin{aligned} \gamma_k &\simeq \frac{4}{\Gamma}\left|\langle k_1|\frac{V}{E_0 - H_0}|k_0\rangle\right|^2 \langle k_1|S^+S^-|k_1\rangle \\ &= \frac{1}{2\Gamma(j+1-\bar{m})}\frac{b^2}{\frac{g_1^2}{(2j+1)g_2^2} + 4g_2^2/\Gamma^2}\left[\frac{2g_1(j+\bar{m})}{\sqrt{2j+1}} + \Delta\right]^2 \end{aligned} \quad (6.34)$$

The expression was derived under the assumption that the state of the system is in a well-defined layer and that the wave function of the system can be approximated by a trapping state+a correction: $|k_0\rangle + |k_0^1\rangle$. We thus expect Eq. (6.34) with $\bar{m}$ and b given by Eqs. (6.23) and (6.26) to give a good agreement with exact calculations in the long time-limit after the superradiant phase. An interesting feature of Eq. (6.34) is that it predicts the onset of fluorescence after a meta-stable state. To illustrate this, we have in Fig. 6.5 plotted γ_k as a function of k for two different values of the detuning. For these values, the decay rate has two peaks. The left peak corresponding to almost full excitation

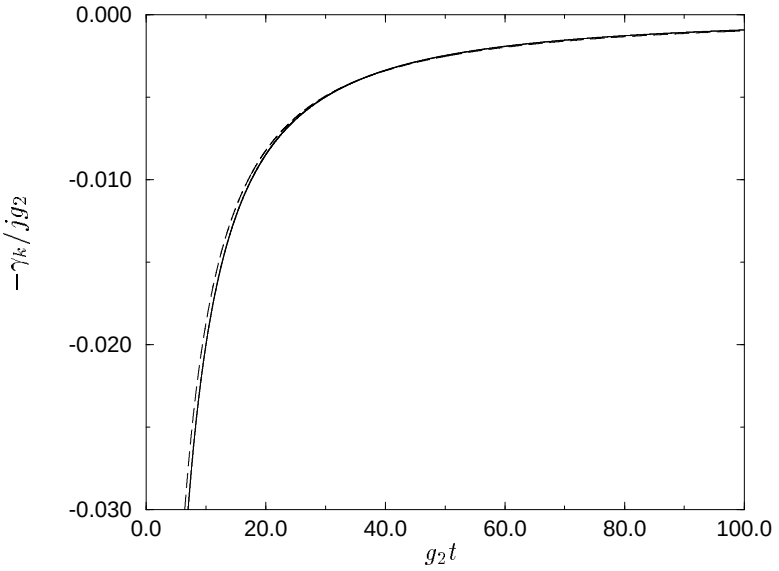

Figure 6.6: The decay rate for the total number of excitations is plotted as function of time in units of g_2. The solid line is the perturbative calculation and the long-dashed line is the master equation calculation. The parameters chosen are $\Delta = 0$, $g_1/g_2 = 0.2$, $V_{12}/g_2 = \sqrt{2j+1}$, $\Gamma/g_2 = 101$ and $j = 100$. The curves are obtained by simulation of the master equation and averaged over 100 trajectories.

($k \approx j$) is the superradiant regime. We do not expect Eq. (6.34) to give a very good agreement with exact calculations in this domain, since Eq. (6.34) was derived under the assumption that the system evolves through a succession of trapping states. Following the superradiant regime, the decay rate for both detunings approaches zero for a range of k values. This corresponds to the meta-stable behavior that we observed in Fig. 6.3 because the system only very slowly decays from layers corresponding to these values of k. When the system has lost a sufficient number of excitations, the trapping effect partly disappears and the decay rate again assumes higher values corresponding to a faster decay. This behavior can be observed in Fig. 6.3 (solid line).
We may convert the k-dependence of γ_k to a time-dependence by inserting $k(t) = \langle a^\dagger a(t)\rangle + \langle J_z(t)\rangle$ obtained from the master equation calculation into Eq. (6.34). In Fig. 6.6, we plot Eq. (6.34) and the excitation loss rate obtained from the master equation Eq. (6.13) as functions of time.
After the system has reached its meta-stable state, we find a very good agree-

ment between the perturbative calculation Eq. (6.34) and the exact results. Eq. (6.34) is a key result of this chapter. In a compact form it provides a very good description of the long-time behaviour of the dynamics for a wide range of parameters.

6.6 Mean-value equations

This section serves to test the results from the mean-field equations against the exact calculations obtained from propagation of the master equation.
In the first decorrelation scheme that we investigate, operator products are decorrelated and we assign non-vanishing mean values or amplitudes to the operators a, J^- i.e. $\langle a^\dagger J^-\rangle \approx \langle a^\dagger\rangle\langle J^-\rangle$. The second approximation decorrelates expectation values containing three operators like $\langle J_z a^\dagger J^-\rangle$ as $\langle J_z\rangle\langle a^\dagger J^-\rangle$ i.e. in such a way that the decorrelated expression contains an equal number of raising and lowering operators and thus only couples states with the same total number of excitations.

6.6.1 Mean-value equations in the symmetry breaking approximation

From the master equation (6.13), we derive the equation of motion for the atomic inversion

$$\begin{aligned}\langle \dot{J}_z\rangle &= \frac{g_1}{i}\left[\langle a J^+\rangle - \langle a^\dagger J^-\rangle\right] - \frac{4g_2^2}{\Gamma}\langle J^+ J^-\rangle \\ &\quad -\frac{2V_{12}g_2}{\Gamma}\left[\langle J^+ a\rangle + \langle a^\dagger J^-\rangle\right] \qquad (6.35)\end{aligned}$$

To find the time evolution of the atomic inversion, we need equations of motion for $\langle a^\dagger J^-\rangle$ and its conjugate. Their equations of motion do, however, involve yet other expectation values and the resulting hierarchy of equations can not be solved without some approximation. The most obvious approximation is to factorize the operator product $\langle a^\dagger J^-\rangle \approx \langle a^\dagger\rangle\langle J^-\rangle$ and $\langle J^+ J^-\rangle \approx (j+\langle J_z\rangle)(j-\langle J_z\rangle+1)$. The resulting equations of motion for $\langle a\rangle, \langle J^+\rangle$ read

$$\begin{aligned}\langle \dot{J}_z\rangle &= \frac{g_1}{i}\left[\langle a\rangle\langle J^+\rangle - \langle a^\dagger\rangle\langle J^-\rangle\right] - \frac{4g_2^2}{\Gamma}(j+\langle J_z\rangle)(j-\langle J_z\rangle+1) \\ &\quad -\frac{2V_{12}g_2}{\Gamma}\left[\langle J^+\rangle\langle a\rangle + \langle a^\dagger\rangle\langle J^-\rangle\right] \qquad (6.36)\\ \langle \dot{J}_+\rangle &= -\frac{\Delta}{i}\langle J^+\rangle + \left(\frac{2g_1}{i} + \frac{4g_2V_{12}}{\Gamma}\right)\langle a^\dagger\rangle\langle J_z\rangle \\ &\quad +\frac{V_{12}g_2}{\Gamma}\langle J^+\rangle\langle J_z\rangle \qquad (6.37)\\ \langle \dot{a}\rangle &= \left(\frac{g_1}{i} - \frac{2V_{12}g_2}{\Gamma}\right)\langle J^-\rangle - \frac{2V_{12}^2}{\Gamma}\langle a\rangle \qquad (6.38)\end{aligned}$$

Equations of motion for $\langle J^-\rangle$ and $\langle a^\dagger\rangle$ are found by hermitian conjugation of the equations of motion for $\langle J^+\rangle$ and $\langle a\rangle$.

Although appealing from a mathematical viewpoint, this approximation has some obvious drawbacks: if the system is started from, say, the product state $|m,0\rangle$, the expectation value $\langle a^\dagger J^-\rangle$ will develop a non-zero expectation value, whereas $\langle a^\dagger\rangle, \langle J^-\rangle$ both remain zero since their equations of motion are uncoupled from the operators with non-zero expectation values. Applying the decorrelation approximation, we thus have to assign a non-zero initial value to at least one of the coherences. In the following we refer to these equations as *mean-field* (MF) equations.
By a formal integration of the equation of motion for the pseudo-mode Eq. (6.38), we can obtain a closed set of equations for the Dicke-system involving only atomic operators

$$\begin{aligned}\langle \dot{J}_z\rangle &= \left[\frac{g_1}{i}-\frac{2}{\Gamma}g_2V_{12}\right]\langle J^+(t)\rangle\int_0^t dt' e^{-2V_{12}^2/\Gamma(t-t')}\langle J^-(t')\rangle \\ &\quad +\text{h.c.}-\frac{4g_2^2}{\Gamma}(j+\langle J_z\rangle)(j-\langle J_z\rangle+1) \qquad (6.39)\\ \langle \dot{J}^-\rangle &= \frac{\Delta}{i}\langle J^-\rangle+\langle J_z\rangle\left[\frac{4g_2^2}{\Gamma}\langle J^-\rangle+2\left(\frac{g_1}{i}-\frac{2g_2V_{12}}{\Gamma}\right)\right. \\ &\quad \left.\int_0^t dt' e^{-2V_{12}^2/\Gamma(t-t')}\langle J^-(t')\rangle\right] \qquad (6.40)\end{aligned}$$

From a practical viewpoint, this set of equations is not an advantage, since it is much more straightforward to implement numerically the slightly larger set of Markovian differential equations Eqs. (6.36)-(6.38) involving the pseudo-mode.

A Heisenberg equation approach

Starting from the structured continuum, we can obtain effective equations of motion for the atomic operators without introducing pseudo-modes. The resulting equations of motion are non-Markovian thus evidencing the structure of the continuum. To obtain a closed set of equations, we have to apply a decorrelation approximation to the operator expectation values and we show that the resulting non-Markovian equations of motion for the atomic operators are the same as Eqs. (6.39) and (6.40).
In the Heisenberg picture the equation of motion for an operator reads $\dot{b}=\frac{1}{i}[b,H_F]$ with H_F given by Eq. (6.1). We then find

$$\langle \dot{J}_z\rangle = -\sum_\lambda g_\lambda^2\int_0^t dt'\left[\langle J^+(t)J^-(t')\rangle e^{-i(\omega_\lambda-\omega_c)(t-t')}+\text{h.c.}\right] \qquad (6.41)$$

where we have eliminated the operator a_λ by a formal integration and transformed to an interaction picture rotating at ω_c. The summation over modes can be evaluated by closing the integration contour with a semi-circle in the lower half of the complex plane and using the Residue theorem to yield

$$\sum g_\lambda^2 e^{-i(\omega_\lambda-\omega_c)(t-t')} = \frac{\Omega^2}{2\pi}\int d\omega\,\rho(\omega)e^{-i(\omega-\omega_c)(t-t')}$$

$$= \frac{4\Omega^2 f}{(\kappa-\gamma)(\gamma+\kappa)}\left[\frac{(q-i\gamma/2)^2}{\gamma}e^{-\gamma/2(t-t')} - \frac{(q-i\kappa/2)^2}{\kappa}e^{-\kappa/2(t-t')}\right] \quad (6.42)$$

and the result is inserted in Eq. (6.41). Assuming that $\kappa \gg q, \Omega, \gamma$, which corresponds to the adiabatic elimination we performed in the master equation calculation, we can perform the time integral over the exponential containing κ which yields

$$\int_0^t dt' J^-(t') e^{-\kappa/2(t-t')} \simeq \frac{2}{\kappa} J^-(t) \quad (6.43)$$

Collecting the terms, the resulting non-Markovian equations of motion for the atomic operators thus read

$$\langle \dot{J}_z \rangle = -\frac{\Omega^2}{\kappa}\frac{1}{q^2/\kappa\gamma + 1/4}\left[\langle J^+ J^-(t)\rangle + \frac{(q-i\gamma/2)^2}{\gamma}\int_0^t dt' e^{-\gamma/2(t-t')}\langle J^+(t)\rangle\langle J^-(t')\rangle\right] \quad (6.44)$$

$$\langle \dot{J}^- \rangle = \frac{\Delta}{i}\langle J^-\rangle + \langle J_z(t)\rangle\frac{\Omega^2}{\kappa}\frac{1}{q^2/\kappa\gamma + 1/4}\left[\langle J^-(t)\rangle + \int_0^t dt' \frac{2(q-i\gamma/2)^2}{\gamma} e^{-\gamma/2(t-t')}\langle J^-(t')\rangle\right] \quad (6.45)$$

where we have used

$$\frac{4f}{(\kappa-\gamma)(\kappa+\gamma)} \simeq \frac{1}{\kappa}\frac{1}{q^2/\kappa\gamma + 1/4} \quad (6.46)$$

Using the explicit expressions for the couplings Eqs. (6.8) to (6.10), one can see that Eqs. (6.39) and (6.40) are equivalent to Eqs. (6.44) and (6.45). The mean-value equations derived from the master equation applying the symmetry breaking approximation are thus equivalent to the non-Markovian equations derived directly from the structured reservoir Eqs. (6.44) and (6.45).
In a recent paper [46], John and Quang derived a set of non-Markovian equations for the atomic operators similar to Eqs. (6.44) and (6.45). They studied superradiance in a PBG with an effective mass dispersion relation $\omega_k = \omega_e + A(k-k_0)^2$ and their integration kernel consequently differs from ours. Since the density of states corresponding to the isotropic dispersion relation is non-analytical in the complex plane, they could not derive a master equation and could thus not test the validity of the mean-field Ansatz against an exact calculation.
On the other hand, since we have a master equation we can test the validity of the MF equations Eqs. (6.39) and (6.40) against the exact solution. Before presenting the numerical solution of Eqs. (6.39) and (6.40), we present a second, slightly more sophisticated decorrelation approximation.

6.6.2 Excitation conserving decorrelation

To improve on this simplest approximation, we go a step beyond, and decorrelate operator expectation values containing three operators in such a way that the resulting expectation values only couple states containing the same number of excitations i.e. $\langle J_z a^\dagger a\rangle \simeq \langle J_z\rangle\langle a^\dagger a\rangle$. With this decorrelation, the equations of motion read

$$\begin{aligned}\langle \dot{J}_z\rangle &= \frac{g_1}{i}\left[\langle aJ^+\rangle - \langle a^\dagger J^-\rangle\right] - \frac{4g_2^2}{\Gamma}\langle J^+J^-\rangle \\ &\quad -\frac{2V_{12}g_2}{\Gamma}\left[\langle J^+a\rangle + \langle a^\dagger J^-\rangle\right] \qquad (6.47)\end{aligned}$$

and

$$\frac{d}{dt}\langle J^+J^-\rangle = 2(-\langle J_z\rangle + 1)\frac{d}{dt}\langle J_z\rangle \qquad (6.48)$$

$$\begin{aligned}\frac{d}{dt}\langle a^\dagger a\rangle &= \frac{g_1}{i}\left[\langle a^\dagger J^-\rangle - \langle aJ^+\rangle\right] \\ &- \frac{2V_{12}}{\Gamma}\left[2V_{12}\langle a^\dagger a\rangle + g_2\langle J^+a\rangle + g_2\langle a^\dagger J^-\rangle\right] \qquad (6.49)\end{aligned}$$

$$\begin{aligned}\frac{d}{dt}\langle aJ^+\rangle &= \frac{g_1}{i}\left[\langle J^+J^-\rangle + 2\langle J_z\rangle\langle a^\dagger a\rangle\right] - \frac{\Delta}{i}\langle aJ^+\rangle \\ &\quad -\frac{2V_{12}}{\Gamma}\left[V_{12}\langle J^+a\rangle + g_2\langle J^+J^-\rangle\right] \\ &+ \frac{4g_2}{\Gamma}\langle J_z\rangle\left[V_{12}\langle a^\dagger a\rangle + g_2\langle J^+a\rangle\right] \qquad (6.50)\end{aligned}$$

Again we find a closed set of differential equations governing the motion of the system. A most satisfying aspect of this decorrelation is that it is not necessary to assign amplitudes by hand to operator expectation values.
Since the equations are non-linear, they can not be solved by Laplace transform. They can, however, be solved in a straightforward manner applying standard numerical methods.
In Fig. 6.7, we compare the two decorrelated equations of motion for the atomic inversion with the exact solution obtained by propagation of the master equation Eq. (6.13).

In particular, we present the dynamics obtained when the system is started in the fully excited state with no photons in the reservoir i.e. $|j,0\rangle$. We find that the simple MF approximation in which we assign mean-values to the atomic and field operators gives a very good agreement with the exact master equation calculation for a wide range of parameters. The accuracy of the MF calculation, however, is very sensitive to the choice of initial conditions. We find that the best agreement is obtained when we take $\langle J^-(0)\rangle = \sqrt{\langle J^+J^-(0)\rangle} = \sqrt{2j}$. We shall now relate this to the semiclassical description of superradiance [71]. In this approach, the wave function for the atomic system is assumed to be in the form $|\psi\rangle = \Pi_i(\sqrt{1-r}|1_i\rangle + \sqrt{r}|2_i\rangle)$, where $|2_i\rangle, |1_i\rangle$ are the upper and lower

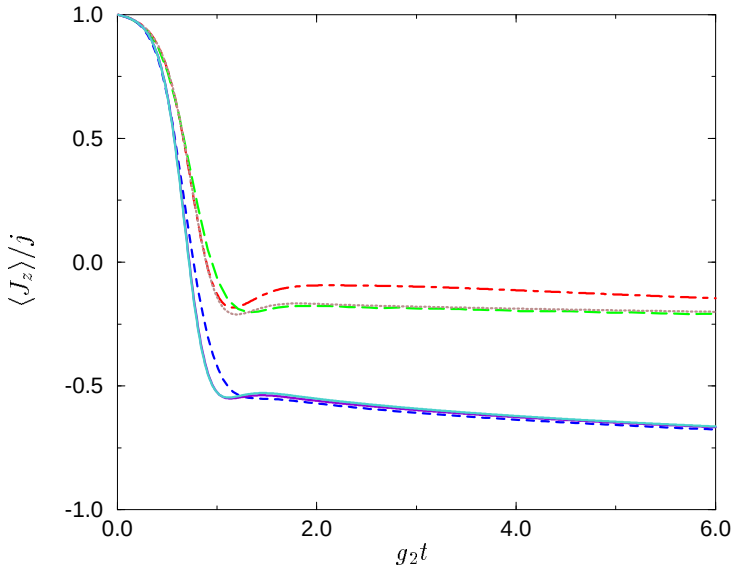

Figure 6.7: The mean-value equations are plotted as functions of time for two values of the detuning Δ. The three lower curves have $\Delta = 0$. The two mean-value calculations coincide (solid line) and the dashed curve is the exact master equation calculation. The three upper curves have $\Delta = -1$. The dot-dashed curve is the MF-solution. The dotted and long-dashed curves are the solutions to the master equation and the equations based on our better decorrelation, respectively. The parameters chosen are $g_1/g_2 = 0.2$, $V_{12}/g_2 = \sqrt{2j+1}$, $\Gamma/g_2 = 101$ and $j = 100$.

states of atom i, respectively and r is a measure of the coherence between the two states. In this state we find $\langle\psi|J^-|\psi\rangle = 2j\sqrt{r(1-r)}$. If we take $r = 1/2j$, then $\langle\psi|J^-|\psi\rangle \approx \sqrt{2j}$ when $j \gg 1$. Our calculations therefore show that in order for this approach to give results in agreement with the exact master equation calculation, r can not be chosen freely but has to be assigned the value $r = 1/2j$. With that choice, however, this approach gives exactly the same results as our MF calculation.

The second approximation Eqs. (6.48)-(6.50) also gives a very good agreement with the exact results and for a wider range of parameters than the simple MF appproximation. Although both approximations predict correctly the atomic inversion where the superradiant phase ceases, both methods overestimate the rapidity of the superradiant phase i.e. the speed at which the atoms lose their excitation.

6.7 Concluding remarks

In this chapter, we investigated an atomic Dicke system coupled to a structured radiation reservoir in the form of a Fano-profile. Introducing two pseudo-modes, a Markovian master equation governing the motion of the atoms+pseudo-modes was derived. For a wide range of parameters, we found that the system reaches a meta-stable state in the long-time limit in which a significant part of the excitation remains bound at the atoms. A trapping state within each layer was identified which diagonalizes the non-hermitian part of the Hamiltonian. Using perturbation theory and a gaussian approximation to the trapping state we derived an analytical expression for the decay rate of the meta-stable state which showed a very good agreement with the decay rate obtained numerically from the master equation.
We further investigated various decorrelation schemes for the equations of motion of the operator expectation values and showed that for a wide range of parameters the mean-field equations give results that are in very good agreement with the exact results obtained by propagation of the master equation. For other problems where multiple excitations of a structured continuum are involved and a master equation for the reduced system is not accessible, the mean-field approximation may thus prove valuable.
The basic motivation for this work stems from new problems that have arisen in connection with new technological developments; PBG materials being one example. A fundamental difficulty inherent in the study of radiation-atom interactions in such environments is the non-Markovian nature of the processes. Although one can always proceed to the derivation of a master equation through a Born-Markov approximation, its range of validity is uncertain. It is useful to have models which share some of the essential features with such materials, while at the same time lend themselves to quantitative analysis of the relevant approximations, providing thus some physical insight into the more complex situations. Our study of the mean-field approximation represents one illustration of the usefulness of this approach.

Chapter VII

Epilogue

7.1 Thesis summary and conclusions

The main theme of this thesis is the interaction of a small quantum system with a strongly modified radiation reservoir and in particular, our focus in this thesis has been on the radiation reservoir existing inside a photonic crystal and here the situation is quite different from cavity quantum electrodynamics (CQED) since the formation of a photonic band structure leads to a density of modes which can no longer be modelled by coupling the quantum system to a few resonant modes and consequently the methods developed in CQED are no longer applicable.
Our investigations as presented in this thesis thus serve a dual purpose: on one side, a whole range of new phenomena occur due to the influence of the modified radiation reservoir such as Rabi-like oscillations in the spontaneous decay of a two-level atom, and the occurrence of the photon-atom bound state in which a significant part of the photon remains localized at the site of the atom. On the other hand our studies aim at investigating the validity of the methods and approximations that are employed when dealing with a conventional radiation reservoir and to develop new methods that are applicable when standard methods fail.
In chapter 3, we address the problem of two identical atoms interacting via the PBG reservoir. The resulting resonant dipole-dipole interaction (RDDI) is strongly modified and we find an analytical expression which gives a very good agreement with the exact numerical results for the RDDI. We can then derive amplitudes governing the motion of the atoms and study the resulting dynamics in time domain. We investigate the system for a wide class of parameters and find that a stable state exists in which a photon tunnels between the two atoms. The state is stable since the photon has an energy in the gap and thus is not allowed to propagate freely in the photonic crystal.
The effects of localization are not easily probed in this system since much of the excitation remains trapped at the atoms located in the bulk of the crystal and in chapter 4, we thus investigate a system for which the effects of the structured

radiation reservoir are easier to demonstrate experimentally. The setup we consider is an atomic ladder system where the atom is initially in the upper level and one of the two transitions is coupled to a PBG-reservoir and the other transition is coupled to a flat radiation reservoir. In this case the photon emitted on the free space transition is allowed to propagate in the photonic crystal and we calculate the resulting emission spectra. Strongly non-Lorentzian emission spectra are obtained and the photon emitted on the free space transition thus carries a strong signature of the PBG-transition.
In chapter 5, we study an atomic lambda-system with one laser-driven transition experiencing a flat background of radiation modes and the other transition coupled to a PBG-reservoir. The presence of the laser implies that a description in terms of wave functions is no longer feasible and we thus derive a master equation for the atomic degrees of freedom employing *only* the Born-approximation. In parallel, we develop a method based on the resolvent operator technique and the Monte-Carlo wave function formalism. Comparing the resulting dynamics from the master equation with the exact dynamics obtained from the Monte-Carlo wave functions, we find a very poor agreement thus invalidating the Born-approximation. The method, we develop is applicable to reservoirs with any density of modes and may thus be a powerful tool in a number of problems involving structured continua. It is, however, essential that only the zero- and one-photon components of the structured reservoir are populated.
In order to circumvent this restriction and thus be able to deal with more excitations in the structured continuum, we investigate in chapter 6, the system consisting of a number of two-level atoms coupled identically to a Fano-profile density of states. The analyticity of the density of states allows us by introduction of two pseudo-modes to derive a Markovian master equation for the system consisting of atoms+the two pseudo-modes. In this system we study superradiance and the influence of multiple excitations in the radiation reservoirs on the atomic dynamics.
We find that following the superradiant regime, a meta-stable state is reached for the atomic system. The decay of the meta-stable state is non-exponential and we derive an analytical expression for the decay based on perturbation theory. The existence of a Markovian master equation for the system further allows us to test the validity of the mean-field approximation. A good agreement is found and the mean-field approximation may therefore be a useful approximation in various contexts where a master equation can not be obtained.

7.2 Outlook

The studies presented in this thesis have a model character since we have not chosen any specific atomic transition or photonic crystal. This choice was partly motivated by our wish to most clearly emphasize the novel features that arise due to the interaction with the modified continuum but it also reflects that experiments probing the interaction of atoms with a PBG-reservoir are not yet performed since appropriate photonic crystals with 3D band gaps in the optical

domain are not yet available. The concept of photonic crystals is, however, still quite new and with the on-going research in the construction of photonic crystals it is likely that photonic crystals with full band gaps in the optical domain will become available in the near future. At that time, calculations using realistic parameters for photonic dispersion relations and atomic matrix elements will be necessary in order to compare theory to experimental data.

The structured continuum gives rise to a range of novel effects as is evidenced in the rapidly growing theoretical literature on the subject. A number of problems deserve attention, but in our view there is one problem which is of particular importance; namely to develop methods to deal with several excitations in the structured continuum. In chapter 5 we proposed a method combining the resolvent operator technique with the Monte-Carlo wave function formalism. This method was used to calculate the dynamics of a system for which no Markovian master equation exists. Our approach is applicable to problems with any density of modes of the reservoir but it is essential that only the zero- and one-photon components of the reservoir Hilbert space are populated. In the case of several excitations in the structured reservoir, a different approach is needed. One such approach was employed in chapter 6 and consists in the introduction of a number of pseudo-modes: one for each of the poles of the density of modes. This approach developed by Garraway assumes that the reservoir density of modes can be approximated by a function which is analytical in the complex plane. In many cases as for instance the reservoir discussed in chapters 3-5 this condition is, however, not fulfilled and a master equation can thus not be derived.

In a recent paper, Quang and John [9] have proposed to use a Monte-Carlo wave function approach based on dressed atomic states to the study of this kind of problems and in particular they study a laser-driven two-level atom with transition frequency in the vicinity of the band gap edge. In appendix A, we argue that their approach is at variance with the physical principles underlying the Monte-Carlo wave function technique and that their approach produces unphysical results [6].

One possible solution to the problem of several excitations in the structured continuum may be to discretize the reservoir. In this approach the structured reservoir is replaced by a large number of harmonic oscillator modes with transition frequencies and coupling strengths determined by the density of modes of the reservoir. The harmonic oscillators are then treated on an equal footing with the atomic degrees of freedom and it is then rather straightforward to propagate the total wave function for atom(s)+harmonic oscillators. To our knowledge this approach of discretizing the structured continuum has not yet been applied. Whether it is a practical technique or whether the number of oscillator modes needed for a satisfactory representation of the structured continuum is simply too large to be tractable, remains to be seen.

It is therefore still an open question how the general case with several excitations in the structured continuum is treated and the development of new theoretical methods to deal with this type of problems will probably be a central theme of the future theoretical research in structured radiation reservoirs.

Appendix A

Comment on "Resonance fluorescence near a photonic band gap edge: Dressed-state Monte-Carlo wave function approach."

Tran Quang and Sajeev John have in a recent paper [*Phys. Rev. A* **56**, 4273 (1997)] proposed a dressed state Monte-Carlo wave function approach to a laser-driven two-level atom coupled to a structured radiation reservoir. In this Comment, we argue that this approach is at variance with basic formal requirements for the MCWF technique to apply, that it is at variance with the underlying physical idea of the technique, and that it produces spurious and un-physical quantitative results for wide ranges of parameters.

A.1 Comment

Atomic systems within photonic band-gap (PBG) materials, microcavities and optical fibres behave differently from atoms in free space. The Born and Markov approximations normally used to derive a master equation fail: the former cannot account for the formation of photon-atom bound states, identified in the seminal papers by Sajeev John *et al.* [31, 32], the latter is at variance with the structured density of states of the radiation reservoir. There is a current need for theoretical methods which can deal with the atomic dynamics in cases with more than one excitation in the structured reservoir and Quang and John have proposed [9] to implement the Monte-Carlo wave function (MCWF) technique [58, 57, 61, 60] to deal with this kind of problems.
They transform the wavefuntion equations to a dressed state basis, and refer to the simulated state vectors as "Dressed-state Monte-Carlo wave functions". This choice of basis diagonalizes the laser coupling at the expense of a more complicated coupling to the reservoir but it does not give a more accurate treatment of the structured continuum and, in particular, it does not justify the omission in Eqs. (8,9) of the coupling to the two-photon sector of the reservoir Hilbert space. An analysis of this approximation is not presented in [9]. The resulting

equations of motion Eqs. (10,11) are exactly equivalent to the much simpler ones obtained within the same approximation in the basis of bare states.
The quantum jumps in the MCWF treatment of resonance fluorescence can be interpreted as consequences of *Gedanken-measurements* of the number of photons in the radiation reservoir, collapsing the system on its zero-photon or on its one-photon component, where the photon in the latter case is annihilated in the detection process. The assumption that such measurements do not alter the dynamics of the system by Quantum Zeno effects or the like, is established by a Markov approximation which does not apply for the interaction studied in Ref. [9].
The quantum jumps applied in Ref. [9] introduce errors by preventing the subsequent atomic reabsorbtion of the light. Quang and John are clearly well aware of the importance of this process and it is partly retained in their time evolution between jumps where it gives rise to oscillations in the squared norm of the zero-photon component of the wave function $P(t)$ (see Fig. A.1). This, however, has the unfortunate consequence that $P(t)$ is not useful as a delay function as in the case of Markovian decay.
Quang and John do not seem to have realized this problem, and they simply apply the procedure as described in [60] and pick a random number ε between zero and unity to simulate the occurrence of a jump at the (first ?) instant t when $P(t) = \varepsilon$. In such a simulation the decay is effectively switched off in time intervals when $P(t)$ exceeds its minimal value at previous times. If one carries out simulations like in [9], one thus finds unphysical spikes in the atomic populations, since a fraction of the atoms experience a sudden turn-on of the decay rate if $P(t)$ at a later time assumes values lower than previous local minima, see the lower part of Fig. A.1.
In the case of a single atom and no laser light, studied in [32], $P(t)$ equals the atomic excited state population, and a simulation will lead to a surviving excited state fraction equal to the minimum value of $P(t)$ rather than its asymptotic value, which is the exact result, see the dashed curve in Fig. A.1.
The problem of an oscillating function $P(t)$ is the symptom of a more fundamental inconsistency of the method, and one cannot conclude that the method is applicable even if $P(t)$ does not show local minima.

In previous applications, the MCWF method has always been formally derived and proved [59] to produce exact results in the limit of many wave functions. It is possible that stochastic wave functions may be useful in the description of problems like the one in Ref. [9] as an *approximate* technique. It is thus interesting to examine more closely the proposal of Ref. [9] and maybe suggest suitable improvements respecting that not all radiation can be made subject of detection. One may for instance identify a discrete eigenstate of the full Hamiltonian restricted to the zero- and one-photon components of the reservoir Hilbert space [33], and implement a jump scheme, where only the one-photon components orthogonal to this bound-photon state are removed during jumps. Exact MCWF treatments of structured reservoirs have been suggested in the

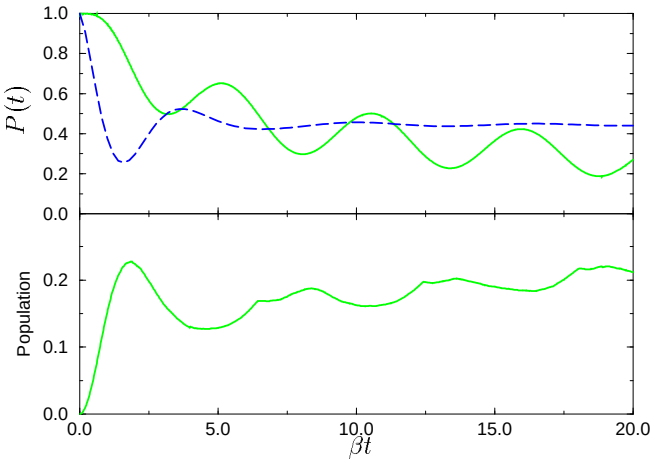

Figure A.1: In the upper figure part of the figure, $P(t)$ is plotted as function of time. The dashed line is the delay function as obtained by John and Quang [32] when the atom is initially excited and without a laser. The solid line is for an atom initially in the ground state. The laser coupling $\Omega/\beta = 0.5$ and $\omega_{21} = \omega_c$ (in the notation of Ref. [9]). In the lower part of the figure, the population in the upper state is plotted after simulation of 10^5 wave functions. The parameters are the same as for the solid curve in the upper part of the figure. The atoms are stable against quantum jumps between $\beta t \approx 3.2$ and $\beta t \approx 6.5$, and at $\beta t \approx 6.5$ the sudden onset of quantum jumps leads to a spike in the mean atomic population. Similar spikes are observed at $\beta t \approx 12.5$ and $\beta t \approx 18$.

literature [65, 67, 5] to deal with reservoir density of states which can be represented by a number of (coupled) oscillator modes. The model in Ref. [9] has, however, a sharp band edge in the density of modes and the approach employed in [65, 67, 5] is therefore less promising for this particular problem.

Appendix B

Resolvent Operator

The resolvent operator was used in chapters 3 and 4 to derive the time evolution operator for a specific system. In this appendix we present in slightly larger detail the connection to the time evolution operator, the analytic properties of the resolvent and the validity of the pole approximation.

B.1 The resolvent operator

The time evolution operator $\mathcal{U}(t,t')$ associated with the Hamiltonian $H = H_0 + V$ is the solution of the differential equation

$$i\hbar\frac{d}{dt}\mathcal{U}(t,t') = (H_0 + V)\mathcal{U}(t,t') \tag{B.1}$$

obeying the initial condition $\mathcal{U}(t',t') = 1$.
One can easily verify that the solution of (B.1) can be written

$$\mathcal{U}(t,t') = \mathcal{U}_0(t,t') + \frac{1}{i\hbar}\int_{t'}^{t} dt_1 \mathcal{U}_0(t,t_1) V \mathcal{U}(t_1,t') \tag{B.2}$$

where $\mathcal{U}_0(t,t') = e^{-iH_0(t-t')}$
Due to the limits of integration, (B.2) is not a convolution product. By introducing the retarded Greens functions

$$K_+(t,t') = \mathcal{U}(t,t')\theta(t-t') \tag{B.3}$$

$$K_{0+}(t,t') = \mathcal{U}_0(t,t')\theta(t-t') \tag{B.4}$$

where

$$\theta(x) = \begin{cases} 1 & x > 0 \\ 0 & x < 0 \end{cases} \tag{B.5}$$

is the Heaviside function, we find however

$$K_+(t,t') = K_{0+}(t,t') + \frac{1}{i\hbar}\int_{-\infty}^{\infty} dt_1 K_{0+}(t,t_1) V K_+(t_1,t') \tag{B.6}$$

which can be simplified greatly through Fourier transform.
Introducing the Fourier transform of K_+

$$K_+(\tau) = -\frac{1}{2\pi i}\int_{-\infty}^{\infty} dE e^{-iE\tau/\hbar} G_+(E) \tag{B.7}$$

which by inversion yields

$$\begin{aligned} G_+(E) &= \frac{1}{i\hbar}\int_{-\infty}^{\infty} d\tau e^{iE\tau/\hbar} K_+(\tau) \\ &= \frac{1}{i\hbar}\int_{0}^{\infty} d\tau e^{i(E-H)\tau/\hbar} \\ &= \lim_{\eta\to 0^+}\frac{1}{i\hbar}\int_{0}^{\infty} d\tau e^{i(E-H+i\eta)\tau/\hbar} \\ &= \lim_{\eta\to 0^+}\frac{1}{E-H+i\eta} \end{aligned} \tag{B.8}$$

In the same way, one defines the advanced Greens functions

$$K_-(t,t') = -\mathcal{U}(t,t')\theta(t'-t) \tag{B.9}$$

$$K_{0-}(t,t') = -\mathcal{U}_0(t,t')\theta(t'-t) \tag{B.10}$$

and introduces the Fourier transform $G_-(E)$ of $K_-(t,t')$

$$K_-(\tau) = -\frac{1}{2\pi i}\int_{-\infty}^{\infty} dE e^{-iE\tau/\hbar} G_-(E) \tag{B.11}$$

which leads to

$$G_-(E) = \lim_{\eta\to 0^+}\frac{1}{E-H-i\eta} \tag{B.12}$$

Defining

$$G(z) = \frac{1}{z-H} \tag{B.13}$$

we thus find

$$G_\pm(E) = \lim_{\eta\to 0_+} G(E\pm i\eta) \tag{B.14}$$

Fourier transform of (B.6) thus yields the simple expression

$$G(z) = G_0(z) + G_0(z)VG(z) \tag{B.15}$$

for the resolvent operator.
Since the evolution operator $\mathcal{U}(\tau) = K_+(\tau) - K_-(\tau)$, it can easily be expressed

by a simple contour integral

$$\begin{aligned} \mathcal{U}(\tau) &= \frac{1}{2\pi i}\int_{-\infty}^{\infty} dE e^{-iE\tau/\hbar}(G_-(E) - G_+(E)) \\ &= \frac{1}{2\pi i}\int_{C_+ + C_-} dz e^{-iz\tau/\hbar} G(z) \end{aligned} \tag{B.16}$$

where C_+, C_- are the paths depicted in Fig. B.1

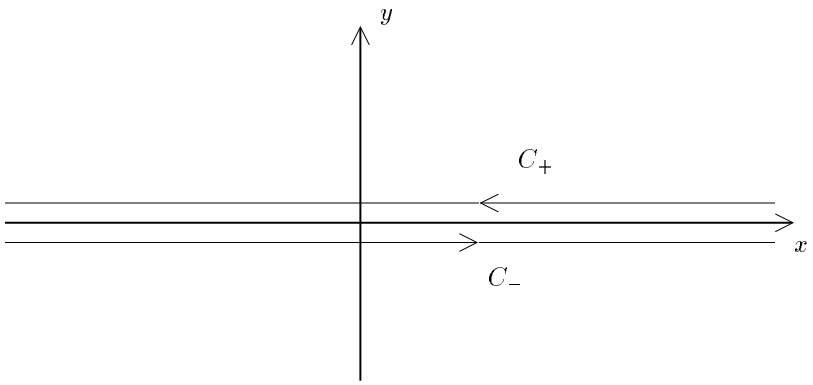

Figure B.1: The two paths C_+ and C_- are infinitesimally close to the real axis

B.2 The inversion

Since $\mathcal{U}(\tau)$ is obtained by a contour integral, the analytic properties of $G(z)$ play an important role.
It is proven by [41] that $G(z)$ is an analytic function in the whole complex plane except from some singularities all located on the real axis. The singularities consist of poles located at the discrete eigenvalues of H, and of cuts extending over the intervals corresponding to the continuous spectrum of H.
At the cut, a matrix element of the resolvent takes the form

$$G_+(E + i\eta) = \frac{1}{E + i\eta - E_b - \hbar\Delta(E) + i\frac{\hbar}{2}\Gamma(E)} \tag{B.17}$$

close to the real axis. Further assuming that $\Delta(E), \Gamma(E)$ are slowly varying as a function of E and $\Delta(E), \Gamma(E) \ll E_b$, $G_+(E + i\eta)$ can be written

$$G_+(E + i\eta) = \frac{1}{E + i\eta - E_b - \hbar\Delta + i\frac{\hbar}{2}\Gamma} \tag{B.18}$$

We note that since η is a positive quantity, this expression has no poles in the upper half of the complex plane. Defining the analytic continuation of G_+ to

the lower half plane by G_+^{II}

$$G_+^{II}(E+i\eta) = \frac{1}{E+i\eta-E_b-\hbar\Delta+i\frac{\hbar}{2}\Gamma} \tag{B.19}$$

this function has a pole at $z_0 = E_b + \hbar\Delta - i\frac{\hbar}{2}\Gamma$.
This continuation is called the second Riemann sheet.
For $\tau > 0$, the contribution of the path C_- in the inversion integral vanishes. The inversion integral thus reduces to

$$\mathcal{U}(\tau) = \frac{1}{2\pi i}\int_{C_+} dz e^{-iz\tau/\hbar} G(z) \tag{B.20}$$

To evaluate this integral by the residue theorem, we should close the contour in the lower half plane. At the cut the matrix elements of $G(z)$ do not tend to the same value, when z tends from below or above towards a point on the cut, and in order to integrate along a closed curve, it is thus necessary to go back to turn around the branch point of the cut at $E = E_a$. The contour is depicted in fig. B.2. The contribution of the semi-circle is zero, if its radius is sufficiently

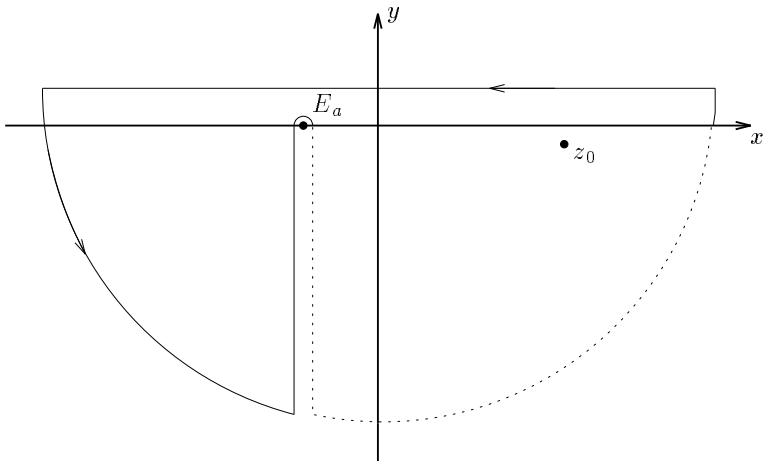

Figure B.2: Contour for inversion.

large. The contribution of the contour formed by turning around the branch point represents a correction to the exponential decay associated with the pole at z_0, but is normally negligible.

B.3 The pole approximation

The replacement of $\Delta(E)$ and $\Gamma(E)$ in (B.18) is known as the pole approximation, and yields a simple expression for the matrix elements of $G(z)$, which can

then easily be inverted using the residue theorem.
To perform the approximation, it is, however, essential, that the continuum is *smooth* i.e. that $\Delta(E), \Gamma(E)$ vary slowly as a function of E. This need not be the case, and one should therefore in general be cautious, when performing the pole approximation.

Appendix C

Resumé

This thesis deals with aspects of the interaction of light and matter and in particular we focus on the atomic dynamics resulting from the coupling to the electromagnetic vacuum field.
In free space, the density of modes of the electromagnetic vacuum field is rather flat and the coupling to the atom gives rise to the Lamb shift in frequency and a finite lifetime (the spontaneous decay) of the excited levels of the atom. The atomic behaviour is, however, sensitive to the density of states of the reservoir, and we investigate the atomic dynamics resulting from the coupling to a radiation reservoir exhibiting gaps and peaks in the density of modes.
Such structured radiation reservoirs are found in photonic crystals in which a periodic modulation of the dielectric constant gives rise to a band structure for the electromagnetic field in close analogy to the *electronic* band structure existing in solids. Experimental and theoretical findings concerning photonic crystals are presented in chapter 2 as well as various schemes for their construction and possible applications.
In chapter 3, we start investigating the influence of the structured radiation reservoir on the atomic dynamics. In particular, we study the problem of two identical atoms near-resonant with a band gap edge and located inside a photonic crystal. One atom is initially excited and the other atom is in the ground state. When the two atoms are far apart their interaction can be neglected and the evolution of the excited atom then reduces to the case of spontaneous decay of one atom. In that case, the atomic inversion in a transient regime exhibits Rabi-like oscillations in which part of the radiation emitted by the atom at previous times is reabsorbed and in the long time limit, a significant part of the excitation remains bound at the site of the atom thus forming what has been termed a "photon-atom bound state". When the interatomic separation is small i.e. comparable to the wavelength of the transition frequency of the atoms, the radiation is exchanged coherently between the two atoms and this coherent oscillation persists even in the long time limit for certain parameters. This, then, corresponds to a photon that tunnels between the two atoms and it remains trapped since it has an energy in the band gap of the reservoir and

thus is not allowed to propagate freely in the solid host.
These novel phenomena are not easy to probe experimentally since most of the radiation remains trapped at the site of the atoms. In order to monitor these effects, we discuss in chapter 4 an atomic ladder system in which one transition is coupled near-resonantly to a band gap edge and the other transition is coupled to a flat radiation reservoir. The radiation emitted into the flat reservoir is allowed to propagate and can thus be detected outside the crystal. In free space, the spectrum for the photon emitted on the upper transition in the radiative cascade is a Lorentzian with a width which is the sum of the decay widths of the upper atomic levels. Observing only the first photon in a radiative cascade thus provides information about the lower transition in the cascade. Indeed, we find that the emission spectra for the photon emitted on the upper transition become strongly non-Lorentzian due to the structured continuum coupled to the other transition.
In addition to the new phenomena arising from the interaction with structured reservoirs, the validity of the standard approximations employed when dealing with flat reservoirs has to be questioned. In chapter 5, we address an atomic lambda system with one laser-driven transition experiencing a flat reservoir and the other transition is coupled near-resonantly to the edge of a photonic band gap. Applying conventional methods, we derive a reduced master equation governing the atomic degrees of freedom employing only the Born approximation. To determine the exact dynamics of this system, we propose a method combining resolvent operator equations with the Monte-Carlo wave function formalism. The dynamics obtained from the master equation is at variance with the exact dynamics thus demonstrating the invalidity of the Born approximation.
These studies demonstrate that the number of fluorescence photons emitted on the free space transition for a weak laser coupling depends on the laser detuning with respect to the band gap edge in a sensitive way. Scanning the laser frequency over the band gap edge and monitoring the fluorescence signal emitted on the free space transition, one can thus experimentally characterize the structured continuum.
The method proposed in this chapter is applicable to problems with any density of states of the structured radiation reservoir but it is essential that only the zero- and one-photon components of the reservoir Hilbert space are populated. In order to circumvent this restriction and thus be able to deal with more excitations in the structured continuum, we investigate in chapter 6, the system consisting of a number of two-level atoms coupled identically to a Fano-profile density of states. The analyticity of the density of states allows us by introduction of two pseudo-modes to derive a Markovian master equation for the system consisting of atoms+the two pseudo-modes. In this system we study superradiance and the influence of multiple excitations in the radiation reservoirs on the atomic dynamics. We find that following the superradiant regime, a meta-stable state is reached for the atomic system. The decay of the meta-stable state is non-exponential and we derive an analytical expression for the decay based on perturbation theory and trapping states identified by the Monte-Carlo wave

function method. The existence of a Markovian master equation for the system further allows us to test the validity of the mean-field approximation in the equations of motion for the operators of the system. A good agreement is found and the mean-field approximation may therefore be a useful approximation in various contexts where a master equation can not be obtained.

Bibliography

[1] S. Bay, P. Lambropoulos, and K. Mølmer, Opt. Comm. **132**, 257 (1996).

[2] S. Bay, P. Lambropoulos, and K. Mølmer, Phys. Rev. A **55**, 1485 (1997).

[3] S. Bay and P. Lambropoulos, Opt. Comm **146**, 130 (1998).

[4] S. Bay, P. Lambropoulos, and K. Mølmer, Phys. Rev. Lett. **79**, 2654 (1997).

[5] S. Bay, P. Lambropoulos, and K. Mølmer, to appear in Phys. Rev. A .

[6] K. Mølmer and S. Bay, subm. to Phys. Rev. A .

[7] E. M. Purcell, Phys. Rev. **69**, 681 (1946).

[8] D. Kleppner, Phys. Rev. Lett. **47**, 233 (1981).

[9] T. Quang and S. John, Phys. Rev. A **56**, 4273 (1997).

[10] E. Yablonovitch, Phys. Rev. Lett. **58**, 2059 (1987).

[11] S. John, Phys. Rev. Lett. **58**, 2486 (1987).

[12] S. John and R. Rangarajan, Phys. Rev. B **38**, 10101 (1988).

[13] K. M. Leung and Y. F. Liu, Phys. Rev. B **41**, 10188 (1990).

[14] K. M. Ho, C. T. Chan, and C. M. Soukoulis, Phys. Rev. Lett. **66**, 393 (1991), comment.

[15] K. M. Ho, C. T. Chan, and C. M. Soukoulis, Phys. Rev. Lett. **65**, 3152 (1990).

[16] E. Yablonovitch, T. J. Gmitter, and K. M. Leung, Phys. Rev. Lett. **67**, 2295 (1991).

[17] E. Yablonovitch, Jour. Mod. Optics **41**, 173 (1994).

[18] E. Ozbay *et al.*, Optics Letters **19**, 1155 (1994).

[19] P. Villeneuve and M. Piche, Prog. Quant. Electr. **18**, 153 (1994).

[20] D. F. Sievenpiper, M. E. Sickmiller, and E. Yablonovitch, Phys. Rev. Lett. **76**, 2480 (1996).

[21] V. N. Bogomolov *et al.*, Appl. Phys. A **63**, 613 (1996).

[22] J. D. Joannopoulos, R. D. Meade, and J. N. Winn, *Photonic Crystals: Molding the Flow of Light* (Princeton University Press, Princeton, 1995).

[23] M. C. Wanke *et al.*, Science **275**, 1284 (1997).

[24] O. Lehmann and M. Stuke, Science **270**, 1644 (1995).

[25] M. Wanke, , private communication.

[26] E. A. Hinds, Adv. At. Mol. Phys. **28**, 237 (1991).

[27] S. Haroche, in *New trends in atomic physics*, edited by G. Grynberg and R. Stora (Elsevier Science Publishers, Holland, 1984).

[28] S. Haroche, in *Fundamental systems in quantum optics*, edited by J. R. J. Dalibard and J. Zinn-Justin (Elsevier Science Publishers, Holland, 1992).

[29] A. Mekis *et al.*, Phys. Rev. Lett. **77**, 3787 (1996).

[30] J. D. Joannopoulos, P. R. Villeneuve, and S. Fan, Nature **386**, 143 (1997).

[31] S. John and J. Wang, Phys. Rev. Lett. **64**, 2418 (1990).

[32] S. John and T. Quang, Phys. Rev. A **50**, 1764 (1994).

[33] A. Kofman, G. Kurizki, and B. Sherman, Journal of Modern Optics **41**, 353 (1994).

[34] S. John, in *Confined electrons and photons*, NATO-ASI (Plenum Publishing Corp., London, England, 1994).

[35] S. John, in *Photonic band gap materials*, NATO Advanced Study Institute (Kluwer Academic Publishers, The Netherlands, 1995).

[36] R. H. Dicke, Phys. Rev. **93**, 99 (1954).

[37] M. Gross and S. Haroche, Physics Reports **93**, 301 (1982).

[38] G. Kurizki, A. G. Kofman, and V. Yudson, Phys. Rev. A **53**, R35 (1996), and references therein.

[39] S. John and T. Quang, Phys. Rev. A **52**, 4083 (1995).

[40] R. G. DeVoe and R. G. Brewer, Phys. Rev. Lett. **76**, 2049 (1996).

[41] C. Cohen-Tannoudji, J. Dupont-Roc, and G. Grynberg, *Atom-Photon Interactions* (Wiley, New York, 1992).

[42] S. John and J. Wang, Phys. Rev. B **43**, 12772 (1991).

[43] G.-I. Kweon and N. M. Lawandy, Journal of Modern Optics **41**, 311 (1994).

[44] M. L. Goldberger and K. M. Watson, *Collision Theory* (Wiley, New York, 1964).

[45] J. H. Eberly and K. Wodkiewicz, J. Opt. Soc. Am. **67**, 1252 (1977).

[46] S. John and T. Quang, Phys. Rev. Lett. **74**, 3419 (1995).

[47] S. John and T. Quang, Phys. Rev. Lett. **76**, 2484 (1996).

[48] G. Kurizki, B. Sherman, and A. Kadyshevitch, J. Opt. Soc. Am. B **10**, 346 (1993).

[49] B. Sherman, A. G. Kofman, and G. Kurizki, Appl. Phys. B **60**, 99 (1995).

[50] S. John, Physics Today 32 (1991).

[51] T. Quang, M. Woldeyohannes, S. John, and G. S. Agarwal, Phys. Rev. Lett. **79**, 5238 (1997).

[52] T. W. Mossberg and M. Lewenstein, J. Opt. Soc. Am. B **10**, 340 (1993).

[53] J. Wang, Physics Letters A **204**, 54 (1995).

[54] B. Sherman, G. Kurizki, and A. Kadyshevitch, Phys. Rev. Lett. **69**, 1927 (1992).

[55] S.-Y. Zhu, H. Chen, and H. Huang, Phys. Rev. Lett. **79**, 205 (1997).

[56] S. John and T. Quang, Phys. Rev. A **54**, 4479 (1996).

[57] H. J. Carmichael, *An Open Systems Approach to Quantum Optics* (Springer Verlag, Berlin, 1992).

[58] J. Dalibard, Y. Castin, and K. Mølmer, Phys. Rev. Lett. **68**, 580 (1992).

[59] K. Mølmer, Y. Castin, and J. Dalibard, J. Opt. Soc. Am. B **10**, 524 (1993).

[60] R. Dum, P. Zoller, and H. Ritsch, Phys. Rev. A **45**, 4879 (1992).

[61] G. C. Hegerfeldt and T. S. Wilser, in *Proceedings of the II International Wigner Symposium*, edited by H. D. Doebner, W. Scherer, and F. Schroeck (World Scientific, Singapore, 1992).

[62] K. Mølmer and Y. Castin, Quantum and Semicl. Opt. **8**, 49 (1996).

[63] P. M. Visser and G. Nienhuis, Phys. Rev. A **52**, 4727 (1995).

[64] P. Meystre and M. Sargent, *Elements of Quantum Optics* (Springer Verlag, Berlin, 1991).

[65] A. Imamoglu, Phys. Rev. A **50**, 3650 (1994).

[66] P. Stenius and A. Imamoglu, Quantum Semicl. Opt. **8**, 283 (1996).

[67] B. M. Garraway, Phys. Rev. A **55**, 2290 (1997).

[68] B. M. Garraway, Phys. Rev. A **55**, 4636 (1997).

[69] R. F. Nabiev, P. Yeh, and J. Sanchez-Mondragon, Phys. Rev. A **47**, 3380 (1993).

[70] J. J. Sakurai, *Modern Quantum Mechanics* (Addison-Wesley, New York, 1995).

[71] L. Allen and J. H. Eberly, *Optical resonance and two-level atoms* (Dover Publications, New York, 1987).